# Adaptive Complex Networks

## An analytical and numerical study of synchronization in complex networks with anti-Hebbian and Hebbian adaptation rules

by

Willemijn F.H. van Varik

to obtain the degree of Bachelor of Science
at the Delft University of Technology,
to be defended publicly on Tuesday July 9th, 2019 at 12:00 PM.


| | | |
|---|---|---|
| Student number: | 4391527 | |
| Project duration: | September 1, 2018 – July 9, 2019 | |
| Thesis committee: | Dr. J.L.A. Dubbeldam, | TU Delft, supervisor |
| | Dr. ing. S. Kenjeres, | TU Delft, supervisor |
| | Prof. dr. Y.M. Blanter, | TU Delft |
| | Dr. ir. J.H. Weber, | TU Delft |


*This thesis is confidential and cannot be made public until July 9, 2019.*

An electronic version of this thesis is available at `http://repository.tudelft.nl/`.

TU Delft

# Summary

Synchrony is a phenomenon that pervades all fields of science. The Kuramoto model is a prominent model that describes synchronization in systems (networks). It models each element of the network as an oscillator with an individual phase. Due to global coupling, a phase transition is realized, such that some oscillators of the network synchronize. An example of this model is the synchronization of chemical oscillators. However, this model is sometimes insufficient. It is found that in some parts of the brain, synchronization is required, but that excessive synchronization may lead to epilepsy. This reveals that negative feedback is required in order to avoid excessive synchronization.
In this study, the Kuramoto model is extended to an adaptive network by introducing two opposing adaptation rules, such that the strength of coupling can differ per pair of oscillators. The anti-Hebbian rule promotes links between oscillators that are in anti-phase. It is found that networks with this adaptation rule organize themselves in a way that links occur between oscillators whose frequencies are most distant, and that other links are weakened or pruned completely. This suggests that networks with this adaptation rule are able to avoid excessive synchronization. However, the network is still able to sustain explosive synchronization.
The second rule, the Hebbian rule, promotes links between oscillators that are in phase. Networks with this rule do not prune links. Again explosive synchronization is revealed in this network.
A stability analysis is performed to obtain more fundamental insights in the dynamics of the network. The results of this thesis can help obtaining deeper understanding the dynamics and principles of link pruning and explosive synchronization in complex networks: phenomena that are observed in, among others, the field of neuroscience.

# Contents

# 1 Introduction

'*Every night along the tidal rivers of Malaysia, thousands of fireflies congregrate in the mangroves and flash in unison, without any leader or cue from the environment*' Steven Strogratz poetically writes in his book[1] about synchronization. It is one of many mysterious examples where a (large) group of individuals spontaneously organize their movements or activities to synchronize as a group. Without noticing, we take part in this synchronizing process on a daily base. For example, think of the applaud after a concert. It may take some time, but the audience will almost always end up clapping their hands in the same rhythm [2]. Recently, Somnox - a spin-off of this university - released a sleep robot that imitates a slow breathing rhythm. By holding the robot, your own breathing rhythm will synchronize to that of the robot. Other examples of synchronization in the human body include the pacemaker cells in our heart that synchronize in order to produce one joint heartbeat [3], and neurons that fire synchronous in some regions of the brain. [4]. On the other hand, oversynchronization may lead to epilepsy [5, 6].
Synchronization occurs not only in the field of biology, it is a phenomenon that pervades all fields of science. Important applications in physics consist of synchronization in superconducting Josephson junctions [7, 8], coupled lasers [9, 10], power grids [11, 12] and coupled microwave oscillators [13].

The existence of the spontaneous order and synchronization of groups astonished many scientists, and triggered them to find an explanation. The first report on the subject originates from Christiaan Huygens [14], who discovered that the phases of pendulums hanging from the same support synchronize. However, the interest in the topic aroused due to the work of Wiener, who was interested in the generation of alpha rhythms in the brain [15]. He already expected that the underlying principle of these rhythms was related to other observed synchronzation mechanisms. However, his ideas were too complex and did not lead to clear analytical results [16, 17]. Winfree was the first to propose an actual mathematical model to describe the synchronization of oscillators [17, 18]. He recognized that synchronization is a threshold process. Only if oscillators are somehow coupled strong enough, a transition will take place from an incoherent state to a synchronous one. This model inspired Kuramoto, who finally simplified the model of Winfree [19, 20, 16]. This simplification led to the Kuramoto model, probably one of the most celebrated and successful models to describe the synchronization of systems. In short, the elements of the elements of the system are modelled as oscillators with a phase. Due to global coupling of all the oscillators, a phase transition occurs, such that some elements synchronize.

It is found that sometimes the Kuramoto model is unsufficient. As stated above, excessive synchronization in the brain may cause epilepsy. It is desired to add negative feedback to the model. To that extend, in this study the model will be extended, such that the strength of the coupling can differ per pair of oscillators. The thesis is organized in the following way. In Chapter 2 the Kuramoto model is discussed and the model is extended to an adaptive network by introducing adaptation rules, such that the strength of coupling can differ per pair of oscillators. The first rule, the anti-Hebbian rule, is adapted from [21]. This rule weakens links between oscillators that are in phase, and promotes links between oscillators that are in anti-phase, while the second rule (Hebbian rule) operates vice-versa. Then, in Chapter 3 the dynamics of a large, adaptive network are considered, by numerically simulating the networks. This is a reproduction of [21], and extended to the Hebbian adaptative network. In particular, it will reveal the existence of Explosive Synchronization (abrupt and irre-

versible transition towards a synchronized state [22, 21]) for both adaptive networks, while having different dynamical properties. Explosive synchronization is currently a subject of many interest, and is for example recently linked to seizures and anesthetic-induced unconsciousness [23, 24, 21]. After that, in Chapter 4 a small network of only two oscillators is considered, and solved analytically. From this solution, some very basic insights in the dynamics of the adaptive network are obtained. This is again based on [21], and extended to the Hebbian network. In Chapter 5 the study will be extended to a network of 3 oscillators. Although this network is not easily solved analytically, by using earlier obtained insights, the dynamics of the network can still be predicted. By doing so, even more dynamics and coupling rules are revealed. Thereafter, in Chapter 6 the coupling of chemical oscillators is considered as an application of the Kuramoto model. Finally, the conclusions are drawn and interpreted in Chapter 7, and some recommendations for further research will be done.

# 2 Theory

## 2.1. Introduction

This chapter short outlines the theoretical background of the model: an adaptive complex network of Kuramoto oscillators. First the basic principles of graph theory will be presented, as graphs and complex networks share the same properties. Thereafter, the model of the complex network of this paper will be introduced.

## 2.2. Algebraic Graph Theory

A complex network can be defined as 'a system made by a large number of single units (individuals, components or agents) interacting in such a way that the behaviour of the system is not a simple combination of the behaviours of the single units' [25]. Using graph theory this system can be described mathematically. The single units are represented by nodes or vertices. The nodes are connected, if there occur interactions between nodes.These connections are represented by edges that connect the corresponding nodes.
The term 'complex network' is usually used to refer to the real system or network, while the graph refers to the mathematical description of the system [26].

### 2.2.1. Definiton of a graph

A graph $G$ is an ordered pair of finite sets $(V,E)$. $V$ is the set of vertices or nodes, and $E$ the set of subsets of $V$, such that $E \subseteq \{\, \{u,v\} \mid u,v \in V \,\}$. An element $\{u,v\}$ of $E$ represents an edge between nodes $u$ and $v$. A graph $G' = (V',E')$ is a subgraph of $G = (V,E)$, if $V' \subseteq V$ and $E' \subseteq E$.
A graph is called an undirected graph, if all edges have no orientation, and thus that for $\{u,v\} \in E$ it holds that $\{u,v\} = \{v,u\}$. In the model of this paper, it is assumed that the network is undirected, that no node is connected to itself and that two nodes are connected by at most one link.
See figure 2.1 for an example of a simple graph [27, 28].

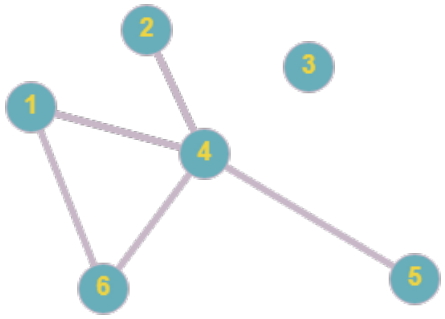


**Figure 2.1.** A graph $G = (V,E)$, where $V = \{1,2,3,4,5,6\}$ and $E = \{\{1,4\},\{1,6\},\{2,4\},\{4,5\},\{4,6\}\}$

### 2.2.2. Walks and paths

By using the links, it is possible to 'walk' through the graph. A walk is an ordered list of nodes $(n_0,\ldots,n_k)$, such that $\{n_{i-1},n_i\} \in E, \forall 1 \leq i \leq k$. If $n_0 = u$ and $n_k = v$, this is called a walk between $u$ and $v$. A path between $u$ and $v$ is a walk between $u$ and $v$ where all visited vertices are unique, such that $n_i \neq n_j, \forall i,j = 0,\ldots,k$ and $i \neq j$ [27, 28].

### 2.2.3. Connectivity and completeness

A graph $G = (V,E)$ is connected if there exists a path between each pair of nodes of $G$. A graph can also consist of multiple connected components. A connected component $G' = (V',E')$ is a maximal subgraph of $G = (V,E)$, that is connected and that is not connected to any other node of $V'$.

If no edges terminate a node, than this node is also a connected component. For example, the graph of Figure 2.1 has two connected components, namely the subsets $V_1' = \{1,2,4,5,6\}$ and $V_2' = \{3\}$
A graph $G = (V, E)$ is complete, if there exists a link $\{u, v\}$ in $E$ for all nodes $u$ and $v$ in $V$ [27, 28].

### 2.2.4. The Adjacency Matrix

The adjacency matrix $A$ contains information about the edges of graph. If a graph has N nodes, than the adjacency matrix is a square $N$-by-$N$ matrix. Its elements are defined as follows:

$$a_{ij} := \begin{cases} 1 & \{i, j\} \in E \\ 0 & \text{otherwise} \end{cases} \tag{2.1}$$

For example, the adjacency matrix of the graph of Figure 2.1 is

$$A = \begin{pmatrix} 0 & 0 & 0 & 1 & 0 & 1 \\ 0 & 0 & 0 & 1 & 0 & 0 \\ 0 & 0 & 0 & 0 & 0 & 0 \\ 1 & 1 & 0 & 0 & 1 & 1 \\ 0 & 0 & 0 & 1 & 0 & 0 \\ 1 & 0 & 0 & 1 & 0 & 0 \end{pmatrix}$$

The adjacency matrix has some interesting properties that are especially useful for larger graphs. In these cases it is more convenient to describe a graph by and perform calculations with an adjacency matrix, instead of drawing the graph.

Since it is assumed that no node is connected to itself, the adjacency matrix is a hollow matrix, meaning that $a_{ii} = 0, \forall i = 1, \ldots, N$. Furthermore, seeing that the graph is undirected, it holds that $a_{ij} = a_{ji}$, and thus that the adjacency matrix is symmetric.

As $a_{ij}$ determines whether node $i$ is linked with node $j$, the $i$th row contains information about all the connections of node $i$. In other words, the number of edges that terminates node $i$ can be found by taking the sum of row $i$. This is also called the degree $d_i$ of node $i$. The diagonal matrix $\Delta := \text{diag}(d_1, d_2, \ldots, d_N)$ is called the degree matrix [29].

### 2.2.5. Laplacian and Connected Components

For the graph of Figure 2.1 it is easy to determine the number of connected components. However, if only the adjacency matrix of a large graph is known, it would be very complicated to first draw the corresponding graph and then determine the number of connected components. Luckily, algebraic graph theory offers an alternative.
This alternative makes use of the spectral analysis of the Laplacian $Q$. This matrix is given by [29]

$$Q = \Delta - A \tag{2.2}$$

With $A$ the adjacency matrix and $\Delta$ the degree matrix of graph $G$. There are multiple formulations of the following theorem, here is chosen for the formulation in [30]

**Theorem 1.** *Let $G$ be an undirected graph with non-negative weights. Then the multiplicity $k$ of the eigenvalue 0 of $Q$ equals the number of connected components $A_1, \ldots, A_k$ in the graph. The eigenspace of eigenvalue 0 is spanned by the indicator vectors $\mathbb{1}_{A1}, \ldots, \mathbb{1}_{Ak}$ of those components.*

The proof (and additional information) can also be found in [30]. As mentioned before, in this model it is assumed that the network is undirected, and it is assumed that the weights are non-negative, such that this theorem may be used. Thus, by determining the algebraic multiplicity of the eigenvalue 0 of $Q$, the number of connected components can be determined.

## 2.3. The Model

As mentioned in section 2.1, the model of interest is an adaptive complex network of Kuramoto oscillators. The nodes of the network are coupled oscillators and the system obeys the dynamics of an extension of the Kuramoto model with an adaptation rule for the coupling of the oscillators. In this section the dynamics and properties of the Kuramoto model will be described, followed by the introduction of two adaptation rules.

### 2.3.1. The Kuramoto Model

A prominent model to describe the synchronization of a large and undirected network of coupled oscillators is the Kuramoto model, described by the Japanese physicist Yoshiki Kuramoto [20]. The model consists of $N \geq 2$ coupled limit-cycle oscillators. The $u$th oscillator ($u = 1, \ldots, N$) is defined by its natural frequency $\omega_u$ and its phase $\theta_u \in [0, 2\pi]$. The natural frequencies are distributed by a unimodal probability g($\omega$) that is symmetric about its mean frequency, and the phase of the oscillators obeys the dynamics

$$\dot{\theta}_u = \omega_u + \frac{\sigma_c}{N} \sum_{v=1}^{N} \sin(\theta_v - \theta_u) \tag{2.3}$$

where $\sigma_c$ denotes the overall coupling strength, thus the strength of an connection between two oscillators. In Figure 2.2(a) a schematic representation of the phases of two Kuramoto oscillators is shown.
The degree of global synchronization can be quantified with the help of the order parameter

$$z := R(t)e^{i\psi(t)} = \frac{1}{N} \sum_{u=1}^{N} e^{i\theta_u(t)} \tag{2.4}$$

where $\psi(t)$ is the average phase of the network at time $t$. $R$ corresponds with the magnitude of the order parameter and can be interpreted as the degree of global synchronization. Figure 2.2(a) shows the order parameter for two Kuramoto oscillators. If all phases are uniformly distributed in the interval $[0, 2\pi]$, then the network is asynchronous (or: incoherent) and $R \approx 0$. This is shown in Figure 2.2(b). On the contrary, if all oscillators have the same phase $\phi(t) = \psi(t)$, then $R = 1$. In this case, the complex network is fully synchronized, and this is shown in Figure 2.2(c). Equation (2.4) can be rewritten as

$$R(t) = \frac{1}{N} \left| \sum_{u=1}^{N} e^{i\theta_u(t)} \right| \tag{2.5}$$

Kuramoto rewrote equation (2.3) with the help of equation (2.4) as [31]

$$\dot{\theta}_u = \omega_u - R\sigma_c \sin(\theta_u - \psi) \tag{2.6}$$

In this equation the evoluation of the phase of the $u$-th oscillator no longer depends on the phase of the other oscillators, but on $R$ and $\psi$. The larger $\sigma_c$, the more the oscillators are attracted to $R(t)e^{i\psi(t)}$, and thereby the network becomes more synchronous[16].

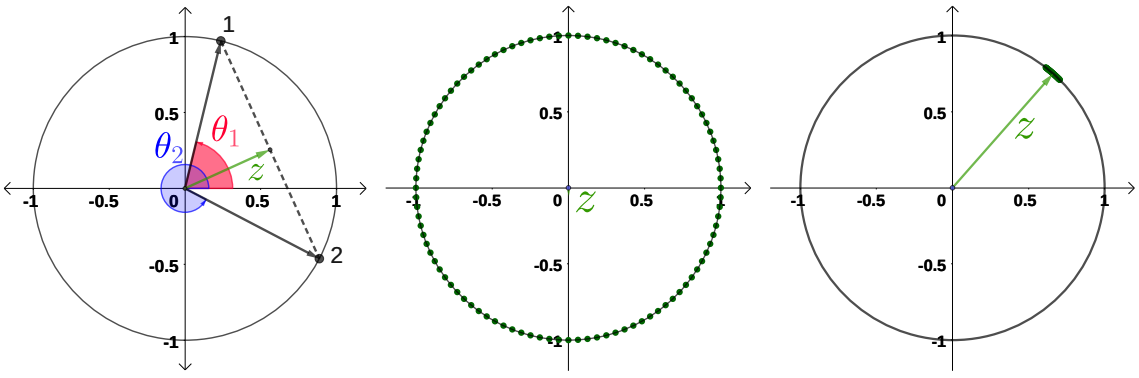


**Figure 2.2.** A visualisation of the parameters of Kuramoto oscillators: (a) The phases $\theta_1, \theta_2$ and the corresponding order parameter $z$, (b) an asynchronous network with $R \approx 0$ and (c) a synchronous network with $R \approx 1$.

There exists a critical coupling strength $\sigma_{critical}$ such that the network transforms from a asynchronous into a synchronous network. Kuramoto analytically proved that for an infinite number of oscillators, and for a continuous, symmetric and unimodal distribution $g(\omega)$ centered above 0, the $\sigma_{critical}$ is given by [19, 20]

$$\sigma_{critical} = \frac{2}{\pi g(0)} \tag{2.7}$$

and that the global synchronization for $\sigma_c > \sigma_{critical}$ is given by

$$R = \sqrt{1 - \frac{\sigma_{critical}}{\sigma_c}} \tag{2.8}$$

And $R \approx 0$ for $\sigma_c < \sigma_{critical}$, as the network is asynchronous for these values of $\sigma_c$. In Figure 2.3, $R$ is plotted as a function of $\sigma_c$ for a network with $\sigma_{critical} = 0.5$, in accordance with (2.8). It shows a very sharp transition from an incoherent network to a synchronous network at $\sigma_c = \sigma_{critical}$.

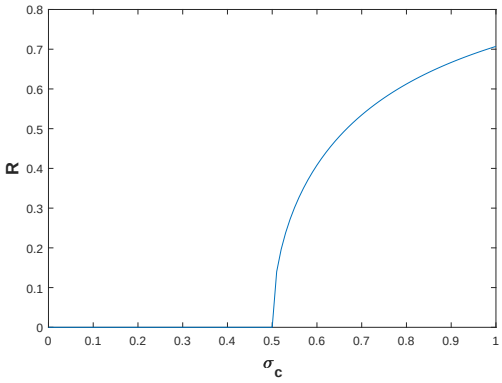


**Figure 2.3.** The order parameter $R$ as a function of overall coupling strength $\sigma_c$ given a critical coupling strength of $\sigma_{critical} = 0.5$.

For the finite dimensional Kuramoto model, the expression of $\sigma_{critical}$ does not hold. However, a necessary condition for the existence of synchronized solutions is given by [32, 33]

$$\sigma_{critical} > \frac{N(\omega_{max} - \omega_{min})}{2(N-1)} \tag{2.9}$$

where $\omega_{min}$/ $\omega_{max}$ are the minimum/maximum values of the natural frequencies of the oscillators of the network. It is emphasised that the above inequality gives a lower bound for $\sigma_{critical}$, and not the exact value.

### 2.3.2. Adaptive Complex Networks

In the Kuramoto model, the strength of a connection between two oscillators is the same for all connections. In the network of this paper however, the strength can differ for every connection. The (modelled) weight of the connection between oscillators $u$ and $v$ is depicted by $\alpha_{uv} \in [0, 1]$. The Kuramoto model can be applied by including the connectivity of the network in the evolution of the phase [34]. The evolution of the phase can then be rewritten into

$$\dot{\theta}_u = \omega_u + \frac{\sigma_c}{N} \sum_{v=1}^{N} \alpha_{uv} \sin(\theta_v - \theta_u) \tag{2.10}$$

In adaptive networks, the weights of connection not only differs for every connection, they can also evolve in time according to an adaptation rule. In the following two adaptation rules will be introduced: the **Hebbian** and the **anti-Hebbian** rule.

#### The Hebbian adaptation rule

First, the Hebbian adaptation rule will be introduced. This rule stimulates connections between oscillators that are in phase. The instantaneous phase correlation $p_{uv}(t)$ between oscillators $v$ and $u$ at time $t$, is measured by:

$$p_{uv}(t) = \tfrac{1}{2} \| e^{i\theta_u(t)} + e^{i\theta_v(t)} \| = \sqrt{\frac{1 + \cos(\theta_u(t) - \theta_v(t))}{2}} \tag{2.11}$$

Of course, oscillator $u$ and $v$ are in phase if $p_{uv} = 1$ and in anti-phase if $p_{uv} = 0$. The Hebbian adaptation rule is then given by

$$\dot{\alpha}_{uv} = (p_{uv} - p_c)\alpha_{uv}(1 - \alpha_{uv}) \tag{2.12}$$

where $p_c$ is the correlation threshold. It can be easily seen that whenever $p_{uv} > p_c$ the weight of the link between oscillator $u$ and $v$ gets increased. On the other hand, whenever $p_{uv} < p_c$ this link will decrease. In other words, given a fixed correlation threshold, the links of pairs with a higher level of instantaneous phase correlation will be reinforced. Furthermore, notice that an equilibrium is reached if $\alpha_{uv} = 0$ or $\alpha_{uv} = 1$, corresponding to the minimum and maximum value of the weight of the link.

### The anti-Hebbian adaptation rule

In a similar way, an anti-Hebbian adaptation rule can be formulated. This rule stimulates connections between oscillators that are out of phase, and is given by [21]

$$\dot{\alpha}_{uv} = (p_c - p_{uv})\alpha_{uv}(1 - \alpha_{uv}) \tag{2.13}$$

where $p_{uv}$ as in equation (2.11) and $p_c$ the correlation threshold. It can be easily seen that now whenever $p_{uv} < p_c$ the weight of the link between oscillator $u$ and $v$ gets increased. On the other hand, whenever $p_{uv} > p_c$ this link will decrease. Thus, given a fixed correlation threshold, the links of pairs with a higher level of instantaneous phase correlation will be weakened. It is emphasized that if the Hebbian adaptation rule stimulates a certain link, then the anti-Hebbian rule would weaken that same link.

### Properties of the adaptive networks

For networks with an anti-Hebbian or Hebbian adaptation rule the global strength $S$ can be defined. $S$ is defined as the sum of all weights of connections, or

$$S := \frac{1}{N-1} \sum_{u,v>u}^{N} \alpha_{uv} \tag{2.14}$$

The maximum total strength of a network is equal to $\frac{1}{N-1}\frac{N\cdot(N-1)}{2} = \frac{N}{2}$.

Finally, to achieve better insight in the topological characteristics of the network, the adjacency matrix $A = \{a_{uv}\}$ of the network is required. This matrix is defined as:

$$a_{uv} := \begin{cases} 1 & \alpha_{uv} > \tau \\ 0 & \text{otherwise} \end{cases} \tag{2.15}$$

where $\tau$ is the threshold to keep relevant (strong enough) links and delete irrelevant (too weak) links. Obviously, $\alpha_{uv}$ is the weight of the link.

# 3

# Numerical simulations of an adaptive complex network

## 3.1. Introduction

In this chapter a network of $N = 300$ oscillators is considered. At $t = 0$, the phases $\theta_u$ of this network are uniformly distributed in the interval $[0, 2\pi]$, the links $\alpha_{uv}$ in the interval [0,1] and the natural frequencies $\omega_u$ in the interval [0.8,1.2]. Modified Euler is applied to simulate the time evolution of $\alpha_{uv}$ and $\theta_u$ for a large range of the coupling strength $\sigma_c$ and the phase correlation threshold $p_c$ for both a network with an anti-Hebbian adaptation rule and a network with a Hebbian adaptation rule. The final degree of the global synchronization $R$, the total strength $S$, the largest component $N_g$ and the average degree $\langle k \rangle$ is measured. In addition, the microscopic structure of the networks will be studied.

## 3.2. Anti-Hebbian Adaptation Rule

First, a numerical simulation is done for a network with an anti-Hebbian adaptation rule, given by equations (2.10) and (2.13).

### 3.2.1. Global Synchronization

The final degree of global synchronization $R$ of the simulated network can be computed with equation (2.5). In Figure 3.1 $R$ is shown as a function of $\sigma_c$ and $p_c$.
Figure 3.1(a) shows $R$ as a function of $\sigma_c$ for different values of $p_c$. For low values of $p_c$, the network is not able to synchronize for any value of $\sigma_c$ and remains incoherent. For higher values of $p_c$ synchronization of the network is possible, and an abrupt transition of the global synchronization is shown for $\sigma_c \approx 0.25$. For these values of $p_c$, the $R,\sigma_c$-characteristics are similar to the $R,\sigma_c$-characteristics of the non adaptive Kuramoto model, as visualized in Figure 2.3 (note that the network in this figure has a different $\sigma_{critical}$). However, it must be noted that the transition from the incoherent network to the synchronous state is more abrupt, and almost discontinuous. This reveals the existence of explosive synchronization (ES). This is the abrupt and irreversible transition from an incoherent state to a fully synchronized state [22, 21]. Explosive synchronization that is currently a subject of many interest, and is for example recently linked to seizures and anesthetic-induced unconsciousness [23, 24, 21]. It is still debated whether this transition is discontinuous or not [35].
The critical value of $\sigma_c$ deduced in Figure 3.1(a) is in line with equation (2.9), which says that synchronized solutions in a network with $N = 300$ can only exists if at least $\sigma_c > 0.2$. Moreover, with the help of equation (2.7), $\sigma_{critical}$ of a network with a infinite number of oscillators can be computed: $\sigma_{critical} = \frac{2}{\pi} \cdot \frac{1}{g(0)} = \frac{2}{\pi} \cdot \frac{\omega_{max} - \omega_{min}}{1} \approx 0.255$. Although finite-size effects are expected for this system, this theoretical value still seems to be a very accurate approximation.

In a similar way, $R$ can be plotted as function of $p_c$ for different values of $\sigma_c$. This is shown in Figure 3.1(b). In accordance with the paragraph above, the network is not able to synchronize for any value of $p_c$ if $\sigma_c < 0.25$. For $\sigma_c > 0.25$, the network is able to synchronize and an abrupt and (almost) discontinuous transition of $R$ is shown at $p_c = 0.65$.

Note that for a network with infinitely many oscillators and a uniformly distribution of all corresponding $\theta_i$, it can be assumed that for each $x \in [0, 2\pi]$ there exists an oscillator $i$ such that $\omega_i = x$. This means that the average value of the instantaneous phase correlation $p_{uv}$ at $t = 0$ ($\frac{1}{N}\sum_{i,j>i} p_{ij}(0)$) can be computed by taking the integral over $\theta$ from 0 to $2\pi$, or:

$$\overline{p_{uv}}(0) = \frac{1}{2\pi - 0}\int_0^{2\pi} \sqrt{\frac{1+\cos(\theta_m - \theta_l)}{2}}\, d\theta_l = \frac{2}{\pi} \approx 0.637 \tag{3.1}$$

Note that this value is almost equal to the critical correlation threshold deduced in 3.1(b). This relationship can be explained using the properties of the anti-Hebbian adaptation rule. This rule stimulates links between oscillators with $p_{uv} < p_c$. Thus, if at $t = 0$ $\overline{p_{uv}}(0) < p_c$, then more than half of the links will be stimulated, forcing the network in the synchronized stated.
Obviously, due to finite-size effects, the real value of $\overline{p_{uv}}(0)$ may slightly differ from this theoretical value. However, equation (3.1) appears to be a very accurate approximation for the critical correlation threshold of a finite network of 300 oscillators.
Figures 3.1(a) and 3.1(b) can be combined in a 3D surface plot and a heat map, see Figure 3.1(c) and 3.1(d) respectively. This figure shows that there exists a large region of parameters $\sigma_c$ and $p_c$ for which the network remains incoherent (i.e. $R \approx 0$). For higher values of $p_c$ and $\sigma_c$ an abrupt and discontinuous transition towards a fully synchronized network is shown, revealing the existence of explosive synchronization (ES). Figure 3.1(d) shows that this abrupt transition indeed occurs for $\sigma_c > 0.25$ and $p_c > 0.65$, which is in line with what was found in Figures 3.1(a) and 3.1(b).

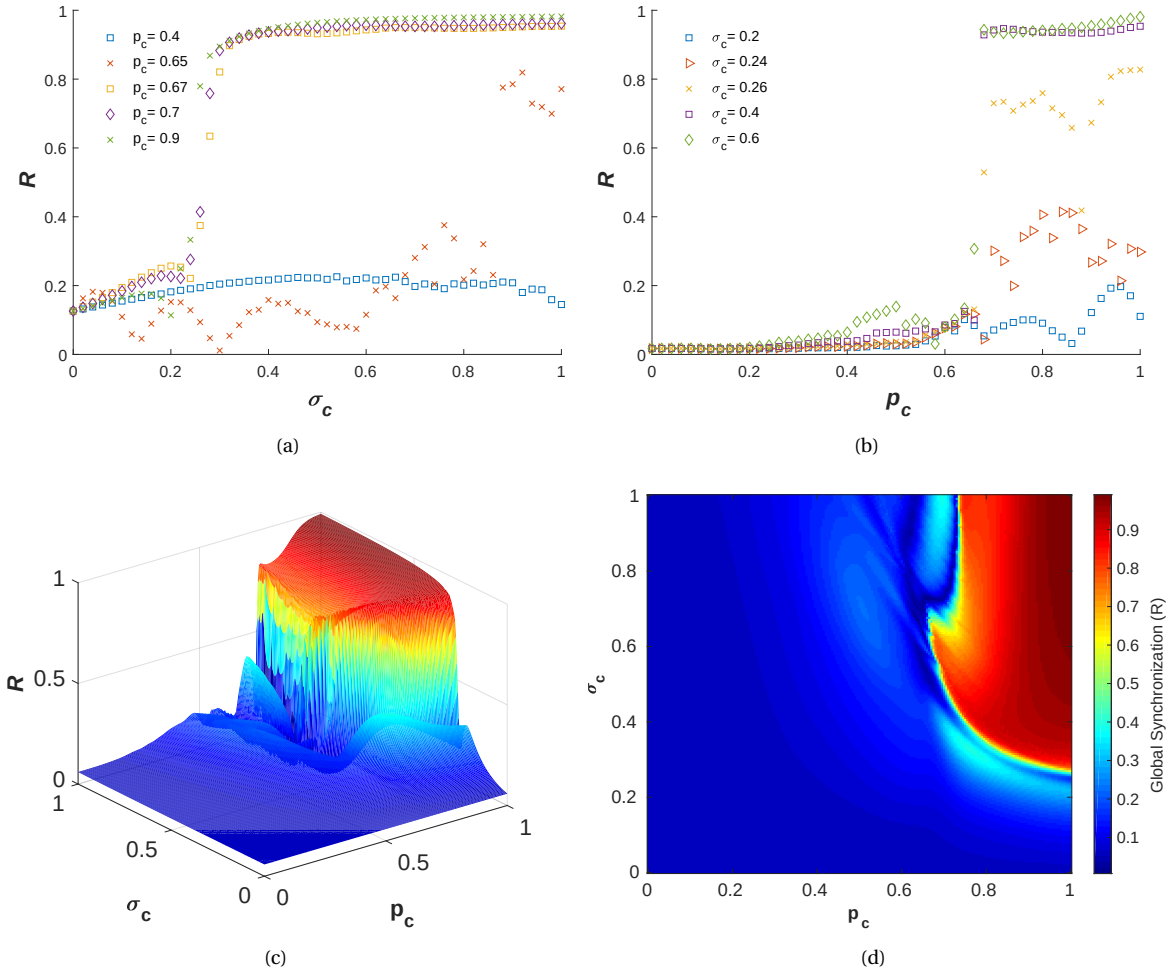


**Figure 3.1.** The final degree of global synchronization $R$. $R$ is shown a) as function of $\sigma_c$ for different values of $p_c$ and b) as function of $p_c$ for different values of $\sigma_c$ and c), d) as function of both $p_c$ and $\sigma_c$. c) underlines the abrupt transition from a asynchronous into an synchronized network (ES). a), b) and d) show that ES occurs for $\sigma_c > 0.25$ and $p_c > 0.65$.

### 3.2.2. Total strength

The global strength $S$ of the evolved network can be computed with equation (2.14). Figure 3.2 shows $S$ as a function of $\sigma_c$ and $p_c$. It points out that for $\sigma_c > 0.25$, $S$ decreases with increasing $\sigma_c$, except for $p_c \approx 1$. This can be explained by investigating equations for $\dot{\theta}_u, \dot{\alpha}_{uv}$ and $p_{uv}$ (given by (2.10), (2.13) and (2.11) respectively) intuitively. If $\sigma_c$ increases, the term $\sum_{v=1}^{N} \alpha_{uv} \sin(\theta_v - \theta_u)$ becomes more significant in the equation for $\dot{\theta}_u$, leading to increasing values of $p_{uv}$. Due to the anti-Hebbian adaptation rule, this will result in more links to be weakened. However, if $p_c \approx 1$, it will always hold that $p_{uv} < p_c$ and thus all links will be strengthened.
Moreover, the figure points out that $S$ suffers an abrupt transition for $\sigma_c < 0.25$ at $p_c = 0.65$. This value of the critical correlation threshold is the same as for $R$ and again corresponds with equation (3.1).
Taking into account both Figure 3.1(d) and Figure 3.2, it should be noticed that (for $p_c > 0.65$) the relations of $S$ and $R$ with $\sigma_c$ are inverse, i.e. $S$ peaks for $\sigma_c < 0.25$, where the network is asynchronous, and $S$ decreases for $\sigma_c > 0.25$, where the network is fully synchronized. This points out that the network first undergoes a phase of strong local synchronization, where clusters are formed, before achieving global coherence. While achieving global coherence, the total strength of the network decreases, implying that links are pruned.

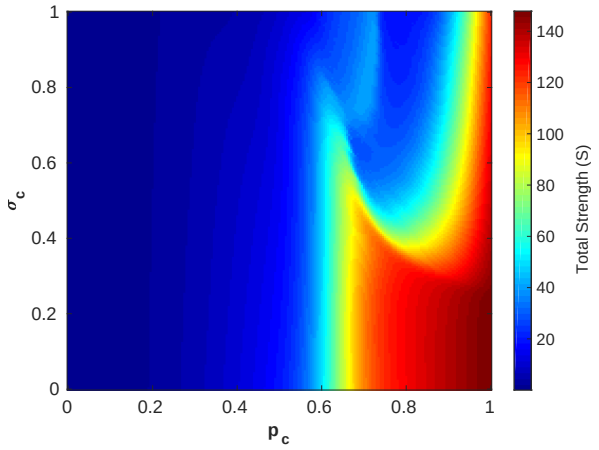


**Figure 3.2.** The total strength $S$ as function of $p_c$ and $\sigma_c$ .

### 3.2.3. Global topological characteristics

Better insight in the topological characteristics of the evolved network can be retrieved by inspecting the largest component $N_g$ and the average degree $\langle k \rangle$ of the evolved network. In order to compute these properties, the adjacency matrix is studied (defined as in equation (2.15)). The threshold is chosen as $\tau = 0.8$ to only keep the significant links. The network is studied in the range of parameters $\sigma_c$ and $p_c$ where the transition into a synchronous and connected network takes place: $p_c \in [0.6,\ 1]$ and $\sigma_c \in [0.2,\ 1]$.
The largest component $N_g$ of the evolved network can be found by analysing the connected components of the graph. Theorem (1) is used to find the number of connected components. Figure 3.3(a) shows the size of $N_g$ as function of $\sigma_c$ and $p_c$. It reveals that for a large region of the parameters the network is fully connected, so that the all the oscillators are part of the same component. In the region $0.4 < \sigma_c$ and $p_c \in [0.7,\ 0.9]$, the network is not fully connected. Again, this can be explained by increasing values of $p_{uv}$, and thus decreasing values of $\alpha_{uv}$ for increasing $\sigma_c$. Only for $p_c$ sufficiently large, links will be reinforced.
Figure 3.3(b) shows $\langle k \rangle$ of the oscillators as function of the parameters. It points out that the network connectivity decreases from $\langle k \rangle = N$ (complete network) to $\langle k \rangle = 2$.
It is interesting to note that $N_g$ remains very large ($N_g > 250$ for almost all combinations of parameters). Since $\langle k \rangle = 2$ is the absolute minimum to enable a fully connected network (required for $R \approx 1$), this points out that all redundant links are pruned in the pruning process (see subsection 3.2.2).

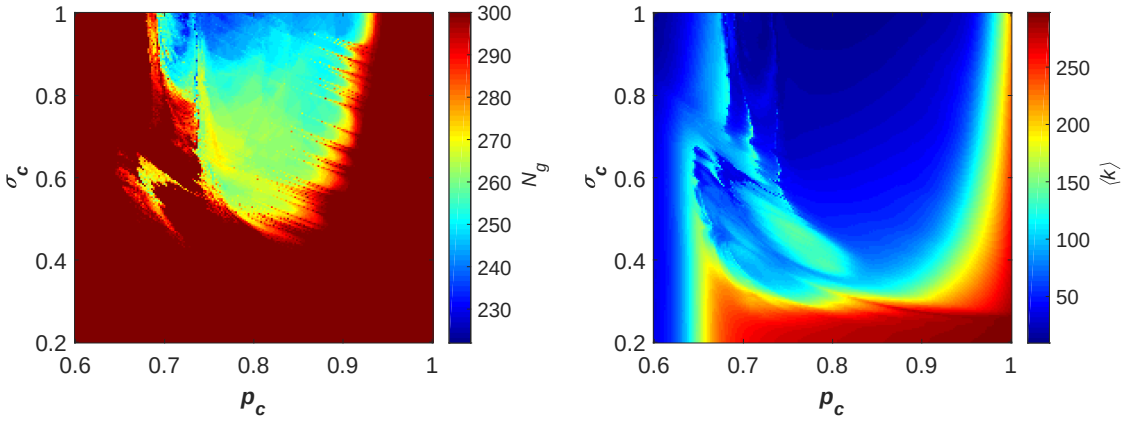


(a) (b)

**Figure 3.3.** Topological characteristics of the binarized network as a function of the coupling strength $\sigma_c$ and of the correlation threshold $p_c$: a) The largest connected component $N_g$, and b) and the average degree $\langle k \rangle$.

### 3.2.4. Microscopic topological characteristics

More information about the topological characteristics of the evolved network can be retrieved by 'zooming in' on the oscillators and inspecting how their natural frequencies and the network structure correlate.
These features are inspected in Figures 3.4, 3.5 and 3.6 for a fixed value $\sigma_c = 0.6$ and three values of $p_c$: $p_c = 0.61$ (left panels), $p_c = 0.75$ (middle panels) and $p_c = 0.95$ (right panels). The value of $\sigma_c$ is fixed such that synchronization is possible (see Figure 3.1). The values of $p_c$ are chosen in such way that the different phases of synchronization are depicted: before the transition ($p_c = 0.61$) and after the transition($p_c = 0.75$ and $p_c = 0.95$). For $p_c = 0.75$, this transition has just occurred, and all redundant links are pruned. For $p_c = 0.95$ the value is sufficiently large to reinforce most links (see Figures 3.1, 3.2 and 3.3).

Figure 3.4 depicts the degree $k_u$ as function of $\omega_u$ of each oscillator $u$ and the different parameter combinations. Just before the transition, $k_u$ and $\omega_u$ are uncorrelated. However, just after the transition a very clear relation is shown between $k_u$ and $\omega_u$. Oscillators whose frequencies are close to the extreme values of the distribution (i.e. $\omega_u \approx 0.8$ or $\omega_u \approx 1.2$) are much more connected than oscillators with an average $\omega_u$ (i.e. $\omega_u \approx 1.0$). This correlation is still present for $p_c = 0.95$, though it is less strong. This is an interesting result, as this shape ($V$-shape) for $k-\omega$-characteristics is known to be an indicator for networks that can sustain explosive characteristics [21]. // The result is explained by inspecting the equation for $\dot{\alpha}_{uv}$ ((2.13)) intuitively: low values of $p_{uv}$ result in increasing $\alpha_{uv}$. It may be expected that the more distance the natural frequencies of two oscillators have, the lower the instantaneous phase correlation $p_{uv}$ is (and thus the stronger $\alpha_{uv}$). Naturally, oscillators with natural frequencies close to the extreme values of the distribution have more distance with the natural frequencies of the other oscillators in the network. In particular, an oscillator $u$ with $\omega_u = 1.0$, can have a maximum distance of $\Delta\omega = 0.2$, whereas an oscillator $v$ with $\omega_u = 0.8$, can have a maximum distance of $\Delta\omega = 0.4$. Thus, as the oscillators with natural frequencies close to the extreme values of the spectrum have on average more distance (in natural frequency), it is expected that $p_{uv}$ is also lower on average, and thus that these oscillators will have a higher degree $k_u$. Note that this implies, that it is also expected that links mainly occur between oscillators with distant frequencies.

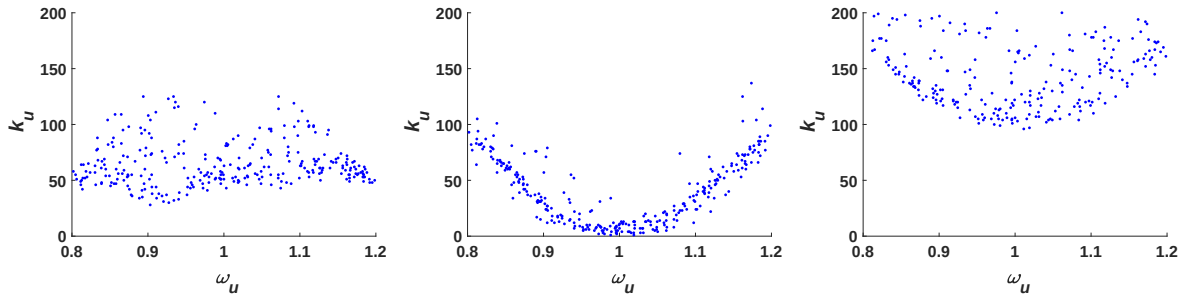


(a) (b) (c)

**Figure 3.4.** Scatter plot of the degree $k_u$ as function of $\omega_l$ of each oscillator $u$ for $\sigma_c = 0.6$ and a) $p_c = 0.61$ b) $p_c = 0.75$ and c) $p_c = 0.95$. A strong correlation appears after the transition in a synchronized network: oscillators whose frequencies are close to extreme values of the distribution are much more connected than the other frequencies.

The implication above (that links are formed between oscillators with distant $\omega$) is confirmed in Figure 3.5, where the node neighborhood detuning $\omega_u - \langle\omega_v\rangle_u$ is shown for each oscillator $u$ for the three combinations of parameters, with $\langle\omega_v\rangle_u$ the average frequency of oscillators $v \in C_u$ and $C_u$ the set of oscillators that are connected to oscillator $u$. The figure shows that after the transition oscillators are much more likely to form links with oscillators whose frequency is distant. This phenomenon is called *frequency dissasortativity* [21], and is particularly remarkable just after the transition. In this phase of synchronization the node neighborhood detuning is discontinuous in $\omega_u$ resulting in a gap in the middle of the frequency spectrum. Here, the preference for connecting with nodes that have frequencies on the right side of the spectrum shifts to a preference for the left side of the spectrum, in order to obtain as much distance in frequency as possible. In addition, all other links are pruned. Again, this can be explained by inspecting the equation for $\dot{\alpha}_{uv}$ ((2.13)) intuitively: low values of $p_{uv}$ result in increasing $\alpha_{uv}$, thus forcing the network to acquire frequency dissasortativity.

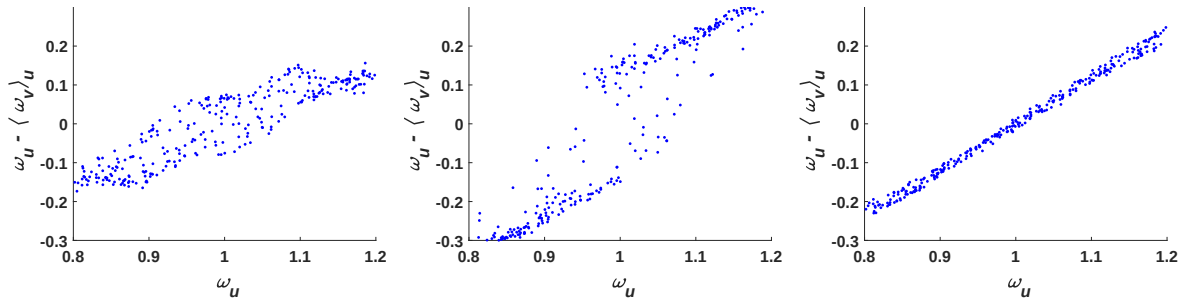


(a) (b) (c)

**Figure 3.5.** Scatter plot of the node neighborhood detuning $\omega_u - \langle\omega_v\rangle_u$, with oscillators $v \in C_u$ for $\sigma_c = 0.6$ and a) $p_c = 0.61$ b) $p_c = 0.75$ and c) $p_c = 0.95$. The network acquires frequency dissasortativity after the transition.

Figure 3.6 shows the connectivity of the network as function of $\omega_u$ and $\omega_v$. This is done by ordering the adjacency matrix according to their natural frequencies. The green regions represent connected oscillators, and red regions represents disconnected oscillators. Inspecting these figures shows the process of pruning and reinforcing links. Before the transition, only links between oscillators with frequencies close to the middle of the spectrum are pruned, corresponding to the red diagonal region. Just after the transition this region of pruning links becomes much larger, leaving unaffected only the links between oscillators with frequencies that are as far away from each other as possible. In the right panel, $p_c$ is sufficiently large to reinforce more links. However, just as in the left panel, links between oscillators with frequencies close to the middle of the spectrum are more likely to be pruned than other links.

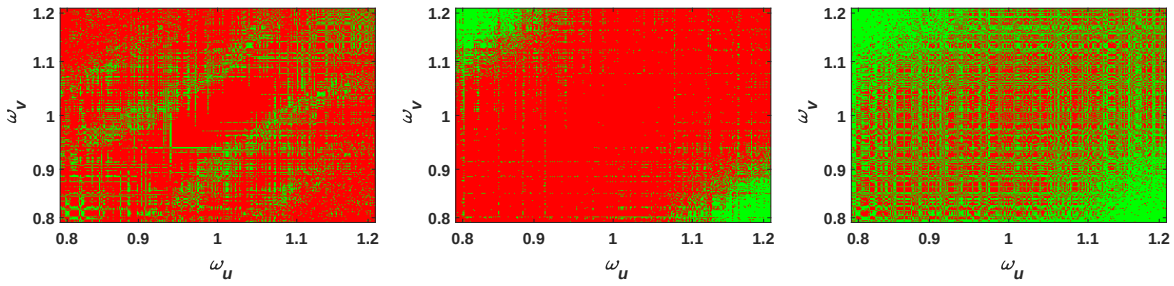


**Figure 3.6.** The connectivity of the network as function of $\omega_u$ and $\omega_v$ for $\sigma_c = 0.6$ and a) $p_c = 0.61$ b) $p_c = 0.75$ and c) $p_c = 0.95$. Links between oscillators with frequencies close to the middle of the spectrum are most likely to be pruned. Just after the transition almost all links are pruned, only leaving links connecting nodes whose frequencies are as far away as possible.

## 3.3. Hebbian Adaptation Rule

The same analysis can be done for a network with an Hebbian adaptation rule, given by equations (2.10) and (2.12).

### 3.3.1. Global Synchronization

The final degree of the global synchronization $R$ of these networks can be computed with equation (2.5). Figure 3.7 shows $R$ as a function of $p_c$ and $\sigma_c$. The surface plot in Figure 3.7(a) shows that there exists a region of parameters $\sigma_c$ and $p_c$ where the network will not synchronize ($R \approx 0$), a region where the network is fully synchronized ($R \approx 1$) and a very small region of parameters where this transition takes places, corresponding with the very abrupt and steep increase of $R$: explosive synchronization. Figure 3.7(b) points out that this transition occurs for $\sigma_c > 0.25$, which is equal to the theoretical critical value for a network with infinite oscillators (given by equation 2.7) and corresponds with the critical value of the network with an Anti-Hebbian adaptation rule (see Figure 3.1).
For values of $\sigma_c$ slightly above this critical value, the network will synchronize for $p_c < 0.63$, again corresponding to $\overline{p_{uv}}(0)$ given in equation (3.1). Thus, the critical correlation threshold is the same as for the network with an anti-Hebbian adaptation rule (see Figure 3.1), but the relation is inverse. This can be explained by the nature of the adaptation rules. Using the Hebbian adaptation rule, links between oscillators $u$ and $v$ with $p_{uv} < p_c$ are stimulated, whereas with the anti-Hebbian adaptation rule links with $p_c < p_{uv}$ are stimulated.
However, if $\sigma_c$ increases, the critical correlation increases, resulting in an expanding region of parameters for which the network is able to synchronize. In a similar way as the investigation of the relationship of $S$ and $\sigma_c$ for the anti-Hebbian network (see section 3.2.2, this relationship can be explained by investigating equations for $\dot{\theta}_u, \dot{\alpha}_{uv}$ and $p_{uv}$ (given by (2.10), (2.12) and (2.11) respectively) intuitively. If $\sigma_c$ increases, the term $\sum_{v=1}^{N} \alpha_{uv} \sin(\theta_v - \theta_u)$ becomes more significant in the equation for $\dot{\theta}_u$, leading to increasing values of $p_{uv}$. Due to the Hebbian adaptation rule, this implies that for a fixed value of $p_c$ more links will be stimulated as $\sigma_c$ increases. This causes the shift to the left of the critical correlation threshold as pointed out in Figure 3.7(b).

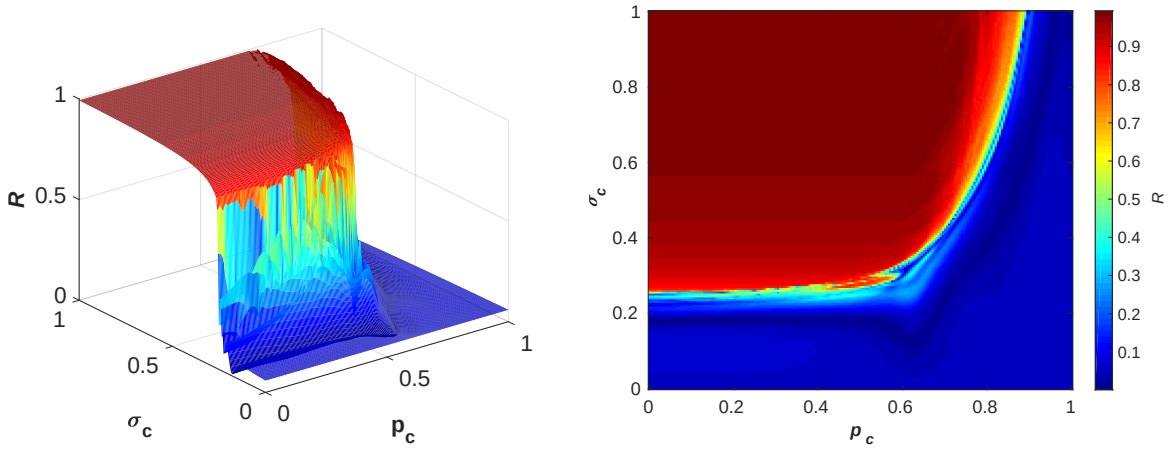


(a) (b)

**Figure 3.7.** The global synchronization $R$ of the evolved network as a function of $\sigma_c$ and $p_c$. The surface plot in a) underlines the explosive transition of the asynchronous to the synchronized state. The heat map in b) points out that this happens for $\sigma_c > 0.25$ and $p_c < 0.63$, and that the latter critical value increases with $\sigma_c$ .

### 3.3.2. Total Strength

The global strength $S$ of the evolved network, defined by equation (2.14), is shown as function of $\sigma_c$ and $p_c$ in Figure 3.8. The figure points out that $S$ suffers an abrupt transition at $p_c = 0.63$ and $\sigma_c = 0.25$, and that the critical value of $p_c$ rises with $\sigma_c$, for $\sigma_c > 0.25$. For values of $p_c$ below this critical value a very strong network is found. This relationship can be explained by investigating equations for $\dot{\theta}_u, \dot{\alpha}_{uv}$ and $p_{uv}$ in a similar way as in the subsection above, finding that for a fixed $p_c$, an increasing $\sigma_c$ results in more stimulated links, and thus an increasing $S$.

Just as with the anti-Hebbian network, the figure points out that $S$ also suffers an abrupt transition for $\sigma_c < 0.25$ (and $p_c = 0.63$), whereas the network does not synchronize for this combination of parameters $\sigma_c$ and $p_c$ (see Figure 3.7. This points out that the network first goes through a phase of strong local synchronization, where clusters are formed, before achieving global coherence. In contrast to the network with the anti-Hebbian adaptation rule, $S$ does not decrease as global coherence is achieved. This thus points out that increasing $\sigma_c$ does not result in the pruning of links.

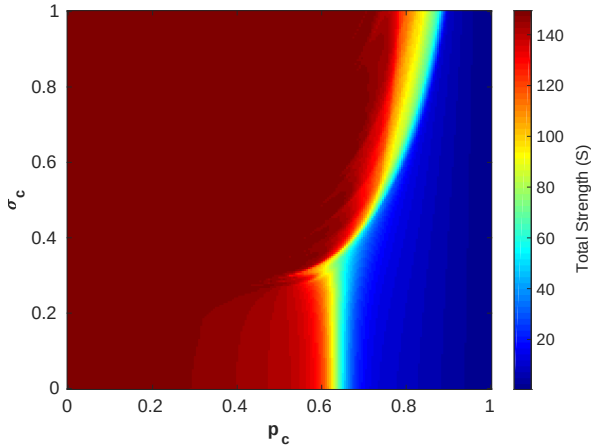


**Figure 3.8.** The total strength $S$ as function of $p_c$ and $\sigma_c$ .

### 3.3.3. Global topological characteristics

The global topological characteristics are studied by inspecting the largest component $N_g$ and the average degree $\langle k \rangle$ of the evolved network. The adjacency matrices (defined as in equation (2.15)) are computed and analyzed for a threshold $\tau = 0.8$ and in the parameter range $p_c \in [0, 0.9]$ and $\sigma_c \in [0.2, 1]$. This is the relevant parameter range where the transition into a synchronous network takes place (see Figure 3.7).

Figure 3.9(a) shows the size of $N_g$ in this parameter range. It reveals that in a large region of parameters the network is fully connected, such that all oscillators belong to the same component. If this region is compared to Figure 3.9(b), where $\langle k \rangle$ is depicted in the same parameter range, it is found that the network is not only fully connected, but also almost complete (i.e. $\langle k \rangle \approx N$) in this region. Comparing Figure 3.9 to Figure 3.8 it is found that same dynamics are found for $N_g$ and $\langle k \rangle$ as for $S$. Since no links are pruned while achieving global coherence, $S$ and therefore $\langle k \rangle$ and (eventually) $N_g$ do not decrease in the synchronized state. In the asynchronous region however, all links are pruned, resulting in $S \approx N_g \approx \langle k \rangle \approx 0$. There are thus only two possible states of the network: either all links are reinforced, or all links are pruned.

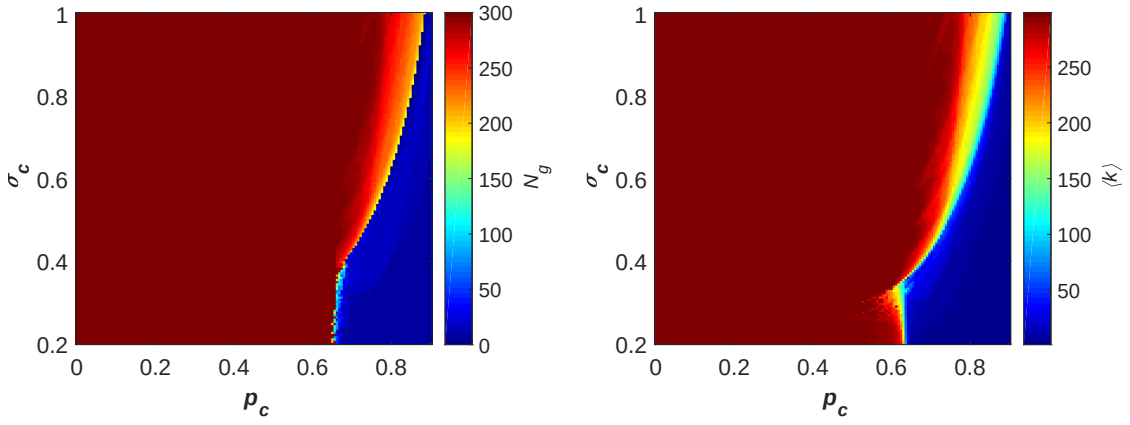


**Figure 3.9.** Topological characteristics of the binarized network as af function of the coupling strength $\sigma_c$ and of the correlation threshold $p_c$. The largest connected component, $N_g$, is shown in a), and the averagede degree, $\langle k \rangle$ is shown in b).

### 3.3.4. Microscopic topological characteristics

Better insight in the topological characteristics of the evolved network can be retrieved by inspecting the correlations between the network structure and the natural frequencies. These microscopic features are shown in Figures 3.10, 3.11 and 3.12 for a fixed value of $\sigma_c = 0.6$ and three values of $p_c$: $p_c = 0.5$ (left panels), $p_c = 0.78$ (middle panels) and $p_c = 0.95$ (right panels). These values are again chosen in such a way that the different phases of synchronization are depicted: the fully synchronized state ($p_c = 0.5$), just before the transition in a asynchronous network ($p_c = 0.78$ and finally the asynchronous state ($p_c = 0.95$)). Note that this are the same phases as studied for the network with an anti-Hebban adaptation rule (see subsection 3.2.4), but in reverse order.

Figure 3.10 shows the degree $k_u$ as function of $\omega_u$ for each oscillator $u$ of the network. For the fully synchronized and the asynchronous phase these two features are uncorrelated, as $k_u$ is constant: $k_u \approx 290$ and $k_u \approx 4$ respectively. Just before the transition a correlation between $k_u$ and $\omega_u$ is shown. Oscillators whose frequencies are close to the extreme values of the distribution (i.e. $\omega_u \approx 0.8$ or $\omega_u \approx 1.2$) are less connected then oscillators whose frequencies are more in the center of the distribution, i.e. $\omega_u \in [0.9, 1.1]$. In comparison to the anti-Hebbian network, this correlation is less strong.

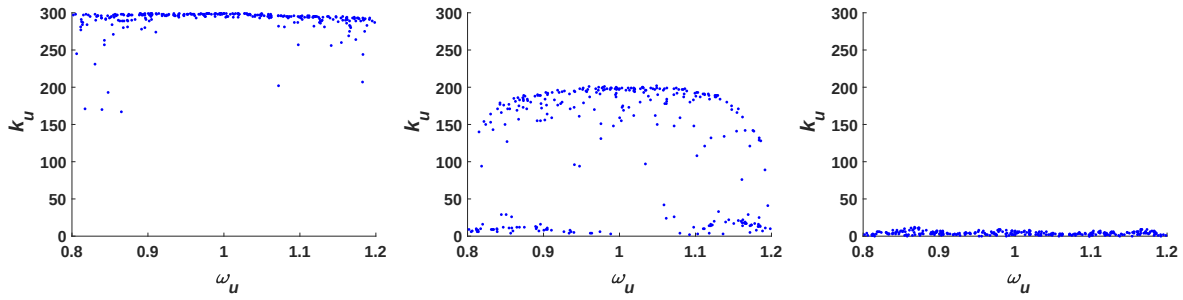


(a) (b) (c)

**Figure 3.10.** Scatter plot of the degree $k_u$ as function of $\omega_l$ of each oscillator $u$ for $\sigma_c = 0.6$ and a) $p_c = 0.5$, b) $p_c = 0.78$ and c) $p_c = 0.95$. A weak correlation appears just before the transition to an asynchronous network. Oscillators whose frequencies are close to extreme values of the distribution are less connected than the other frequencies

Figure 3.11 shows the node neighborhood detuning $\omega_u - \langle\omega_v\rangle_u$ for each oscillator $u$ for the three combinations of parameters, with $\langle\omega_v\rangle_u$ the average frequency of oscillators $v \in C_u$ and $C_u$ the set of oscillators that are connected to oscillator $u$. For the fully synchronized network a linear relation is shown. Figure 3.10(a) showed that $k_u \approx 290 \approx N$ for all $\omega_u$. Therefore, $\langle\omega_v\rangle_u \approx 1$ for all $\omega_u$, resulting in the linear relation in the synchronized phase. A few deviations from this relation are shown for oscillators whose frequencies are close to the extreme values of the distribution, where the (absolute value of the) node neighborhood detuning is slightly smaller, pointing out that these oscillators are not able to link with oscillators whose frequencies are on the other side of the spectrum. For the asynchronous network, the node neighborhood detuning is contant, with $\omega_u - \langle\omega_v\rangle_u \approx 0$. In this phase, oscillators are only able to link with oscillators whose frequencies are very close to each other. Finally, just before the transition a mix of these two relations is found. It is noted that the (absolute value of the) node neighborhood detuning is smaller than in the completely synchronized phase (and larger than the asynchronous phase), pointing out that links linking oscillators whose frequencies are close are favored (and that a larger distance is allowed than in the asynchronous phase). This phenomenon is the opposite of frequency dissasortativity, which is acquired in networks with an anti-Hebbian adaptation rule.

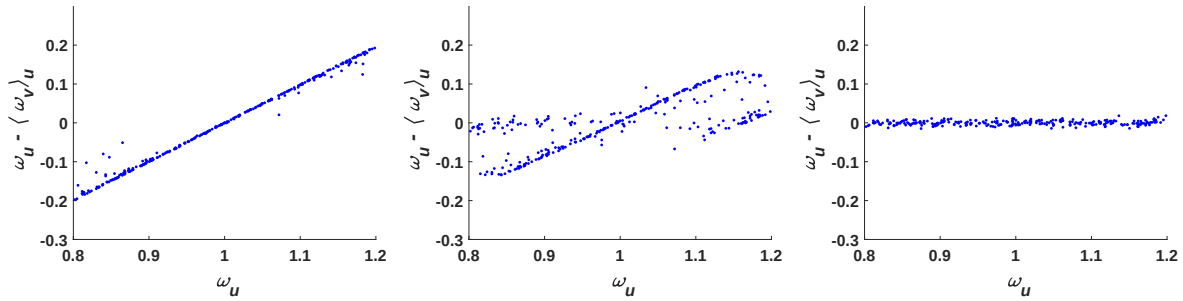


(a) (b) (c)

**Figure 3.11.** Scatter plot of the node neighborhood detuning $\omega_u - \langle\omega_v\rangle_u$, with oscillator $v \in C_u$

Figure 3.12 depicts the connectivity of the network as a function of $\omega_u$ and $\omega_v$, by ordering the adjacency matrix according to their natural frequencies. The green regions represent linked oscillators, and red regions represent disconnected oscillators. For the fully synchronized network only a few links between oscillators with frequencies that are as far away from each other as possible are pruned, all the other oscillators are connected. Just before the transition, this pruning region becomes much larger, and many links between oscillators whose frequencies are close to the extreme values of the distribution are pruned, especially those between oscillators with very distant frequencies with respect to each other. In the asynchronous network, all links are pruned, except for those linking two oscillators with almost similar frequencies. This results in the thin diagonal line.

The pruning of links only occurs if $p_c$ becomes too large, resulting in the transition in an asynchronous network. This is an essential difference with the anti-Hebbian network, where link pruning also occurs in the

synchronous network.

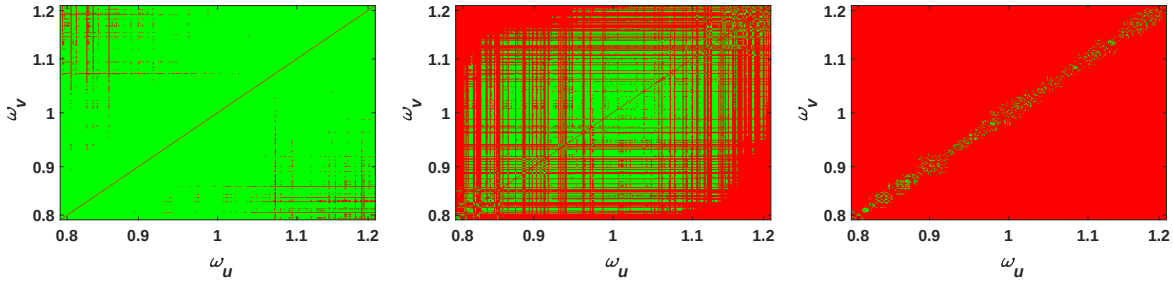


(a) (b) (c)

**Figure 3.12.** Scatter plot of the node neighborhood detuning $\omega_u - \langle \omega_v \rangle_u$, with oscillator $v \in C_u$

# 4

# Analysis of an adaptive network of 2 oscillators

## 4.1. Introduction

The dynamics of the two networks in the previous chapter may be better understood by analyzing a much more simplified system. Vanesa Avalos-Gaytan et al. [21] analytically derived the equilibrium points and their stability for a network of two oscillators with an anti-Hebbian adaptation rule. In this section the results of this study will be briefly presented and the analytical study will be extended to an analysis of a network of two oscillators with a Hebbian adaptation rule. In addition both analysis will be compared to a numerical simulation of the networks.

## 4.2. Anti-Hebbian adaptation rule

First a network with an anti-Hebbian adaptation rule is considered. The network consists of two oscillators $\theta_1$ and $\theta_2$ that are coupled by a single weighted link $\alpha$. The two oscillators have an instantaneous phase correlation $p$ given by equation (2.11). The dynamics of the network are described by the differential equations for $\dot{\theta}_u$ and $\dot{\alpha}$, given by (2.10) and (2.13) respectively.

### 4.2.1. Analytical study

The analytical study can also be found in [21], and therefore only the results will be presented in this subsection. If few more details are desired, it may be useful to first read the analytical study of the Hebbian network (section 4.3), which is a bit more extensive and has many similarities with the anti-Hebbian case.
In order to transform the of equations given by equations (2.10) and (2.13) into a two-dimensional system, the phase difference $\phi := \theta_2 - \theta_1$ and natural frequency difference $\Delta = \omega_2 - \omega_1$ is defined. Without loss of generality, it is supposed that $\Delta > 0$. The two-dimensional system is given by:

$$\begin{aligned} \dot{\phi} &= \Delta - \sigma_c \alpha \sin(\phi) \\ \dot{\alpha} &= \left( p_c - \sqrt{\frac{1+\cos(\phi)}{2}} \right) \alpha \, (1-\alpha) \end{aligned} \tag{4.1}$$

Where $p_c$ is the correlation threshold and $\sigma_c$ the coupling strength. It is not possible to integrate the set of equations (4.9) explicitly, therefore the stability of the system is analyzed to better understand its behavior. In order to do so, the equilibrium points (i.e. $\dot{\phi} = 0$ and $\dot{\alpha} = 0$) are determined, and $(\phi^*, \alpha^*)_1$ and $(\phi^*, \alpha^*)_2$ are found:

$$\phi^* = \arcsin\left(\frac{\Delta}{\sigma_c}\right), \qquad \alpha^* = 1 \tag{4.2}$$

$$\phi^* = \arccos\left(2p_c^2 - 1\right), \qquad \alpha^* = \frac{\Delta/\sigma_c}{2p_c\sqrt{1-p_c^2}} \tag{4.3}$$

Where the star stands for an equilibrium value of $\alpha$ and $\phi$. The stability conditions can be found by studying the sign of the eigenvalues of the Jacobian matrix of these two equilibrium points.
In this study two critical coupling strengths $\Upsilon_1, \Upsilon_2$ are found, given by

$$\Upsilon_1 := \frac{\Delta}{2p_c\sqrt{1-p_c^2}} \tag{4.4}$$

$$\Upsilon_2 := \left(\frac{1}{\Upsilon_1} - \frac{\left(1-2p_c^2\right)^2}{4p_c\left(1-p_c^2\right)}\right)^{-1} \tag{4.5}$$

Note that $\Delta < \Upsilon_1 < \Upsilon_2$ for all values of $p_c$ and $\Delta$. Furthermore, note that both equilibrium points are not defined for $\sigma_c < \Delta$.
Equilibrium point (4.2) is stable for $p_c > \frac{1}{\sqrt{2}}$ and $\Delta < \sigma_c < \Upsilon_1$.
Equilibrium point (4.3) is stable for $p_c > \frac{1}{\sqrt{2}}$ and $\Upsilon_1 < \sigma_c$. For $\Upsilon_1 < \Upsilon_2 < \sigma_c$ the point has a sink node, and for $\Upsilon_1 < \sigma_c < \Upsilon_2$ the point has a spiral sink. The latter case converges slower to the asymptotic state, as the rate of convergence $\min \|Re(\lambda_{1,2}(p_c, \sigma_c))\|$ drops.
It is interesting to note that for $N = 2$ the necessary condition for the existence of synchronized solutions (see equation (2.9)) simplifies to

$$\sigma_c > \frac{N(\omega_{max} - \omega_{min})}{2(N-1)} = \Delta \tag{4.6}$$

This condition for $\sigma_c$ is also found in the analysis. Thus, for $N = 2$, this lower boundary is in fact the exact value of $\sigma_{critical}$.

### 4.2.2. Numerical study

In this subsection a network of two oscillators will be simulated, and this network will be compared to the analytical derived asymptotic values of the network. At $t = 0$ the simulated network has the following properties:

$$\begin{aligned} \omega_1 &= 0.8, & \omega_2 &= 1.2, & \Delta &= 0.4 \\ \theta_1 &= 0, & \theta_2 &= \pi, & \phi &= \pi \\ \alpha &= 0.5 \end{aligned} \tag{4.7}$$

The value of $\phi$ is chosen such that at $t = 0$ a minimum value of $p$ ($p = 0$) is obtained, which is the most optimal situation for the anti-Hebbian network to evolve. This network is developed in time using modified Euler for the differential equations (2.10) and (2.13) for $\dot{\theta}$ and $\dot{\alpha}$, respectively.
First, the weighted link $\alpha$ is studied as function of $\sigma_c$ and $p_c$. Figure 4.1(a) shows the value of $\alpha$ in the simulated network, and Figure 4.1(b) shows the asymptotic value of $\alpha$, as derived in the analytical study. In region $A1$ the network is disconnected ($\alpha = 0$). In region $A2$ the network is connected ($\alpha = 1$), but since $\sigma_c < \Delta$, the network will not synchronize. Thus, in both regions $A1$ and $A2$ phase-locking is not possible. $A1$ is defined by $p_c < \frac{1}{\sqrt{2}}$, and $A2$ is defined by $p_c > \frac{1}{\sqrt{2}}$ and $\sigma_c < \Delta$. On the other hand, synchronization is possible in regions $B1$ and $B2$. In $B1$ equilibrium point (4.2) is stable, and thus in this region $\alpha = 1$. Region $B1$ is given by $\Delta < \sigma_c < \Upsilon_1$ (given by (4.4)) and $p_c > \frac{1}{\sqrt{2}}$. Finally, in region $B2$ equilibrium point (4.3) is stable, and thus the link converges to $\frac{\Upsilon_1}{\sigma_c}$. Region $B2$ is enclosed by $\Upsilon_1 < \sigma_c$ and $p_c > \frac{1}{\sqrt{2}}$.

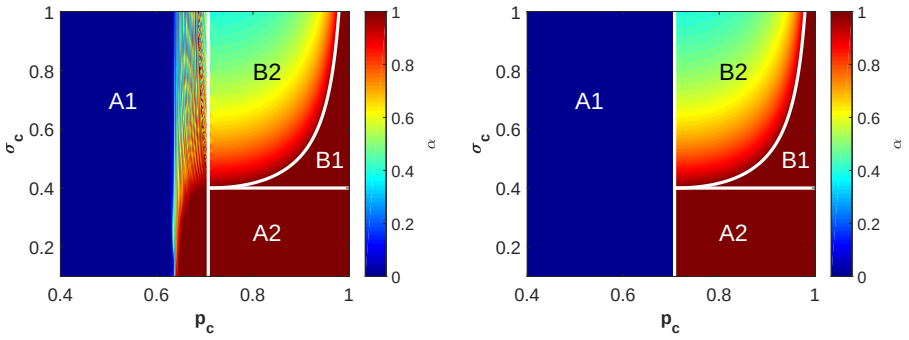


(a) Simulated network (b) Asymptotic value

**Figure 4.1.** The weight of the link as function of $\sigma_c$ and $p_c$ in a) a simulated network and b) the asymptotic value of an analytical study. The analytical study is verified by the simulation, however for $0.64 < p_c < \frac{1}{\sqrt{2}}$ the link does not converge.

The analytical study is verified by the numerical simulation, as Figures 4.1(a) and 4.1(b) are indeed very similar. However, around $p_c = \frac{1}{\sqrt{2}}$ the transition from the incoherent network to the synchronous one is less abrupt for the simulated network than the analytical study predicts. In this region, the link does not seem to converge. Figure 4.2 depicts the development of $\alpha$ in time for $\sigma_c = 0.6$ and $p_c = 0.5$ (4.2(a)), $p_c = 0.95$ (4.2(b)) and $p_c = 0.64$ (4.2(c), 4.2(d)) after $n$ time steps ($h = 0.01$). These values of $p_c$ correspond to the incoherent state, the synchronous state, and the region of transition, respectively. The figures reveal a fast convergence of $\alpha$ for $p_c = 0.5$ and $p_c = 0.95$, but that, as $t \to \infty$, $\alpha$ indeed does not converge to any value $0.64 < p_c < \frac{1}{\sqrt{2}}$. It may be assumed that this is causes by errors of the Modified Euler method, and not by errors of the analytical study. This results in the fluctuating pattern in this region in Figure 4.1(a).

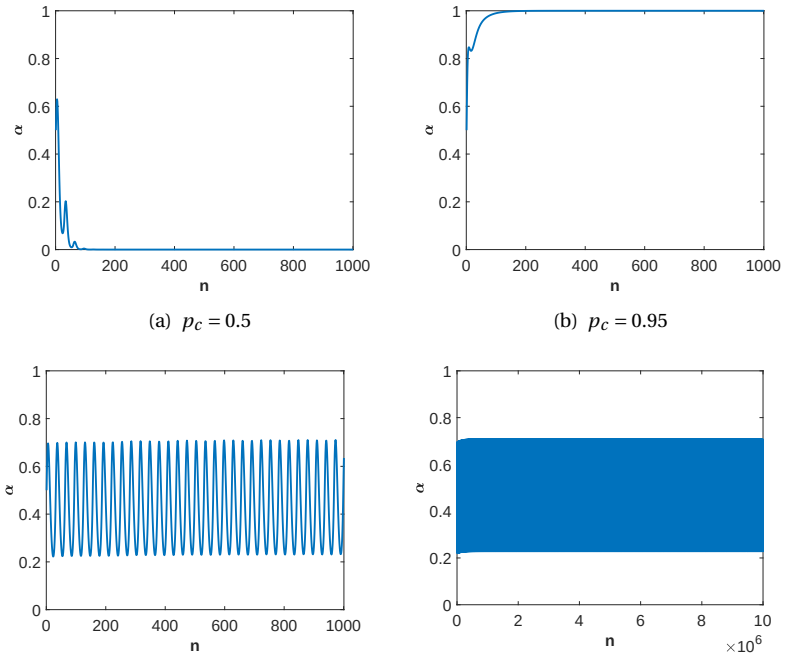


(a) $p_c = 0.5$ (b) $p_c = 0.95$

(c) $p_c = 0.64$ (d) $p_c = 0.64$

**Figure 4.2.** The value of $\alpha$ after $n$ time steps ($h = 0.01$) for $\sigma_c = 0.6$. In a) $p_c = 0.5$ corresponding to the incoherent state, in b) $p_c = 0.95$ corresponding to the synchronous state and in c), d) $p_c = 0.64$ corresponding to the region of transition. It is shown that for $p_c = 0.64$ $\alpha$ does not converge.

Moreover, in the analytical study it was found that for $\sigma_c > \Upsilon_2$ (given by (4.5)) the convergence of $\alpha$ is slower than for $\sigma_c < \Upsilon_2$. In Figure 4.3(a) $\alpha$ is shown in regions $B1$, $B2-I$ and $2B-II$ while the network is still evolving (after 1000 time steps, $h = 0.01$). In Figure 4.3(b) the asymptotic value in this region is depicted. Region $B2-I$ is enclosed by $\Upsilon_1 < \sigma_c < \Upsilon_2$ and $p_c > \frac{1}{\sqrt{2}}$, and region $B2-II$ by $\Upsilon_2 < \sigma_c$ and $p_c > \frac{1}{\sqrt{2}}$. Indeed, in region $B2-II$ the value of $\alpha$ deviates more from the asymptotic value. However, this claim is not correct for the whole

region. The rate of convergence does not drop significantly for every combination of $\sigma_c$ and $p_c$ in region $B2-II$.

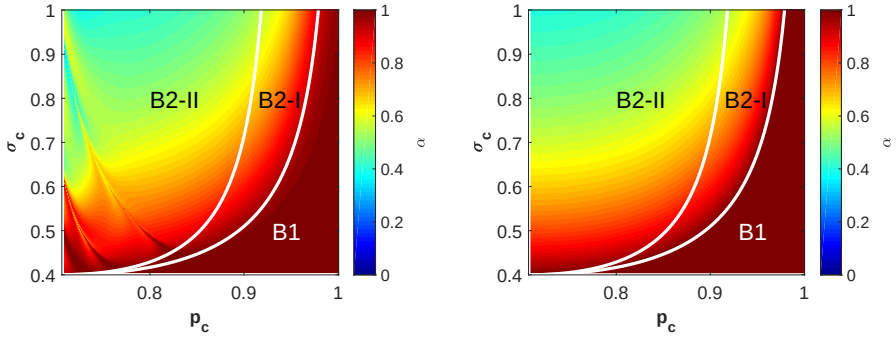


(a) Evolving network (b) Asymptotic value

**Figure 4.3.** The value of $\alpha$ in regions $B1, B2-I, B2-II$. In a) the network is shown after 1000 time steps ($h = 0.01$) and in b) the asymptotic values are shown. The convergence in some parts of region $B2-II$ is indeed slower, but not for all combinations of $\sigma_c$ and $p_c$ in the region.

Figure 4.4(a) shows the value of $\phi$ in the simulated network, and Figure 4.4(b) shows the asymptotic value of $\phi$, as derived in the analytical study. It was already found that in region $A1$ and $A2$ no phase-locking is possible. In region $A1$ this means that $\phi$ does not converge, as $\dot{\phi} = \Delta$, en thus $\phi$ changes at a constant rate. In region $A2$, $\dot{\phi} = \Delta - \sigma_c \sin(\phi)$, resulting in the fluctuating pattern. In region $B1$ and $B2$ $\phi$ is given by the corresponding equilibrium points (4.2) and (4.3). As in Figure 4.1 in the region $0.64 < p_c < \frac{1}{\sqrt{2}}$ the simulated network does not converge to the asymptotic value.

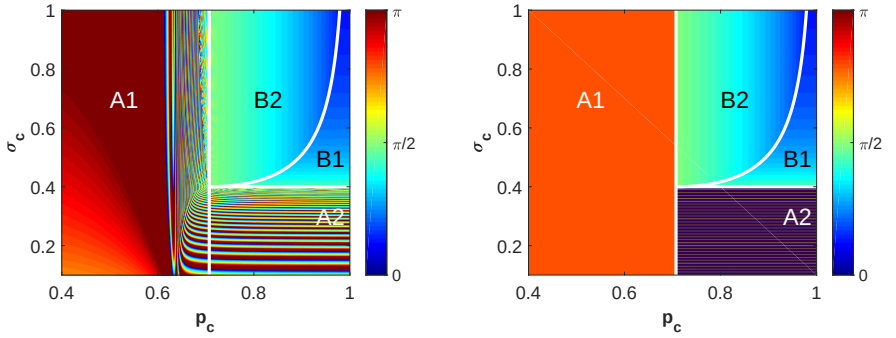


(a) Simulated network (b) Asymptotic value

**Figure 4.4.** The value of the $\phi$ as a function of $\sigma_c$ and $p_c$. In a) the simulated network and in b) the asymptotic value of $\phi$. For $0.64 < p_c < \frac{1}{\sqrt{2}}$ the simulated network does not converge to the asymptotic value.

Finally, in Figure 4.5(a) the global synchronization $R$ is shown as function of $\sigma_c$ and $p_c$ of the evolved network. In Figure 4.5(b) the asymptotic value is depicted. Indeed, the final degree of global synchronization can be described very precise.

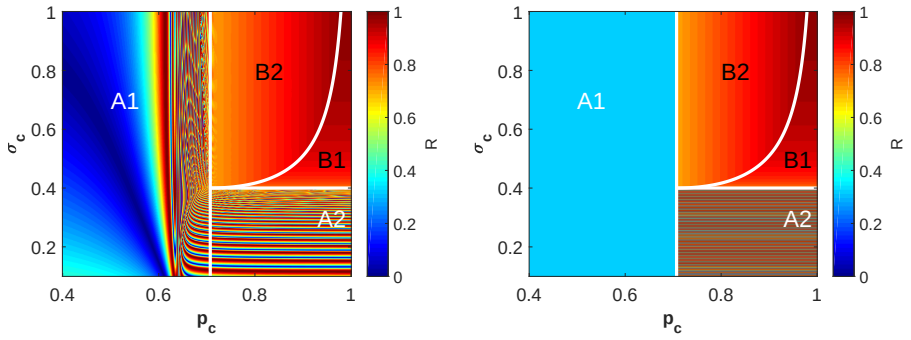


(a) (b)

**Figure 4.5.** The value of the $R$ as a function of $\sigma_c$ and $p_c$. The global synchronization can be described very precise. In the region $0.64 < p_c < \frac{1}{\sqrt{2}}$ the simulated network does not converge.

Note that the value of $R$ in regions $A1$ and $A2$ is based on non converging values of the phases of two oscillators. Therefore, in a small network the value of $R$ fluctuates rapidly in time between 0 and 1, as the phases are sometimes in phase and sometimes in anti-phase. If there are more oscillators, the rate of change of the phases will still differ per oscillator (as there are many different values of $\Delta$). As the phases are not related (and now $N = 300$), the phases will now cancel each other and $R$ will tend to 0. Including this result, the dynamics in Figure 4.5 are very similar to those obtained for a network of 300 oscillators with an anti-Hebbian adaptation rule (see Figure 3.1(d)).
Moreover, comparing $\alpha$ (see Figure 4.1) to the total strength $S$, which directly depends on the value of $\alpha$, once again reveals that the dynamics in parameter space of these networks are very similar.
These similarities suggest that the analysis of this elementary network actually captures the dynamics of large-scale adaptive networks, that are impossible to analyze analytically.

## 4.3. Hebbian adaptation rule

The same analytical and numerical study can be preformed for a network with a Hebbian adaptation rule. Again, this network consists of two oscillators $\theta_1$ and $\theta_2$ that are coupled by a single weighted link $\alpha$ and have an instantaneous phase correlation $p$ given by equation (2.11). The dynamics of the network are described by the differential equations for $\dot{\theta}_u$ and $\dot{\alpha}$, given by (2.10) and (2.12) respectively. The latter differential equation characterizes the Hebbian adaptation rule.

### 4.3.1. Analytical study

The analytical study of the Hebbian network has the same structure as the anti-Hebbian network. However, the study presented in this subsection will be more detailed, as this study is not preformed yet.
The dynamics of the network obey the differential equations for $\dot{\theta}_u$ and $\dot{\alpha}$ (equations (2.10) and (2.12)). This gives the following set of equations:

$$\begin{aligned} \dot{\theta}_1 &= \omega_1 + \frac{\sigma_c}{2}\alpha\sin(\theta_2-\theta_1) \\ \dot{\theta}_2 &= \omega_2 + \frac{\sigma_c}{2}\alpha\sin(\theta_1-\theta_2) \\ \dot{\alpha} &= \left(p-p_c\right)\alpha(1-\alpha) \end{aligned} \tag{4.8}$$

If the first two equations are added, it is found that $\dot{\theta}_1 + \dot{\theta}_2 = \omega_1 + \omega_2$. This reveals that the system can be reduced with one equation. To do so, the phase difference $\phi := \theta_2 - \theta_1$ and natural frequency difference $\Delta = \omega_2 - \omega_1$ are defined. The numbering of the oscillators may be arbitrary, so without loss of generality, it is assumed that $\Delta > 0$. The two-dimensional system is then given by:

$$\begin{aligned} \dot{\phi} &= \Delta - \sigma_c\alpha\sin(\phi) \\ \dot{\alpha} &= \left(\sqrt{\frac{1+\cos(\phi)}{2}} - p_c\right)\alpha\,(1-\alpha) \end{aligned} \tag{4.9}$$

This set of equations can not be integrated explicitly. Therefore, to grasp better insight in its behavior, the stability of the system is analyzed. To this end, the equilibrium points (i.e. $\dot{\phi} = 0$ and $\dot{\alpha} = 0$) are determined, and $(\phi^*, \alpha^*)_1$ and $(\phi^*, \alpha^*)_2$ are found:

$$\phi^* = \arcsin\left(\frac{\Delta}{\sigma_c}\right), \qquad \alpha^* = 1 \tag{4.10}$$

$$\phi^* = \arccos\left(2p_c^2 - 1\right), \qquad \alpha^* = \frac{\Delta/\sigma_c}{2p_c\sqrt{1-p_c^2}} \tag{4.11}$$

Note that this is the same set of equilibrium points as in the anti-Hebbian network. Again, $\phi^*$ in (4.2) is not defined if $\Delta > \sigma_c$. Moreover, note that for $p_c \in [0,1]$ it holds that $1/(2p_c\sqrt{1-p_c^2}) \geq 1$. This implies that for $\alpha$ in (4.3) it holds that $\alpha \geq \Delta/\sigma_c$, thus $\alpha > 1$ if $\Delta > \sigma_c$, which is not possible. From this, it is concluded that for both equilibrium points to be well defined it is required that $\Delta \leq \sigma_c$.
The stability of a certain equilibrium point can be determined by constructing the Jacobian matrix $J$ and evaluating its eigenvalues at that point. If all eigenvalues of $J$ have $\mathbb{R}\mathrm{e}\{\lambda_i\} < 0$, then the equilibrium point is asymptotically stable. If at least one eigenvalue has $\mathbb{R}\mathrm{e}\{\lambda_i\} > 0$, then the point is unstable. If $J$ has an eigenvalue $\lambda_i = 0$, that is not due to symmetry in the system, $J$ provides no conclusions about the stability of the equilibrium point. [36] The Jacobian of the system (4.9) has the form

$$J(\phi,\alpha) = \begin{bmatrix} \frac{\partial\dot{\phi}}{\partial\phi} & \frac{\partial\dot{\phi}}{\partial\alpha} \\ \frac{\partial\dot{\alpha}}{\partial\phi} & \frac{\partial\dot{\alpha}}{\partial\alpha} \end{bmatrix} = \begin{bmatrix} -\sigma_c\alpha\cos(\phi) & -\sigma_c\sin(\phi) \\ \frac{\alpha(\alpha-1)\sin(\phi)}{2\sqrt{2+2\cos(\phi)}} & \left(\sqrt{\frac{1+\cos(\phi)}{2}} - p_c\right)(1-2\alpha) \end{bmatrix} \tag{4.12}$$

Spectral analysis of the Jacobian evaluated at $(\phi^*, \alpha^*)_1$ reveals the spectrum $\lambda(J(\phi^*, \alpha^*)_1)$, that is

$$\lambda_1 = -\sigma_c\cos(\phi^*) \tag{4.13}$$

$$\lambda_2 = p_c - \sqrt{\frac{1+\cos(\phi^*)}{2}} \tag{4.14}$$

Note that $\lambda_1 < 0$, if $\cos(\phi^*) > 0$. Indeed, since $\cos(\phi*) = \cos\left(\arcsin\left(\frac{\Delta}{\sigma_c}\right)\right) = \sqrt{1-\left(\frac{\Delta}{\sigma_c}\right)^2}$ and the equilibrium point is only defined for $\sigma_c > \Delta$, it is found that $\lambda_1 < 0$.
Moreover, the result $\cos(\phi^*) > 0$ implies that, for $p_c < \frac{1}{\sqrt{2}}$, it always holds that $\lambda_2 < 0$. Thus, the equilibrium point is stable in this region.
For $p_c > \frac{1}{\sqrt{2}}$, the region of stability can be determined by solving $\lambda_2 < 0$ for $\sigma_c$. This yields the same critical coupling strength $\Upsilon_1$ as obtained in the anti-Hebbian network:

$$\Upsilon_1 := \frac{\Delta}{2p_c\sqrt{1-p_c^2}} \tag{4.15}$$

However, the relation of $\sigma_c$ and $\Upsilon_1$ is opposite: If $\sigma_c < \Upsilon_1$ the point is unstable, and for $\Upsilon_1 < \sigma_c$ the point is stable.
Next, the stability of the second equilibrium point, i.e. $(\phi^*, \alpha^*)_2$, is inspected. The spectrum of the Jacobian evaluated at this point contains the following eigenvalues:

$$\lambda_\pm = \frac{A \pm \sqrt{A^2 + B\left(\frac{1}{\Upsilon_1} - \frac{1}{\sigma_c}\right)}}{C} \tag{4.16}$$

where $A := 2(1-2p_c^2)\Delta$, $B := 16p_c(1-p_c^2)\Delta^2$ and $C := 8p_c\sqrt{1-p_c^2}$.
Note that $B$ and $C$ are always positive for $p_c \in [0,1]$. This implies that $\lambda_+ > 0$ for $\sigma_c > \Upsilon_1$.
Moreover, note that $\alpha^* = \frac{\Upsilon_1}{\sigma_c}$. As $\alpha$ is constrained to be in the unit interval, this equilibrium point is only well defined for $\sigma_c > \Upsilon_1$.

It is concluded that the second equilibrium point is not stable for any value of $\sigma_c$ and $p_c$. Thus, the Hebbian network has only one stable equilibrium point, whereas the anti-Hebbian network has two stable equilibrium points. In other words, in the Hebbian network the weight of the link will always evolve to one of the extreme values, i.e. $\alpha = 1$ or $\alpha = 0$, and there is no intermediate (stable) value like in the anti-Hebbian network.

### 4.3.2. Numerical study

In this subsection a network of two oscillators will be simulated at each $(p_c, \sigma_c)$. The resulting network will be compared to the analytical derived asymptotic values of the network. At $t = 0$ the simulated network has the following properties:

$$\begin{aligned} \omega_1 &= 0.8, & \omega_2 &= 1.2, & \Delta &= 0.4 \\ \theta_1 &= 0, & \theta_2 &= 2\pi, & \phi &= 2\pi \\ \alpha &= 0.5 \end{aligned} \tag{4.17}$$

The value of $\phi$ is chosen such that at $t = 0$ a maximum value of $p$ ($p = 1$) is obtained, which is the most optimal situation for the Hebbian network to evolve. This network is developed in time using modified Euler for the differential equations (2.10) and (2.12) for $\dot{\theta}$ and $\dot{\alpha}$, respectively.

First, the weighted link $\alpha$ is studied as function of $\sigma_c$ and $p_c$. Figure 4.6(a) shows the value of $\alpha$ in the simulated network, and Figure 4.6(b) shows the asymptotic value of $\alpha$ as derived in previous analytical study. In region $A1$ the network is connected ($\alpha = 1$), but since $\sigma_c < \Delta$, this is not strong enough to synchronize the network. In region $A2$ the network is disconnected ($\alpha = 0$). Thus, in both $A1$ and $A2$ phase-locking is not possible and the network will not synchronize. Region $A1$ is defined by $p_c < \frac{1}{\sqrt{2}}$, $\sigma_c < \Delta$, and region $A2$ by $p_c > \frac{1}{\sqrt{2}}$, $\sigma_c < \Upsilon_1$. In region $B$ synchronization is possible, and here $\alpha = 1$. This region is given by $p_c < \frac{1}{\sqrt{2}}$, $\sigma_c > \Delta$. Regions $A1, A2$ and $B$ are similar to regions $A2, A1$ and $B1$ of the anti-Hebbian network, respectively (see Figure 4.1).
The two figures correspond almost exactly, indicating that the analytical study is verified. Indeed, $\alpha = 0$ and $\alpha = 1$ are the only possible values in the evolved network, just like the analytical study predicted. However, the critical value of $p_c$ in the evolved network is shifted to the left relative to the analytical study. This is almost similar to the anti-Hebbian network, where the numerical and analytical study also differed at the transition from a synchronized towards an asynchronous network. Again, it may be assumed that this is due to errors of the modified Euler method. However, in this case $\alpha$ does converge, but not to the asymptotic value.

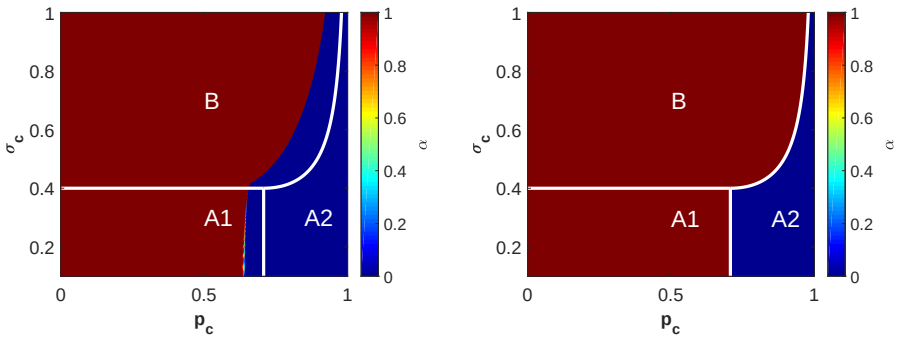


(a) Simulated network (b) Asymptotic value

**Figure 4.6.** The weight of the link $\alpha$ as function of $\sigma_c$ and $p_c$ in a) a simulated network and b) the asymptotic value obtained in the analytical study. The numerical study verifies that $\alpha$ only takes the values 0 and 1. The critical value of $p_c$ in the evolved network is shifted to the left relative to its asymptotic prediction

Figure 4.7(a) shows the value of $\phi$ of the simulated network, and Figure 4.7(b) shows its asymptotic value, both as function of $\sigma_c$ and $p_c$. In regions $A1$ and $A2$ it was found that no phase-locking is possible, as $\dot{\phi} \neq 0$. Similar to corresponding regions of the anti-Hebbian network (see Figure 4.4), in region $A1$ $\dot{\phi} = \Delta - \sigma_c \sin(\phi)$, in region $A2$ $\dot{\phi} = \Delta$. Finally, in region $B$ $\dot{\phi} = 0$ and $\phi$ is given by 4.10.

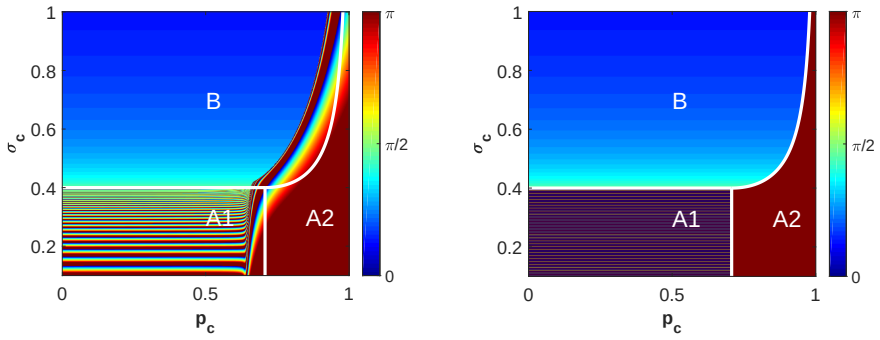


(a) Simulated network (b) Asymptotic value

**Figure 4.7.** The value of $\phi$ as function of $\sigma_c$ and $p_c$. In a) the simulated network and in b) the asymptotic value of $\phi$.

Finally, Figure 4.8(a) shows the final degree of synchronization $R$ of the evolved network, and Figure 4.8(b) depicts its asymptotic value, both as a function of $\sigma_c$ and $p_c$. Indeed, using the analytical analysis a very precise description of $R$ can be obtained. However, as with 4.6, the critical values of $p_c$ are sligthly shifted to the left for the simulated network.

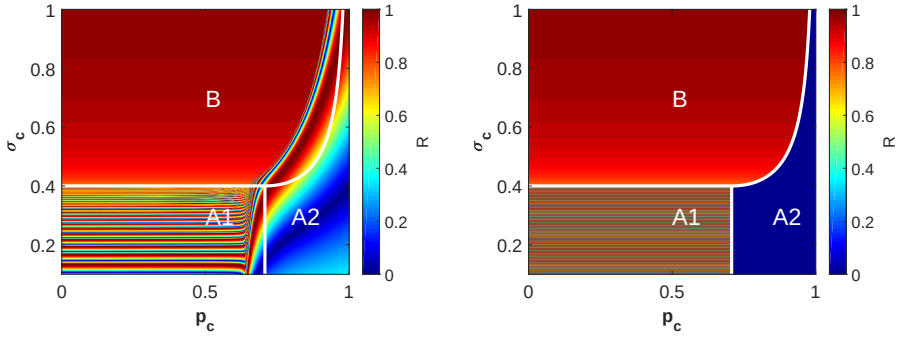


(a) (b)

**Figure 4.8.** The value of $R$ as function of $\sigma_c$ and $p_c$. In a) the simulated network and in b) the asymptotic value of $R$. The global synchronization can be described very precise, although the critical values of $p_c$ are slightly shifted to the left

As with the anti-Hebbian network, it must be noted that the value of $R$ in regions $A1$ and $A2$ would tend to 0 as $N$ grows (see subsection 4.2.2). Including this result, it is again found that the dynamics of Figure 4.8 fits closely to the final degree of synchronization of a network of 300 oscillators, as is shown in Figure 3.7. Moreover, the diagram of $\alpha$ (see Figure 4.1) is very similar to the total strength $S$ of the large network, which directly depends on $\alpha$.

These similarities suggest that the analysis of this elementary network actually captures the dynamics of large-scale adaptive networks, that are impossible to analyze analytically.

# 5

# Analysis of an adaptive network of 3 oscillators

## 5.1. Introduction

In the previous chapter it was shown that the dynamics of a network of two oscillators can be analyzed analytically and that it may be suggested that this analysis captures the relevant dynamics of the large-scale networks. The Hebbian network is only stable for $\alpha = 1$ or $\alpha = 0$, and has no intermediate stable value. It may be expected that this is also the case for larger networks (of $N$ oscillators). Therefore, the dynamics of this network are less interesting to study. For this reason, the analysis will be extended to a network of three oscillators with an anti-Hebbian network only. The network consists of the oscillators with phases $\theta_1$, $\theta_2$ and $\theta_3$. Note that the number of possible links increases from 1 to 3, immediately raising the complexity of the problem.

First the results of the stability analysis will be presented and compared to a numerical simulation of the network. Thereafter, all details of the stability analysis will be presented in 5.4-5.7. Finally some basic 'linking' rules will be given, that are obtained in the stability analysis.

## 5.2. Numerical study

In the stability analysis there were found 26 equilibrium points. These points and their derivation can be found in 5.4-5.6. The stability of the points are summarized in Figure 5.1. The different colors depict different (stable) equilibrium points. The boundary of each region is analytically derived of estimated in the stability analysis.
In region $A$, it is found that $\alpha_{12} = 0$ and $0 < \alpha_{23,13} < 1$. Region $B$, corresponds to $\alpha_{12} = 0, 0 < \alpha_{23} < 1, \alpha_{13} = 1$. In region $C$, it holds that $0 < \alpha_{12,23}$, and $\alpha_{13} = 1$. In region $D$, the weight of the links are given by $0 < \alpha_{12} < 1, \alpha_{23} = \alpha_{13} = 1$. In region $E$ all links are equal to 1. Finally, in the regions $F1, F2$ no equilibrium point is stable. In the region $F2$ (where $p_c > \frac{1}{\sqrt{2}}$), it is expected that the weight of the links will tend the maximum value 1, which is not enough for synchronizing the oscillators (just as with 2 oscillators). In region $F1$, the weight of the links will tend to 0, resulting in 3 disconnected oscillators.

The exact value of the equilibrium points and the stability conditions can be found in 5.6. After studying all the equilibrium points, this bifurcation diagram will be discussed more extensively in section 5.7.

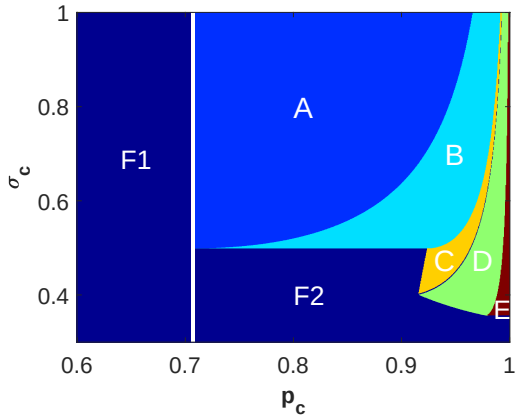


**Figure 5.1.** Stability diagram of all the equilibrium points of the network (with $\Delta_1 = 0.1, \Delta_2 = 0.3$, by using the (estimated) conditions for stability.

Now, a network of three oscillators will be simulated at each $(p_c, \sigma_c)$ using the modified Euler method. The characteristics of the resulting network will be compared with the predicted characteristics based on the bifurcation diagram above. At $t = 0$ the simulated network has the following properties:

$$\begin{aligned} \omega_1 &= 0.8, & \omega_2 &= 0.9, & \omega_3 &= 1.2 \\ \theta_1 &= 0, & \theta_2 &= \frac{2}{3}\pi, & \theta_3 &= \frac{4}{3}\pi \\ \alpha_{12} &= 0.5, & \alpha_{23} &= 0.5, & \alpha_{13} &= 0.5 \end{aligned} \tag{5.1}$$

And thus $\Delta_1 = 0.1, \Delta_2 = 0.3$, and $\phi_1 = \phi_2 = \frac{2}{3}\pi$. Here, $\phi_1, \phi_2$ are chosen such that the instantaneous phase correlations $p_{ij}$ are as low as possible.

Figure 5.2 shows the total strength $S$ as a function of $p_c$ and $\sigma_c$. Figure 5.2(a) shows the value of $S$ of the simulated network, and Figure 5.2(b) shows the asymptotic values of $S$. The regions $A, B, C, D, E$ are not labeled in this figure (as this would be a bit chaotic), but of course the asymptotic value of $S$ is determined by using the values of $\alpha^*_{ij}, \alpha^*_{jk}, \alpha^*_{ki}$ of the equilibrium point that is stable in these regions. Comparing the left and right panel shows that the asymptotic values indeed correspond almost exactly to the simulated values of $S$ in these regions.
Region $F1$ and $F2$ correspond to those of Figure 5.1, but they are expanded as a larger interval is considered. Indeed, in region $F1$, it is shown that $S = 0$ in both the right and left panel. However, around $p_c = \frac{1}{\sqrt{2}}$ the transition towards the (a)synchronous network is less abrupt for the simulated network than the analytical study predicts. This is very similar to the case of 2 oscillators, see Figure 4.1. In this region, the link does not seem to converge at all. Moreover, the boundaries of region $F2$ seem to correspond to those of the simulated network, as the value of $S$ becomes irregular in this region. However, it is seen that is not true that all links tend to the maximum value in this region. However, as it is expected that this region is still asynchronous, the exact dynamics in $F2$ are beyond the scope of this study and will therefore not be divided further in separate regions (of different values of $S$).
Finally, the lines $\sigma_c = \frac{\max\{\Delta_1+2\Delta_2\ ;\ 2\Delta_1+\Delta_2\}}{2} = 0.35$ and $\sigma_c = \min\{\Delta_1+2\Delta_2\ ;\ 2\Delta_1+\Delta_2\} = 0.5$ are shown. The first corresponds to a lower bound on $\sigma_c$ for the existence of possible synchronized solutions that is found in the analysis (see equation (5.67)). The latter depicts the lower bound for which the network is stable for all $p_c > \frac{1}{\sqrt{2}}$.

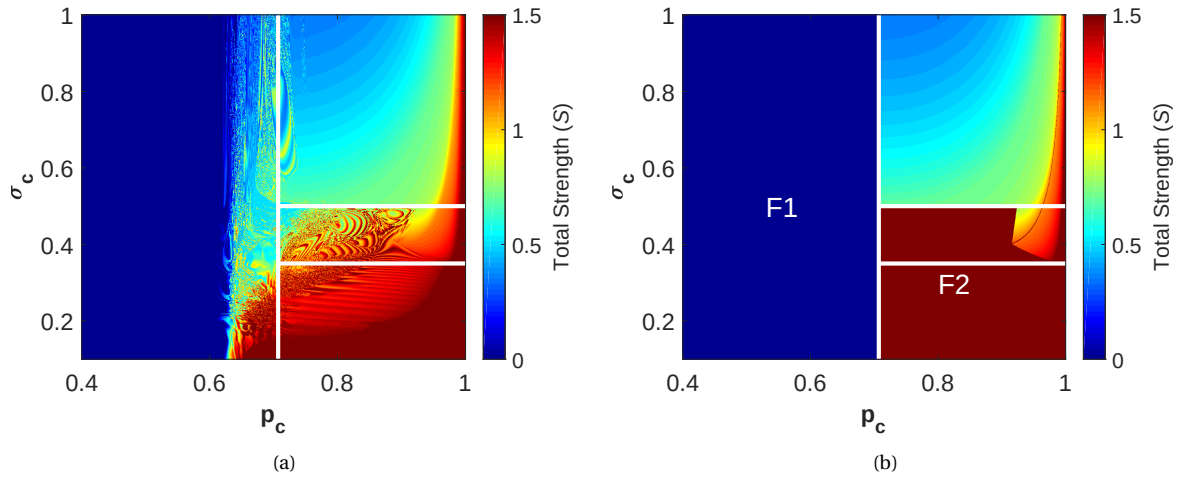


(a) (b)

**Figure 5.2.** Total strength $S$ of the network as a function of $\sigma_c$ and $_c$. In a) the network is simulated, in b) the asymptotic value of $S$ is shown.

In order to find the global synchronization $R$, so that it can be verified that the regions $A, B, C, D, E$ correspond to synchronous states (and $F1, F2$ to asynchronous ones), the phase differences $\phi_{1,2}$ must be known. Figure 5.3(a) shows the value of $\phi_1$ in the simulated network, and Figure 5.3(b) shows its asymptotic value, both as a function of $\sigma_c$ and $p_c$. In regions $A, B, C, D, E$ phase-locking is possible ($\dot{\phi} = 0$), so it is expected that in these regions the $\phi_1$ converges to the asymptotic value. Indeed, the left and right panel correspond almost exactly in these regions.
In region $F1, F2$ here is no phase-locking, and thus no convergence of $\phi_1$. In region $F1$ $\dot{\phi}_1 = \Delta_1$, en thus $\phi_1$ changes at a constant rate. However, note that due to different convergence times (to $\alpha_{ij,jk,ki} = 0$), $\phi_1$ does not have to be constant in this region. In the right panel this is only done for simplicity.
In region $F2$, $\dot{\phi}_1 = \Delta_1 + \frac{\sigma_c}{3}[-2\sin(\phi_1) + \sin(\phi_2) - \sin(\phi_1 + \phi_2)$, resulting in a more rapidly fluctuating pattern. Obviously, a figure with similar dynamics can be constructed for $\phi_2$.

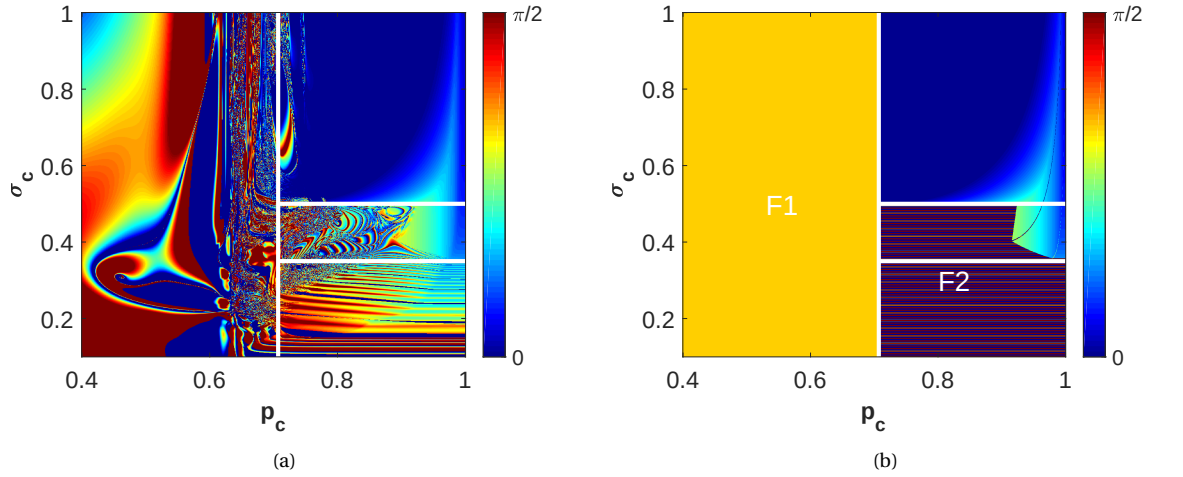


(a) (b)

**Figure 5.3.** The phase difference $\phi_1$ of the network as a function of $\sigma_c$ and $p_c$. In a) the network is simulated, in b) the asymptotic value of $\phi_1$ is shown.

Finally, Figures 5.4(a) and 5.4(b) shows the global degree of synchronization $R$ of the simulated network for different evolving times, and 5.4(c) shows the asymptotic value of $R$.
Indeed, the states in $F1, F2$ are asynchronous and the value of $R$ changes with time. This is confirmed by comparing figures 5.4(a) and 5.4(b). It is clear that for different times, $R$ has different values in these regions. Moreover, synchronized states only occur in regions $A, B, C, D, E$. Here the value of $R$ is stationary, and thus remains the same for different evolving times. It is noted in these regions a very precise description of $R$ can be obtained.

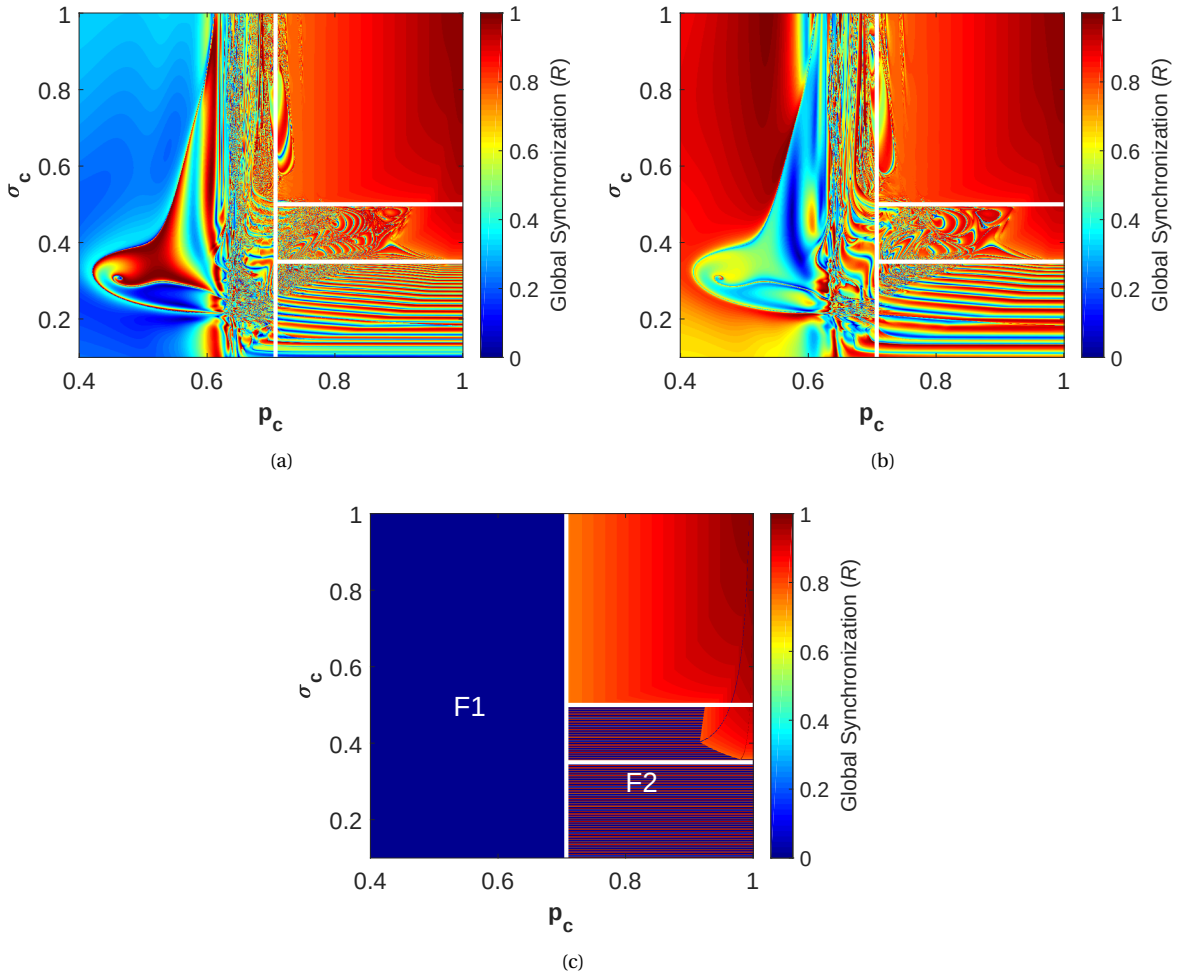


(a) (b)

(c)

**Figure 5.4.** The global synchronization $R$ of the network as a function of $\sigma_c$ and $_c$. In a) and b) the network is simulated, but for different evolving times, and in c) the asymptotic value of $\phi_1$ is shown. In regions $F1, F2$ the network is asynchronous and non-stationary.

To emphasize the similarity between the simulated and asymptotic values of $R$ in the regions $A, B, C, D, E$ the color scale is adjusted. This is shown in Figure 5.5. Indeed, the value of $R$ correspond almost exactly. Therefore, it may be suggested that the stability analysis is performed correctly.

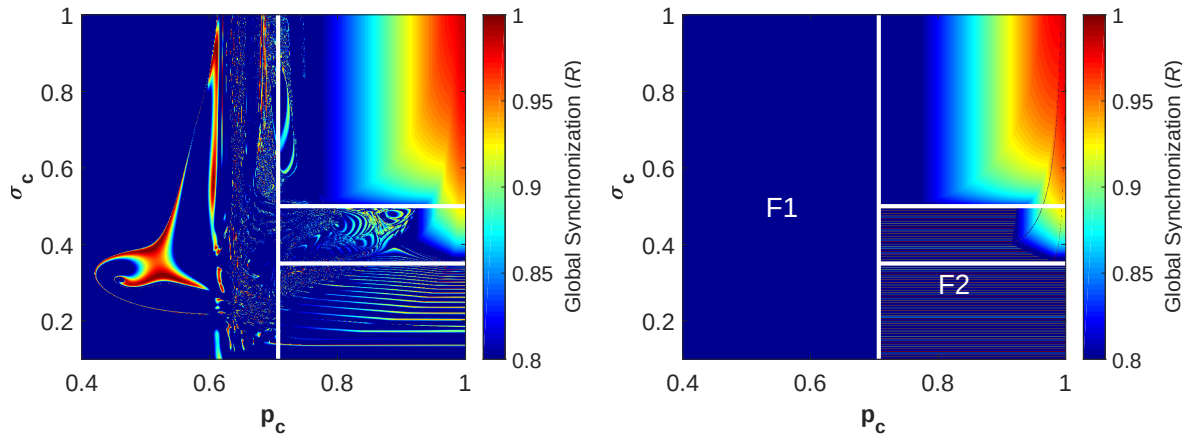


(a) (b)

**Figure 5.5.** The phase difference $\phi_1$ of the network as a function of $\sigma_c$ and $_c$. In a) the network is simulated, in b) the asymptotic value of $\phi_1$ is shown.

Finally, it must be noted that the value of $R$ in regions $F1$ and $F2$ depends on the non-stationary values of the phases of two oscillators. Therefore, in a small network the value of $R$ fluctuates strongly in time between 0 and 1. If there are more oscillators, the rate of change of the phases will differ per oscillator (as there are many different values of $\Delta$). Therefore, the value of the phase differences will be random and $R$ will tend to 0. This was already found in the network of 2 oscillators, see section 4.2.2.
Including this result, the dynamics in Figure 5.4 are again quite similar to those obtained for a network of two oscillators (Figure 4.5) and for a network of 300 oscillators (see Figure 3.1(d)) with an anti-Hebbian adaptation rule. In comparison with the the network of 2 oscillators, the critical value of $\sigma_c$ of a network of 3 oscillators became smaller, and thus closer to the critical value of the network of 300 oscillators.
Moreover, the dependence of total strength $S$ on $\sigma_c, p_c$ (see Figure 5.2) are very similar to those of the network of 2 and 300 oscillators (Figures 4.1 and 3.2, resp.). In a network of three oscillators, $S$ becomes relatively smaller for increasing $\sigma_c$, then it does in a network of two oscillators. This again is a better representation of the dynamics of $S$ of the large network.
However, it must be noted that the region where synchronized states occur for $0.35 < \sigma_c < 0.5$, has a remarkable shape, that is not observed in the large network. Therefore, the dynamics of both $S$ and $R$ differ here from those of the large-scale network. However, in general it may be suggested that the dynamics of the 3-network capture the dynamics of the large-scale networks.

## 5.3. Introduction analytical study

In the following sections the set of equations will be simplified, the equilibrium points will be presented, and the stability conditions will be derived for a network of three oscillators. The procedure is similar to the one followed for the network of 2 oscillators, although the analysis is (much) more complex for the network of three oscillators.

## 5.4. Transformation of the set of equations

The three oscillators $\theta_1$, $\theta_2$ and $\theta_3$ are coupled by three weighted links $\alpha_{12}$, $\alpha_{23}$ and $\alpha_{13}$ through an anti-Hebbian adaptation rule. The evolution of the phases and the weight of the links are given by equations (2.10) and (2.13), respectively and result in a six-dimensional system of equations. In the following, this set of equations will be transformed into a set of five equations.

The differential equations $\dot{\theta}_1$, $\dot{\theta}_2$ and $\dot{\theta}_3$ are given by

$$\dot{\theta}_1 = \omega_1 + \frac{\sigma_c}{3}\left[\alpha_{12}\sin(\theta_2-\theta_1) + \alpha_{13}\sin(\theta_3-\theta_1)\right] \tag{5.2}$$

$$\dot{\theta}_2 = \omega_2 + \frac{\sigma_c}{3}\left[\alpha_{12}\sin(\theta_1-\theta_2) + \alpha_{23}\sin(\theta_3-\theta_2)\right] \tag{5.3}$$

$$\dot{\theta}_3 = \omega_3 + \frac{\sigma_c}{3}\left[\alpha_{23}\sin(\theta_2-\theta_3) + \alpha_{13}\sin(\theta_1-\theta_3)\right] \tag{5.4}$$

Adding these equation gives $\dot{\theta}_1+\dot{\theta}_2+\dot{\theta}_3 = \omega_1+\omega_2+\omega_3$, which is a constant factor. This reveals that the system can be reduced by one equation. To that extend, the phase difference $\phi_i$ and natural frequency difference $\Delta_i$ is defined:

$$\phi_i := \theta_{i+1} - \theta_i \tag{5.5}$$

$$\Delta_i := \omega_{i+1} - \omega_i \tag{5.6}$$

for $i = 1,2,3$ and with the cyclic boundary condition that $\theta_{i+3} = \theta_i$. Note that: $\Delta_i = -\Delta_j - \Delta_k$ and $\phi_i = -\phi_j - \phi_k + n\cdot 2\pi$, $\forall i,j,k = 1,2,3$, $i \neq j \neq k$ and $n \in \mathbb{Z}$.
Subtracting equations (5.3) - (5.2) and (5.4) - (5.3), the differential equations for $\phi_1$ and $\phi_2$ are obtained. Finally, by substituting $\phi_3 = -\phi_1 - \phi_2$, the system is reduced to two differential equations.
Next, the differential equations for $\dot{\alpha}_{12}$, $\dot{\alpha}_{23}$ and $\dot{\alpha}_{13}$ are included to find the set of equations that describes the dynamics of a network of 3 oscillators. These are in the form of $\dot{\alpha}_{ij} = \left(p_c - p_{ij}\right)\ \alpha_{ij}\ (1-\alpha_{ij})$. The instantaneous phase correlation $p_{ij}$ between oscillators $i$ and $j$ is given by (2.11) and can be rewritten as

$$\begin{aligned} p_{12} &= \sqrt{\frac{1+\cos(\phi_1)}{2}} \\ p_{23} &= \sqrt{\frac{1+\cos(\phi_2)}{2}} \\ p_{13} &= \sqrt{\frac{1+\cos(\phi_3)}{2}} \end{aligned} \tag{5.7}$$

Finally, the five-dimensional set of equations is given by

$$\dot{\phi}_1 = \Delta_1 + \frac{\sigma_c}{3}\left[-2\alpha_{12}\sin(\phi_1) + \alpha_{23}\sin(\phi_2) - \alpha_{13}\sin(\phi_1+\phi_2)\right] \tag{5.8}$$

$$\dot{\phi}_2 = \Delta_2 + \frac{\sigma_c}{3}\left[-2\alpha_{23}\sin(\phi_2) + \alpha_{12}\sin(\phi_1) - \alpha_{13}\sin(\phi_1+\phi_2)\right] \tag{5.9}$$

$$\dot{\alpha}_{12} = \left(p_c - \sqrt{\frac{1+\cos(\phi_1)}{2}}\right)\ \alpha_{12}\ (1-\alpha_{12}) \tag{5.10}$$

$$\dot{\alpha}_{23} = \left(p_c - \sqrt{\frac{1+\cos(\phi_2)}{2}}\right)\ \alpha_{23}\ (1-\alpha_{23}) \tag{5.11}$$

$$\dot{\alpha}_{13} = \left(p_c - \sqrt{\frac{1+\cos(\phi_1+\phi_2)}{2}}\right)\ \alpha_{13}\ (1-\alpha_{13}) \tag{5.12}$$

As it is not possible to integrate equations (5.8) - (5.12) explicitly, the stability of the system is analyzed to better understand its behavior.

## 5.5. Equilibrium Points

Just as in the previous chapter, the stability of the system can be analyzed by computing the equilibrium points of the system and checking the stability of these points. The equilibrium points of this system are the values of $\alpha_{ij}$ and $\phi_i$ for which all differential equations (5.8) - (5.12) are all equal to zero.
Observing that equations (5.10)-(5.12) are equal to 0 if and only if $\alpha^*_{ij} = 0 \vee \alpha^*_{ij} = 1 \vee \phi^*_i = \arccos(2p_c^2 - 1)$, where $\phi^*_i$ is the corresponding phase difference in the equation for $\dot{\alpha}_{ij}$. For each combination of these values (such that all three equations are equal to 0) an equilibrium point can be found by substituting them in

equations (5.8)-(5.9), resulting in a system of 2 equations with 2 unknown variables, except in the case that $\phi_1^* = \phi_2^* = \arccos(2p_c^2 - 1) \mod (2\pi)$. The latter results in a system of 2 equations with 3 unknown variables, but then an implicit expression for the equilibrium point can be found. The same holds for larger networks, i.e. each combination of $\alpha_{ij}^* = 0 \vee \alpha_{ij}^* = 1 \vee \phi_i^* = \arccos(2p_c^2 - 1)$ will give an equilibrium point. Moreover, note that the case $\alpha_{12}^* = \alpha_{23}^* = \alpha_{13}^* = 0$ is not considered, as this yields $\Delta_i = 0$ for all $\omega_i$, while it is assumed that $\omega_i$ is distributed in an interval (that contains more than one point). Thus, it can be concluded that the total number of possible equilibrium points of the network is given by $3^{N_\alpha} - 1$, where $N_\alpha = \frac{N(N-1)}{2}$ is the total number of links connecting $N$ oscillators. Thus, there are 26 equilibrium points for a network of 3 oscillators.

In this section the 26 equilibrium points will be found by considering the three possible situations: the network has 1, 2 or 3 links in total, or equivalently: 2 links are equal to 0, 1 link is equal to 0 and all links are nonzero. These equilibrium points will be arranged in 9 different sets of alike equilibrium points.

### 5.5.1. One link

#### Set 1

In this case, the weight of two links is equal to 0. If the weight of the third link is chosen to be equal to 1, the equations for $\dot{\alpha}_{ij}$ ((5.10) - (5.12)) are all equal to 0. By filling in the values of the weight of the links in equations for $\dot{\phi}_1$ ((5.8)-(5.9)) and equating them to 0, the equilibrium points can be found. For example, using $\alpha_{12}^* = 1$, and $\alpha_{23}^* = \alpha_{13}^* = 0$, equations (5.8)-(5.9) will take the form of two constraints on $\phi_1$. This results in the asymptotic value $\phi_1^* = \arcsin\left(\frac{3\Delta_1}{2\sigma_c}\right)$ for $\phi_1$. The other phase difference $\phi_2$ can have any value. However, later it will be shown that the value of $\phi_2$ is restricted to be 'large enough', otherwise an extra link will appear.
The same procedure can be followed for $\alpha_{23} = 1$ or $\alpha_{13} = 1$ to obtain constraints for $\phi_2$ and $\phi_1 + \phi_2$, respectively. The following three equilibrium points are found, where for each point only the condition for the constrained phase difference is given:

$$\phi_1^* = \arcsin\left(\frac{3\Delta_1}{2\sigma_c}\right), \qquad \alpha_{12}^* = 1, \alpha_{23}^* = \alpha_{13}^* = 0, \qquad \Delta_2 = \Delta_3 = -\tfrac{\Delta_1}{2} \tag{5.13}$$

$$\phi_2^* = \arcsin\left(\frac{3\Delta_2}{2\sigma_c}\right), \qquad \alpha_{23}^* = 1, \alpha_{12}^* = \alpha_{13}^* = 0, \qquad \Delta_1 = \Delta_3 = -\tfrac{\Delta_2}{2} \tag{5.14}$$

$$\phi_1^* + \phi_2^* = \arcsin\left(\frac{3(\Delta_1 + \Delta_2)}{2\sigma_c}\right), \qquad \alpha_{13}^* = 1, \alpha_{12}^* = \alpha_{23}^* = 0, \qquad \Delta_1 = \Delta_2 \tag{5.15}$$

#### Set 2

Now consider the situation where two links have a weight of 0, and the weight of the third link is $0 < \alpha_{ij} < 1$. In that case, the corresponding equation for $\dot{\alpha}_{ij}$ is only equal to zero, if for the $\phi_i$ appearing in this equation it holds that $\phi_i = \arccos\left(2p_c^2 - 1\right)$. Filling in the two links with weight 0 and the $\phi_i = \arccos\left(2p_c^2 - 1\right)$ in the equations for $\dot{\phi}_1$, $\dot{\phi}_2$ ((5.8)-(5.9)), and equating them to 0, an explicit expression can be found for the weight of the nonzero link. Again, the value of the other phase is not prescribed (yet). The following three equilibrium points are obtained:

$$\phi_1^* = \arccos\left(2p_c^2 - 1\right), \qquad \alpha_{12}^* = \frac{3\Delta_1}{4\sigma_c p_c \sqrt{1 - p_c^2}} \qquad \alpha_{23}^* = \alpha_{13}^* = 0, \qquad \Delta_2 = \Delta_3 = -\tfrac{\Delta_1}{2} \tag{5.16}$$

$$\phi_2^* = \arccos\left(2p_c^2 - 1\right), \qquad \alpha_{23}^* = \frac{3\Delta_2}{4\sigma_c p_c \sqrt{1 - p_c^2}} \qquad \alpha_{12}^* = \alpha_{13}^* = 0, \qquad \Delta_1 = \Delta_3 = -\tfrac{\Delta_2}{2} \tag{5.17}$$

$$\phi_1^* + \phi_2^* = \arccos\left(2p_c^2 - 1\right), \qquad \alpha_{13}^* = \frac{3(\Delta_1 + \Delta_2)}{4\sigma_c p_c \sqrt{1 - p_c^2}} \qquad \alpha_{12}^* = \alpha_{23}^* = 0, \qquad \Delta_1 = \Delta_2 \tag{5.18}$$

There are 6 equilibrium points found in total with one link.

### 5.5.2. Two links

#### Set 3

Now the case is considered, where one link is equal to 0, and the other two links are nonzero.
First, the weight of the two nonzero links is chosen to be one. Again $\dot{\alpha}_{12} = \dot{\alpha}_{23} = \dot{\alpha}_{13} = 0$ is satisfied. To find

the equilibrium points, the equations for $\dot{\phi_1}$, $\dot{\phi_2}$ ((5.8)-(5.9)) are equated to 0, and the method of substitution is used to solve for $\phi_1^*, \phi_2^*$. The following three points are found:

$$\phi_1^* = \arcsin\left(\frac{\Delta_2 + 2\Delta_1}{\sigma_c}\right) \qquad \phi_2^* = \arcsin\left(\frac{\Delta_1 + 2\Delta_2}{\sigma_c}\right), \qquad \alpha_{12}^* = \alpha_{23}^* = 1 \qquad \alpha_{13}^* = 0 \tag{5.19}$$

$$\phi_1^* = \arcsin\left(\frac{\Delta_1 - \Delta_2}{\sigma_c}\right) \qquad \phi_1^* + \phi_2^* = \arcsin\left(\frac{\Delta_1 + 2\Delta_2}{\sigma_c}\right), \qquad \alpha_{12}^* = \alpha_{13}^* = 1 \qquad \alpha_{23}^* = 0 \tag{5.20}$$

$$\phi_2^* = \arcsin\left(\frac{\Delta_2 - \Delta_1}{\sigma_c}\right) \qquad \phi_1^* + \phi_2^* = \arcsin\left(\frac{\Delta_2 + 2\Delta_1}{\sigma_c}\right), \qquad \alpha_{23}^* = \alpha_{13}^* = 1 \qquad \alpha_{12}^* = 0 \tag{5.21}$$

### Set 4

Just like shown before, the two links can also be chosen to be $0 < \alpha_{ij} < 1$. Then again, the corresponding $\phi_i$ of the equation of $\dot{\alpha}_{ij}$ has to be $\phi_i = \arccos\left(2p_c^2 - 1\right)$. By equating equations (5.8)-(5.9) ($\dot{\phi_1}$, $\dot{\phi_2}$) to 0 and using substitution the following three equilibrium points are found:

$$\phi_1^* = \phi_2^* = \arccos\left(2p_c^2 - 1\right), \qquad \alpha_{12}^* = \frac{\Delta_2 + 2\Delta_1}{2\sigma_c p_c\sqrt{1-p_c^2}} \qquad \alpha_{23}^* = \frac{\Delta_1 + 2\Delta_2}{2\sigma_c p_c\sqrt{1-p_c^2}} \qquad \alpha_{13}^* = 0 \tag{5.22}$$

$$\phi_1^* = \phi_1^* + \phi_2^* = \arccos\left(2p_c^2 - 1\right), \qquad \alpha_{12}^* = \frac{\Delta_1 - \Delta_2}{2\sigma_c p_c\sqrt{1-p_c^2}} \qquad \alpha_{13}^* = \frac{\Delta_1 + 2\Delta_2}{2\sigma_c p_c\sqrt{1-p_c^2}} \qquad \alpha_{23}^* = 0 \tag{5.23}$$

$$\phi_2^* = \phi_1^* + \phi_2^* = \arccos\left(2p_c^2 - 1\right), \qquad \alpha_{23}^* = \frac{\Delta_2 - \Delta_1}{2\sigma_c p_c\sqrt{1-p_c^2}} \qquad \alpha_{13}^* = \frac{\Delta_2 + 2\Delta_1}{2\sigma_c p_c\sqrt{1-p_c^2}} \qquad \alpha_{12}^* = 0 \tag{5.24}$$

### Set 5

Finally, as there are two nonzero links, it is also possible to find equilibrium points that have one link equal to 1, and one link with $0 < \alpha_{ij} < 1$. This implies that the asymptotic value of the $\phi_i$ appearing in the equation for $\dot{\alpha}_{ij}$ has to equal $\phi_i^* = \arccos\left(2p_c^2 - 1\right)$. Filling in the known values of $\alpha(=1,0)$ and $\phi(=\arccos\left(2p_c^2-1\right))$ in equations (5.8) and (5.9) ($\dot{\phi_1}$, $\dot{\phi_2}$) results in the following six equilibrium points:

$$\phi_1^* = \arccos\left(2p_c^2 - 1\right) \qquad \phi_2^* = \arcsin\left(\frac{\Delta_1 + 2\Delta_2}{\sigma_c}\right), \qquad \alpha_{12}^* = \frac{\Delta_2 + 2\Delta_1}{2\sigma_c p_c\sqrt{1-p_c^2}} \qquad \alpha_{23}^* = 1 \qquad \alpha_{13}^* = 0 \tag{5.25}$$

$$\phi_2^* = \arccos\left(2p_c^2 - 1\right) \qquad \phi_1^* = \arcsin\left(\frac{2\Delta_1 + \Delta_2}{\sigma_c}\right), \qquad \alpha_{23}^* = \frac{\Delta_1 + 2\Delta_2}{2\sigma_c p_c\sqrt{1-p_c^2}} \qquad \alpha_{12}^* = 1 \qquad \alpha_{13}^* = 0 \tag{5.26}$$

$$\phi_1^* = \arccos\left(2p_c^2 - 1\right) \qquad \phi_1^* + \phi_2^* = \arcsin\left(\frac{\Delta_1 + 2\Delta_2}{\sigma_c}\right), \qquad \alpha_{12}^* = \frac{\Delta_1 - \Delta_2}{2\sigma_c p_c\sqrt{1-p_c^2}} \qquad \alpha_{13}^* = 1 \qquad \alpha_{23}^* = 0 \tag{5.27}$$

$$\phi_2^* = \arccos\left(2p_c^2 - 1\right) \qquad \phi_1^* + \phi_2^* = \arcsin\left(\frac{2\Delta_1 + \Delta_2}{\sigma_c}\right), \qquad \alpha_{23}^* = \frac{\Delta_2 - \Delta_1}{2\sigma_c p_c\sqrt{1-p_c^2}} \qquad \alpha_{13}^* = 1 \qquad \alpha_{12}^* = 0 \tag{5.28}$$

$$\phi_1^* + \phi_2^* = \arccos\left(2p_c^2 - 1\right) \qquad \phi_1^* = \arcsin\left(\frac{\Delta_1 - \Delta_2}{\sigma_c}\right), \qquad \alpha_{13}^* = \frac{2\Delta_2 + \Delta_1}{2\sigma_c p_c\sqrt{1-p_c^2}} \qquad \alpha_{12}^* = 1 \qquad \alpha_{23}^* = 0 \tag{5.29}$$

$$\phi_1^* + \phi_2^* = \arccos\left(2p_c^2 - 1\right) \qquad \phi_2^* = \arcsin\left(\frac{\Delta_2 - \Delta_1}{\sigma_c}\right), \qquad \alpha_{13}^* = \frac{2\Delta_1 + \Delta_2}{2\sigma_c p_c\sqrt{1-p_c^2}} \qquad \alpha_{23}^* = 1 \qquad \alpha_{12}^* = 0 \tag{5.30}$$

This looks like many different equilibrium points, but it is emphasized that all equilibrium points are in fact very similar. They all depend on $\sigma_c$ and $p_c$ in the same way. In addition, as $\Delta_3 = -\Delta_1 - \Delta_2$, the numerators $\Delta_1 - \Delta_2$ can also be written as $2\Delta_1 + \Delta_2$, etc. Now it is even more clear that all equilibrium points in this set are similar under exchange of subscripts.

There are found 12 equilibrium points with two nonzero links.

### 5.5.3. Three links

#### Set 6

Now, the case is considered where all links are nonzero. Obviously, all links can be chosen to be 1, and then it follows that $\dot{\alpha_{12}}, \dot{\alpha_{12}}, \dot{\alpha_{12}} = 0$ ( (5.10)-(5.12)). By equating the equations for $\dot{\phi_1}$, $\dot{\phi_2}$ ((5.8) and (5.9)) to 0, a system of two nonlinear equations with two unknown variables ($\phi_1$ and $\phi_2$) is obtained. From this set of equations, $\phi_2^*$ and $\phi_1^* + \phi_2^*$ can be expressed as a function of $\phi_1^*$, giving the following equilibrium point:

$$\phi_2^* = \arcsin\left(\sin(\phi_1) + \frac{\Delta_2 - \Delta_1}{\sigma_c}\right) \qquad \phi_1^* + \phi_2^* = \arcsin\left(\frac{2\Delta_1 + \Delta_2}{\sigma_c} - \sin(\phi_1)\right) \qquad \alpha_{12}^* = \alpha_{23}^* = \alpha_{13}^* = 1 \quad (5.31)$$

Finally, a condition on $\phi_1^*$ can be obtained by substituting $\phi_2^*$ in equation $\dot{\phi_1}$(5.8) and using the relevant trigonometric identities. This condition is given by the following equality:

$$\frac{2\Delta_1 + \Delta_2}{\sigma_c} = \sin(\phi_1)\left(1 + \sqrt{1 - \left(\frac{\Delta_2 - \Delta_1}{\sigma_c} + \sin(\phi_1)\right)^2} + \sqrt{1 - \sin^2(\phi_1)}\right) + \frac{\Delta_2 - \Delta_1}{\sigma_c}\sqrt{1 - \sin^2(\phi_1)} \qquad (5.32)$$

There is no explicit solution to this equality. However, using numerical methods, $\sin(\phi_1^*)$ (and thus $\phi_2^*$ and $\phi_1^* + \phi_2^*$) can be solved found for each value of $\sigma_c$.

#### Set 7

The next set of equilibrium points can be found by choosing all links to be $0 < \alpha_{ij} < 1$. Then, all phase differences have to obey $\phi_i = \arccos\left(2p_c^2 - 1\right)$. Equating equations (5.8) and (5.9) to 0 results in a system of two equations with three unknown variables ($\alpha_{12}, \alpha_{23}$ and $\alpha_{13}$). This gives an implicit expression for $\alpha_{23}$ and $\alpha_{13}$ in terms of $\alpha_{12}$:

$$\phi_1^* = \phi_2^* = \phi_1^* + \phi_2^* = \arccos\left(2p_c^2 - 1\right) \qquad \alpha_{23}^* = \frac{\Delta_2 - \Delta_1}{2\sigma_c p_c\sqrt{1 - p_c^2}} + \alpha_{12}^* \qquad \alpha_{13}^* = \frac{2\Delta_1 + \Delta_2}{2\sigma_c p_c\sqrt{1 - p_c^2}} - \alpha_{12}^* \quad (5.33)$$

In order to satisfy $\cos(\phi_1^*) = \cos(\phi_2^*) = \cos(\phi_1^* + \phi_2^*)$, it must hold that $p_c = 1 \vee p_c = \frac{1}{2}$. Note that for $p_c = 1$ the value of $\alpha_{23}$ and $\alpha_{13}$ goes to infinity, whereas it should be bounded in the unit interval. Thus, it follows that $p_c = \frac{1}{2}$, resulting in

$$\phi_1^* = \phi_2^* = \tfrac{2}{3}\pi, \quad \phi_1^* + \phi_2^* = \tfrac{4}{3}\pi \qquad \alpha_{23}^* = \frac{2(\Delta_2 - \Delta_1)}{\sigma_c\sqrt{3}} + \alpha_{12} \qquad \alpha_{13}^* = \alpha_{12} - \frac{2(2\Delta_1 + \Delta_2)}{\sigma_c\sqrt{3}} \qquad (5.34)$$

#### Set 8

As before, the next set of equilibrium points can be found by choosing one link equal to 1, and two links with $0 < \alpha_{ij}^* < 1$, again implying that the corresponding phase differences are given by $\phi_i^* = \arccos(2p_c^2 - 1)$. However, now it must be noted that $\phi_i^* = -\arccos(2p_c^2 - 1)$, is also a solution. This is now relevant, as this implies different values for the last phase difference. For example, if $\phi_1^* = \phi_2^* = \arccos\left(2p_c^2 - 1\right)$, then $\phi_1^* + \phi_2^* = 2\arccos\left(2p_c^2 - 1\right)$, while $\phi_1^* = -\phi_2^* = \arccos\left(2p_c^2 - 1\right)$, would imply $\phi_1^* + \phi_2^* = 0$. Below, the equilibrium points are given. If in point (5.35) the signs were chosen to be opposite, the additions term $-2(2p_c^2 - 1)$ would vanish. For the other two points, the terms between brackets originate from phase differences with opposite sign.

$$\phi_1^* = \phi_2^* = \arccos\left(2p_c^2 - 1\right), \qquad \alpha_{12}^* = \frac{2\Delta_1 + \Delta_2}{2\sigma_c p_c\sqrt{1 - p_c^2}} \pm 2(2p_c^2 - 1) \qquad \alpha_{23}^* = \frac{2\Delta_2 + \Delta_1}{2\sigma_c p_c\sqrt{1 - p_c^2}} \pm 2(2p_c^2 - 1) \qquad \alpha_{13}^* = 1 \quad (5.35)$$

$$(-)\phi_1^* = \phi_1^* + \phi_2^* = \arccos\left(2p_c^2 - 1\right), \quad \alpha_{12}^* = \frac{\Delta_1 - \Delta_2}{2\sigma_c p_c\sqrt{1 - p_c^2}}(\pm 2(2p_c^2 - 1)) \quad \alpha_{13}^* = \frac{2\Delta_2 + \Delta_1}{2\sigma_c p_c\sqrt{1 - p_c^2}}(\mp 2(2p_c^2 - 1)) \quad \alpha_{23}^* = 1 \quad (5.36)$$

$$(-)\phi_2^* = \phi_1^* + \phi_2^* = \arccos\left(2p_c^2 - 1\right), \quad \alpha_{23}^* = \frac{\Delta_2 - \Delta_1}{2\sigma_c p_c\sqrt{1 - p_c^2}}(\pm 2(2p_c^2 - 1)) \quad \alpha_{13}^* = \frac{2\Delta_1 + \Delta_2}{2\sigma_c p_c\sqrt{1 - p_c^2}}(\mp 2(2p_c^2 - 1)) \quad \alpha_{12}^* = 1 \quad (5.37)$$

**Set 9**

Finally, the last set of equilibrium points can be found by choosing two links equal to 1, and one link with $0 < \alpha^*_{ij} < 1$. This implies that the asymptotic value of the $\phi_i$ appearing in $\dot{\alpha}_{ij}$ has to equal $\phi^*_i = \arccos(2p_c^2 - 1)$. For example, choose $\alpha^*_{23} = \alpha^*_{13} = 1$ and $\phi^*_1 = 2\arccos(2p_c^2 - 1)$, such that equations (5.10)-(5.12) are equal to 0, and a system of two equations and two unknown variables ($\alpha_{12}$ and $\phi_2$) is left. From this set of equations an expression for $\alpha_{12}$ as function of $\phi^*_2$ is found, giving the equilibrium point

$$\phi^*_1 = \arccos(2p_c^2 - 1) \qquad \alpha^*_{12} = \frac{\Delta_1 - \Delta_2 + \sigma_c \sin(\phi^*_2)}{2\sigma_c p_c \sqrt{1-p_c^2}} \qquad \alpha^*_{23} = \alpha^*_{13} = 1 \tag{5.38}$$

Moreover, by again using the relevant trigonometric identities, a condition on $\phi^*_2$ can be found:

$$\frac{2\Delta_2 + \Delta_1}{\sigma_c} = 2p_c^2 \sin(\phi^*_2) + 2p_c\sqrt{1-p_c^2}\cos(\phi^*_2) \tag{5.39}$$

In addition, it must also hold that $0 < \alpha^*_{12} < 1$. These equality's can not be solved analytically, but they can be solved numerically. This gives the allowed parameter space and the corresponding values of $\sin(\phi^*_2)$.

In the same way expressions can be found for the case $0<\alpha_{23}<1$, giving the equilibrium point

$$\phi^*_2 = \arccos(2p_c^2 - 1) \qquad \alpha^*_{23} = \frac{\Delta_2 - \Delta_1 + \sigma_c \sin(\phi^*_1)}{2\sigma_c p_c \sqrt{1-p_c^2}} \qquad \alpha^*_{12} = \alpha^*_{13} = 1 \tag{5.40}$$

with the following condition on $\phi^*_1$

$$\frac{2\Delta_1 + \Delta_2}{\sigma_c} = 2p_c^2 \sin(\phi^*_1) + 2p_c\sqrt{1-p_c^2}\cos(\phi^*_1) \tag{5.41}$$

and the equilibrium point with $0<\alpha_{13}<1$

$$\phi^*_1 + \phi^*_2 = \arccos(2p_c^2 - 1) \qquad \alpha^*_{13} = \frac{2\Delta_1 + \Delta_2 - \sigma_c \sin(\phi^*_1)}{2\sigma_c p_c \sqrt{1-p_c^2}} \qquad \alpha^*_{12} = \alpha^*_{23} = 1 \tag{5.42}$$

and a condition on $\phi^*_1$ (this could also be written as a condition on $\phi^*_2$)

$$\frac{\Delta_1 - \Delta_2}{\sigma_c} = 2p_c^2 \sin(\phi^*_1) + 2p_c\sqrt{1-p_c^2}\cos(\phi^*_1) \tag{5.43}$$

There are found 8 equilibrium points with three nonzero links. It is now concluded that all 26 equilibrium points are found.

## 5.6. Stability of Equilibrium Points

In this section the stability of the equilibrium points found in section 5.5 will be analysed by studying the spectrum of the Jacobian, just as is done in subsection 4.3.1

The Jacobian matrix of the system (equations (5.8) - (5.12)) is given by:

$$\begin{pmatrix}
-\frac{2\sigma_c\alpha_{12}\cos(\phi_1)}{3} - \frac{\sigma_c\alpha_{13}\cos(\phi_1+\phi_2)}{3} & \frac{\sigma_c\alpha_{23}\cos(\phi_2)}{3} - \frac{\sigma_c\alpha_{13}\cos(\phi_1+\phi_2)}{3} & -\frac{2\sigma_c\sin(\phi_1)}{3} & \frac{\sigma_c\sin(\phi_2)}{3} & -\frac{\sigma_c\sin(\phi_1+\phi_2)}{3} \\
\frac{\sigma_c\alpha_{12}\cos(\phi_1)}{3} - \frac{\sigma_c\alpha_{13}\cos(\phi_1+\phi_2)}{3} & -\frac{2\sigma_c\alpha_{23}\cos(\phi_2)}{3} - \frac{\sigma_c\alpha_{13}\cos(\phi_1+\phi_2)}{3} & \frac{\sigma_c\sin(\phi_1)}{3} & -\frac{2\sigma_c\sin(\phi_2)}{3} & -\frac{\sigma_c\sin(\phi_1+\phi_2)}{3} \\
\frac{\alpha_{12}(1-\alpha_{12})\sin(\phi_1)}{2\sqrt{2+2\cos(\phi_1)}} & 0 & (p_c - p_{12})(1-2\alpha_{12}) & 0 & 0 \\
0 & \frac{\alpha_{23}(1-\alpha_{23})\sin(\phi_2)}{2\sqrt{2+2\cos(\phi_2)}} & 0 & (p_c - p_{23})(1-2\alpha_{23}) & 0 \\
\frac{\alpha_{13}(1-\alpha_{13})\sin(\phi_1+\phi_2)}{2\sqrt{2+2\cos(\phi_1+\phi_2)}} & \frac{\alpha_{13}(1-\alpha_{13})\sin(\phi_1+\phi_2)}{2\sqrt{2+2\cos(\phi_1+\phi_2)}} & 0 & 0 & (p_c - p_{13})(1-2\alpha_{13})
\end{pmatrix}$$

where the phase correlations $p_{ij}$ are given as in (5.7). In the following the eigenvalues of the equilibrium

points will be computed and the stability conditions formulated per set of equilibrium point. For each set, the stability conditions are first summarized, followed by the derivation of these conditions. For some sets of equilibrium points, the derivation is quite technical and/or extensive. It is sufficient to read the stability conditions only for understanding the bifurcation diagram and ultimately the dynamics of the network.

### 5.6.1. One link

#### Set 1

**Stability conditions**
It can be concluded that an equilibrium point of this set is stable, if

1. $\Delta_i = \Delta_j = -\frac{\Delta_k}{2}$, where $\Delta_k > 0$
2. $p_c > \frac{1}{\sqrt{2}}$
3. $\frac{3}{2}\Delta_k \leq \sigma_c < \Sigma_{1,k}$ ((5.45),(5.47),(5.48))
4. $\sigma_c > f(p_c)$, where $f(p_c)$ is determined by $p_c < p_{ij}$ and $p_c < p_{jk}$ (such that corresponding $\alpha_{ij,jk} = 0$) (see eq. (5.46)).

Moreover, it is found that frequency dissartovity is required, i.e. the link occurs between the oscillators whose frequencies are most distant.

**Derivation**
The equilibrium points in this set are given by (5.13)-(5.15). For the sake of completeness, the first point is also stated below:

$$\phi_1^* = \arcsin\left(\frac{3\Delta_1}{2\sigma_c}\right), \qquad \alpha_{12}^* = 1, \alpha_{23}^* = \alpha_{13}^* = 0, \qquad \Delta_2 = \Delta_3 = -\frac{\Delta_1}{2}$$

For $\phi_1^*$ to be well defined, it is required that $\left|\frac{3\Delta_1}{2\sigma_c}\right| \leq 1$, or $\frac{3}{2}|\Delta_1| \leq \sigma_c$. Evaluating the Jacobian matrix of this equilibrium point gives the following eigenvalues:

$$\begin{aligned}
\lambda_1 &= \sqrt{\frac{1+\cos(\phi_1^*)}{2}} - p_c = \sqrt{\frac{1+\sqrt{1-\frac{9\Delta_1^2}{4\sigma_c^2}}}{2}} - p_c \\
\lambda_2 &= p_c - \sqrt{\frac{1+\cos(\phi_2^*)}{2}} = p_c - p_{23} \\
\lambda_3 &= p_c - \sqrt{\frac{1+\cos(\phi_1^*+\phi_2^*)}{2}} = p_c - p_{13} \\
\lambda_4 &= -\frac{2\sigma_c\cos(\phi_1^*)}{3} = -\frac{2\sigma_c\sqrt{1-\frac{9\Delta_1^2}{4\sigma_c^2}}}{3} \\
\lambda_5 &= 0
\end{aligned} \tag{5.44}$$

If $p_c < \frac{1}{\sqrt{2}}$, then $\lambda_1 > 0$ for all allowed $\phi_1^*$ and the equilibrium point is a saddle point.
If $p_c > \frac{1}{\sqrt{2}}$, the inequality $\lambda_1 < 0$ can be solved for $\sigma_c$, resulting in the critical coupling strength $\Sigma_{1,1}$:

$$\Sigma_{1,1} := \frac{3\Delta_1}{4p_c\sqrt{1-p_c^2}} \tag{5.45}$$

If $\sigma_c > \Sigma_{1,1}$ then the equilibrium point is a saddle point $\lambda_1 > 0$. If $\sigma_c < \Sigma_{1,1}$ then $\lambda_1 < 0$. Moreover, note that this implies that $\Delta_1 > 0$, as $\sigma_c$ can not be negative.
It is clear that $\lambda_2 < 0$ and $\lambda_3 < 0$, if $p_c < p_{23}$ and $p_c < p_{13}$. Thus, if

$$2p_c^2 - 1 < \cos(\phi_1^*+\phi_2^*) = \cos(\phi_1^*)\cos(\phi_2^*) - \frac{3\Delta_1}{2\sigma_c}\sin(\phi_2^*) \qquad \wedge \qquad 2p_c^2 - 1 < \cos(\phi_2^*) \tag{5.46}$$

This can be solved numerically and implies a lower bound for $\sigma_c$ as function of $p_c$ (in the region where $\lambda_1 < 0$). Note that $p_c < p_{23}$ and $p_c < p_{13}$ is required to obtain $\alpha_{23} = 0$ and $\alpha_{13} = 0$ in a network with an anti-Hebbian adaptation rule.
Finally, $\lambda_4 < 0$ for all $\sigma_c$, as $\frac{9\Delta_1^2}{4\sigma_c^2} < 1$.
The same analysis can be done for equilibrium points 2 and 3, given by (5.14) and (5.15) respectively. The critical coupling strength for the second equilibrium point is given by

$$\Sigma_{1,2} := \frac{3\Delta_2}{4p_c\sqrt{1-p_c^2}} \tag{5.47}$$

and for the third equilibrium point by

$$\Sigma_{1,3} := \frac{3(\Delta_1+\Delta_2)}{4p_c\sqrt{1-p_c^2}} \tag{5.48}$$

It is noted that $\lambda_5 = 0$, and thus that nothing can be said about the stability.[36] It gives rise to the center manifolds, which are curves that capture the asymptotic features of the point. [37] In this stability analysis however, it is just assumed that by studying the center manifolds, it is found that the point is stable. In other words, the eigenvalues with zero real part are ignored for now. In the following section, the stability analysis will be compared to a numerical simulation, and this will reveal if this assumption is correct or not.

Finally, it is noted that for a certain network only one of the three equilibrium points can be stable, due to the condition on $\Delta_{i,j,k}$ ($\Delta_i = \Delta_j = -\frac{\Delta_k}{2}, \Delta_k > 0$). Without loss of generality, the system can be ordered such that $\omega_1 > \omega_2 > \omega_3$. Then, if $\omega_2 = \frac{\omega_1+\omega_3}{2}$, this condition is satisfied (with $\Delta_k = \Delta_3$) and the first and third oscillator are connected, i.e. the oscillators whose frequencies are most distant. This phenomenon, called *frequency dissasortativity* was already observed in large networks (3.2.4), and is here analytically confirmed!

### Set 2

**Stability conditions**
An equilibrium point of this set is stable, if

1. $\Delta_i = \Delta_j = -\frac{\Delta_k}{2}$, where $\Delta_k > 0$
2. $p_c > \frac{1}{\sqrt{2}}$
3. $\sigma_c > \Sigma_{1,k} \geq \frac{3}{2}\Delta_k$, where two eigenvalues have complex part for $\sigma_c > \Sigma_{2,k}$ (,(5.52),(5.53))

Again, the link occurs between the oscillators whose frequencies are most distant.

**Derivation**
The equilibrium points of this set are given by (5.16) - (5.18). Recall that for the first point of this set is described by:

$$\phi_1^* = \arccos\left(2p_c^2 - 1\right), \qquad \alpha_{12}^* = \frac{3\Delta_1}{4\sigma_c p_c\sqrt{1-p_c^2}} \qquad \alpha_{23}^* = \alpha_{13}^* = 0, \qquad \Delta_2 = \Delta_3 = -\frac{\Delta_1}{2}$$

The weight of the link $\alpha_{12}^*$ can also be written as $\alpha_{12}^* = \frac{(3\Delta_1/2\sigma_c)}{2p_c\sqrt{1-p_c^2}}$. This implies that $\frac{3\Delta_1}{2\sigma_c} \leq \alpha_{12}^*$, as for $0 \leq p_c \leq 1$ it holds that $0 \leq 2p_c\sqrt{1-p_c^2} \leq 1$. Taking into account that $0 \leq \alpha_{12}^* \leq 1$, it can be concluded that $0 \leq \frac{3\Delta_1}{2} \leq \sigma_c$.

The Jacobian matrix of this point yields more complex eigenvalues. These eigenvalues can be rewritten into:

$$\begin{aligned}
\lambda_1 &= \frac{A + \sqrt{A^2 + B(\frac{1}{\sigma_c} - \frac{1}{\Sigma_{1,1}})}}{C} \\
\lambda_2 &= \frac{A - \sqrt{A^2 + B(\frac{1}{\sigma_c} - \frac{1}{\Sigma_{1,1}})}}{C} \\
\lambda_3 &= p_c - \sqrt{\frac{1+\cos(\phi_2^*)}{2}} = p_c - p_{23} \\
\lambda_4 &= p_c - \sqrt{\frac{1+\cos(\phi_1^* + \phi_2^*)}{2}} = p_c - p_{13} \\
\lambda_5 &= 0
\end{aligned} \tag{5.49}$$

where $A := 2\Delta_1(1-2p_c^2)$, $B := 24p_c(1-p_c^2)\Delta_1^2$, $C := 8p_c\sqrt{1-p_c^2}$ and $\Sigma_{1,1}$ the critical coupling strength given by (5.45).
Notice that $B$ and $C$ are always positive, so it can be shown easily that if $\sigma_c < \Sigma_{1,1}$, that $\lambda_1 > 0$ and $\lambda_2 < 0$, regardless the sign of $A$. Hence the equilibrium point is unstable for these values of $\sigma_c$.
If $\sigma_c > \Sigma_{1,1}$, the stability depends on a second critical coupling strength $\Sigma_{2,1}$ that determines the sign of the radicand:

$$\frac{1}{\Sigma_{2,1}} := \frac{1}{\Sigma_{1,1}} - \frac{A^2}{B} = \frac{1}{\Sigma_{1,1}} - \frac{(1-2p_c^2)^2}{6p_c(1-p_c^2)} \tag{5.50}$$

Using $\Sigma_{2,1}$, the eigenvalues $\lambda_1$ ($\lambda_+$) and $\lambda_2$ ($\lambda_-$) can be rewritten as

$$\lambda_\pm = \frac{A \pm \sqrt{\frac{1}{\sigma_c} - \frac{1}{\Sigma_{2,1}})}}{C} \tag{5.51}$$

Since $A^2$ and $B$ are both positive, it holds that $\Sigma_{2,1} > \Sigma_{1,1}$, and thus the following cases need to be considered: $\Sigma_{1,1} < \sigma_c < \Sigma_{2,1}$ and $\Sigma_{1,1} < \Sigma_{2,1} < \sigma_c$.
If $\Sigma_{1,1} < \sigma_c < \Sigma_{2,1}$, the sign of $\lambda_\pm$ is the same as the sign of $A$.
On the other hand, if $\Sigma_{1,1} < \Sigma_{2,1} < \sigma_c$, then the radicand is negative and thus the eigenvalues are complex. The sign of the real part is again the same as the sign of $A$.
Hence, in both cases it holds that $\mathbb{R}\text{e}\{\lambda_\pm\} < 0$ if $A < 0$, thus if $\Delta_1 < 0$ and $p_c < \frac{1}{\sqrt{2}}$, or if $\Delta_1 > 0$ and $p_c > \frac{1}{\sqrt{2}}$. Only the latter is valid, since it is required that $\Delta_1 > 0$ for $\alpha_{12}$ to be well-defined.

Moreover, $\lambda_3, \lambda_4 < 0$, if $p_c < p_{23}$ and $p_c < p_{13}$. As with the previous set of equilibrium points, these conditions are necessary to obtain $\alpha_{23} = 0$ and $\alpha_{13} = 0$ in a network with an anti-Hebbian adaptation rule. However, in this case, these conditions do not yield an extra lower bound for $\sigma_c$. To verify this, note that equation 5.46 is met for small negatives values of $\phi_2^*$, as long as $p_c < 1$. The latter is satisfied as $\sigma_c > \Sigma_{1,1}$.

A similar analysis can be done for equilibrium points 5 and 6.
For the fifth equilibrium point, the critical coupling strength (distinguishing real and complex eigenvalues) is given by

$$\frac{1}{\Sigma_{2,2}} := \frac{1}{\Sigma_{1,2}} - \frac{(1-2p_c^2)^2}{6p_c(1-p_c^2)} \tag{5.52}$$

And for equilibrium point 6, by

$$\frac{1}{\Sigma_{2,3}} := \frac{1}{\Sigma_{1,3}} - \frac{(1-2p_c^2)^2}{6p_c(1-p_c^2)} \tag{5.53}$$

Finally, just as in the previous group, it is noted that for a certain network only one point of this set can possibly be stable. If the point is stable, then the nonzero link connects the oscillators whose frequencies are most distant.

### 5.6.2. Two links

#### Set 3

**Stability conditions**
It is found that this point is always unstable.

**Derivation**
The points of this set are given by (5.19), (5.20) and (5.21). Recall that the first point is given by

$$\phi_1^* = \arcsin\left(\frac{\Delta_2 + 2\Delta_1}{\sigma_c}\right) \qquad \phi_2^* = \arcsin\left(\frac{\Delta_1 + 2\Delta_2}{\sigma_c}\right), \qquad \alpha_{12}^* = \alpha_{23}^* = 1 \qquad \alpha_{13}^* = 0$$

The solution is feasible if $\left|\frac{\Delta_2+2\Delta_1}{\sigma_c}\right| \leq 1$ and $\left|\frac{\Delta_1+2\Delta_2}{\sigma_c}\right| \leq 1$. Otherwise, $\phi_1^*$ and $\phi_2*$ are not defined.
The eigenvalues of the Jacobian matrix for this point are

$$\begin{aligned}
\lambda_1 &= \left(-\frac{\cos(\phi_2^*)}{3} - \frac{\cos(\phi_1^*)}{3} + \frac{\sqrt{\cos(\phi_2^*)^2 - \cos(\phi_1^*)\cos(\phi_2^*) + \cos(\phi_1^*)^2}}{3}\right)\sigma_c \\
\lambda_2 &= \left(-\frac{\cos(\phi_2^*)}{3} - \frac{\cos(\phi_1^*)}{3} - \frac{\sqrt{\cos(\phi_2^*)^2 - \cos(\phi_1^*)\cos(\phi_2^*) + \cos(\phi_1^*)^2}}{3}\right)\sigma_c \\
\lambda_3 &= \sqrt{\frac{1+\cos(\phi_1^*)}{2}} - p_c = \sqrt{\frac{1+\sqrt{1-\left(\frac{\Delta_2+2\Delta_1}{\sigma_c}\right)^2}}{2}} - p_c \\
\lambda_4 &= \sqrt{\frac{1+\cos(\phi_2^*)}{2}} - p_c = \sqrt{\frac{1+\sqrt{1-\left(\frac{\Delta_1+2\Delta_2}{\sigma_c}\right)^2}}{2}} - p_c \\
\lambda_5 &= p_c - p_{13} = p_c - \sqrt{\frac{1+\cos(\phi_1^* + \phi_2^*)}{2}}
\end{aligned} \tag{5.54}$$

Note that $\cos\left(\phi_1^*\right) \geq 0$ and $\cos\left(\phi_2^*\right) \geq 0$, since $\left|\frac{\Delta_2+2\Delta_1}{\sigma_c}\right| \leq 1$ and $\left|\frac{\Delta_1+2\Delta_2}{\sigma_c}\right| \leq 1$. Therefore, it holds that $\cos(\phi_1^*) + \cos(\phi_2^*) = \sqrt{\cos(\phi_2^*)^2 + 2\cos(\phi_1^*)\cos(\phi_2^*) + \cos(\phi_1^*)^2} > \sqrt{\cos(\phi_2^*)^2 - \cos(\phi_1^*)\cos(\phi_2^*) + \cos(\phi_1^*)^2}$. This implies that $\lambda_1 < 0$. Moreover, it is trivial that $\lambda_2 < 0$.
If $p_c < \frac{1}{\sqrt{2}}$, then it holds that $\lambda_3, \lambda_4 > 0$ and thus that this point is unstable for this region.
If $p_c > \frac{1}{\sqrt{2}}$, the sign of $\lambda_3$ depends on the critical coupling strength

$$\Sigma_{3,1} := \frac{\Delta_2 + 2\Delta_1}{2p_c\sqrt{1-p_c^2}} \tag{5.55}$$

If $\sigma_c > \Sigma_{3,1}$, then $\lambda_3 > 0$, or, the other way around, $\sigma_c < \Sigma_{3,1}$, then $\lambda_3 < 0$. Note that $\sigma_c$ is positive, and thus it must hold that $0 < \Delta_2 + 2\Delta_1 \leq \sigma_c < \Sigma_{3,1}$.
The sign of $\lambda_4$ (for $p_c > \frac{1}{\sqrt{2}}$) depends on the critical coupling strength

$$\Sigma_{3,2} := \frac{\Delta_1 + 2\Delta_2}{2p_c\sqrt{1-p_c^2}} \tag{5.56}$$

and also here applies: If $\sigma_c < \Sigma_{3,2}$, then $\lambda_4 < 0$ and vice-versa. In addition, this is a valid statement if it also holds that $0 < \Delta_1 + 2\Delta_2 \leq \sigma_c$.
Define $\Delta_{max(min)} = \max(\min)\{\Delta_1 + 2\Delta_2, \Delta_2 + 2\Delta_1\}$ and $\Sigma_{min/max} = \frac{\Delta_{min/max}}{2p_c\sqrt{1-p_c^2}}$. Then $\lambda_3, \lambda_4 < 0$ for $0 < \Delta_{\max} < \sigma_c < \Sigma_{min}$ and $p_c > \frac{1}{\sqrt{2}}$.
Finally, $\lambda_5 < 0$ if $p_c < p_{13}$. This condition is required in order to obtain $\alpha_{13} = 0$ in a network with an anti-Hebbian adaptation rule. However, it can be proven that if $0 < \Delta_{\max} < \sigma_c < \Sigma_{min}$ and $p_c > \frac{1}{\sqrt{2}}$, then $\lambda_5 > 0$, and thus that this equilibrium point is unstable. As this is nontrivial, the proof is given below:

*Proof.* Consider $\Delta_{\min}, \Delta_{\max}, \Sigma_{min}, \phi_1^*, \phi_2^*$ and $\lambda_3, \lambda_4, \lambda_5$ defined as above. Furthermore, consider $0 < \Delta_{\min} < \Delta_{\max} < \sigma_c < \Sigma_{min}$ and $p_c > \frac{1}{\sqrt{2}}$, such that we have that $\lambda_3, \lambda_4 > 0$. We need to prove that this implies that $\lambda_5 > 0$, thus that $p_c > \sqrt{\frac{1+\cos(\phi_1^*+\phi_2^*)}{2}}$. Or equivalently: $\cos(\phi_1^*+\phi_2^*) < 2p_c^2 - 1$.

$$
\begin{aligned}
\cos(\phi_1^*+\phi_2^*) &= \cos\left(\arcsin\left(\frac{\Delta_{max}}{\sigma_c}\right) + \arcsin\left(\frac{\Delta_{min}}{\sigma_c}\right)\right) && \Longleftrightarrow \\
&= \cos\left(\arcsin\left(\frac{\Delta_{max}}{\sigma_c}\right)\right)\cdot\cos\left(\arcsin\left(\frac{\Delta_{min}}{\sigma_c}\right)\right) \\
&\quad - \sin\left(\arcsin\left(\frac{\Delta_{max}}{\sigma_c}\right)\right)\cdot\sin\left(\arcsin\left(\frac{\Delta_{min}}{\sigma_c}\right)\right) && \Longleftrightarrow \\
&= \sqrt{1-\left(\frac{\Delta_{max}}{\sigma_c}\right)^2}\cdot\sqrt{1-\left(\frac{\Delta_{min}}{\sigma_c}\right)^2} - \frac{\Delta_{max}\Delta_{min}}{\sigma_c^2} && \Longleftrightarrow \\
&< \sqrt{\left(1-\left(\frac{\Delta_{min}}{\sigma_c}\right)^2\right)^2} - \frac{\Delta_{max}\Delta_{min}}{\sigma_c^2} && \Longleftrightarrow \\
&< \sqrt{\left(1-\left(\frac{\Delta_{min}}{\sigma_c}\right)^2\right)^2} && \Longleftrightarrow \\
&= 1-\left(\frac{\Delta_{min}}{\sigma_c}\right)^2 && (*) \Longleftrightarrow \\
&< 1-4p_c^2(1-p_c^2) && (**) \Longleftrightarrow \\
&= \left(2p_c^2-1\right)^2 && \Longleftrightarrow \\
&< 2p_c^2-1, \text{ for } p_c \in (\tfrac{1}{\sqrt{2}}, 1)
\end{aligned}
$$

Note that at $(*)$ we used that $1-\left(\frac{\Delta_{min}}{\sigma_c}\right)^2 > 0$, implying that the square and the root cancel out. At $(**)$ we used that $\sigma_c < \frac{\Delta_{\min}}{2p_c^2-1}$ implies $2p_c^2 - 1 < \frac{\Delta_{\min}}{\sigma_c}$. We conclude that $\cos(\phi_1^*+\phi_2^*) < 2p_c^2-1$, as required. □

In a similar way it can be proven that equilibrium point 8 and 9 are unstable.
It can thus be conluded that all points in this set are unstable.

### Set 4

**Stability conditions**
By using earlier obtained insights, and by assuming that only links occur between oscillators whose natural frequencies are most distant, it is found that the first equilibrium point of this set is always unstable. For a given network, the oscillators can be ordered (such that $\omega_1 < \omega_2 < \omega_3$), and the other two points are then stable if

1. $\Delta_1 \neq \Delta_2$, and $\Delta_{1,2} > 0$
2. $p_c > \frac{1}{\sqrt{2}}$
3. Equilibrium point 2: $\Delta_1 > \Delta_2$, and $\sigma_c > \Sigma_{4,2} > \Delta_{max} > 0$, with $\Delta_{max}$ the numerator of $\Sigma_{4,2}$ ((5.58)
4. Equilibrium point 3: $\Delta_2 > \Delta_1$, and $\sigma_c > \Sigma_{4,3} > \Delta_{max} > 0$, with $\Delta_{max}$ the numerator of $\Sigma_{4,2}$ ((5.59)

Moreover, this reveals that the strongest link (equal to 1), occurs between the two oscillators whose frequencies are most distant. The less stronger, but nonzero link occurs between the two oscillators whose frequencies are second most distant.

**Derivation**
The equilibrium points in this set are given by (5.22), (5.23) and (5.24) respectively. The first point of this set is also shown below:

$$\phi_1^* = \phi_2^* = \arccos\left(2p_c^2-1\right), \qquad \alpha_{12}^* = \frac{\Delta_2+2\Delta_1}{2\sigma_c p_c\sqrt{1-p_c^2}} \qquad \alpha_{23}^* = \frac{\Delta_1+2\Delta_2}{2\sigma_c p_c\sqrt{1-p_c^2}} \qquad \alpha_{13}^* = 0$$

To determine the stability of these points, the Jacobian is again evaluated at this equilibrium point by filling in the corresponding values for $\phi_1^*, \phi_2^*, \alpha_{12}^*, \alpha_{23}^*$,and $\alpha_{13}^*$. However, this time the spectrum of the resulting matrix can not be found as straightforward as in the previous cases. Therefore, it might be better to take a different approach for this problem by finding the stability numerically and to compare the results with earlier obtained insights.
The stability is determined numerically by computing the eigenvalues of the (simplified) Jacobian for different values of $\sigma_c$ and $p_c$, and checking whether these have all real negative part. It is found that the first equilibrium point of this set is never stable, but that the second and third equilibrium point are stable under certain conditions. The following paragraph will elaborate on these conditions. Thereafter, it will be explained why the first equilibrium point is never stable.

Note that for equilibrium points from the first en second set it was found that these points are stable for $\sigma_c < \Sigma_i$ and $\sigma_c > \Sigma_i$, respectively. Moreover, note that set 1 and 2 are in fact very similar to set 3 and 4, respectively. Namely, the values of $\alpha_{ij}^*$ and $\phi_i^*$ are related in the same way to the parameters $\sigma_c$ and $p_c$, but have a different constant in the numerator and - in the case of set 3 and 4- an extra nonzero link and prescribed phase difference.

Moreover, note that the critical coupling strength of set 2 (and 1) is in fact the curve where $\alpha_{ij}^* = \frac{3\Delta_i}{4\sigma_c p_c \sqrt{1-p_c^2}} = 1$, and thus that for $\sigma_c < \Sigma_i$, an equilibrium point from this set would have $\alpha_{12} > 1$, which is not allowed. It was found that beneath this curve, $\alpha_{ij}$ is just equal to 1.

The equilibrium points of this set have two nonzero links. In the following, the stability will be determined by considering each link apart, as if the other two links have vanished. The appropriate conditions (found from set 1 and 2) will be selected and combined. Therefore, it may be expected that there are two critical coupling strengths per point, namely the curves where the nonzero links $\alpha_{ij}$ and $\alpha_{jk}$ of such a point are equal to 1 (as this is the stability condition for one link to be nonzero and smaller than 1). Just as with the first two sets, it would be reasonable to suggest that equilibrium point *i* of set 3 and equilibrium point *i* of set 4 share the same critical coupling strengths.

For set 3, it was found that the critical coupling strengths, $\Sigma_{min/max}$, were given by $\Sigma_i = \frac{\sigma_c \sin(\phi_i^*)}{2p_c\sqrt{1-p_c^2}}$, and these curves correspond exactly to those predicted (namely, the curves where $\alpha_{ij}^* = 1, \alpha_{jk}^* = 1$). As with set 1, it is expected to have $\sigma_c < \Sigma_{min}$ as one of the conditions for stability for set 3. This is indeed a condition for stability, though combined with other conditions the point is still unstable.

Now, for set 4, it would be reasonable to require $p_c > \frac{1}{\sqrt{2}}$ and $\sigma_c > \Sigma_{max}$ (so that $p_c > p_{12}, p_{23}$). For set 3, it was proven that it is not possible to have $p_c < p_{13}$, if $\sigma_c < \Sigma_{min}$ and $p_c > \frac{1}{\sqrt{2}}$. However, it can be proven that for $\sigma_c > \Sigma_{max}$ and $p_c > \frac{1}{\sqrt{2}}$, it holds that $p_c < p_{13}$, and thus that the point may be stable. Thus the critical coupling strengths for an equilibrium point of this set are given by

$$\Sigma_{4,1} := \frac{\max\{\Delta_1 + 2\Delta_2; 2\Delta_1 + \Delta_2\}}{2p_c\sqrt{1-p_c^2}} \tag{5.57}$$

$$\Sigma_{4,2} := \frac{\max\{\Delta_1 - \Delta_2; \Delta_1 + 2\Delta_2\}}{2p_c\sqrt{1-p_c^2}} \tag{5.58}$$

$$\Sigma_{4,1} := \frac{\max\{\Delta_2 - \Delta_1; 2\Delta_1 + \Delta_2\}}{2p_c\sqrt{1-p_c^2}} \tag{5.59}$$

Note that these critical coupling strengths can also be written as $\max\{\sigma_c\alpha_{ij}^*; \sigma_c\alpha_{jk}^*\}$, with $\alpha_{ij}^*, \alpha_{jk}^*$ the nonzero links. The point is stable for $\sigma_c > \Sigma_{4,i}$

Finally, the equilibrium point must also be well defined. Without loss of generality, a given network can be ordered such that $\omega_1 < \omega_2 < \omega_3$, and thus that $\Delta_1, \Delta_2 > 0$. Then the second equilibrium point (of set 4) is well defined, if $\Delta_1 > \Delta_2$, and the third equilibrium point is well defined if $\Delta_2 > \Delta_1$. If $\Delta_1 = \Delta_2$, all points are unstable.

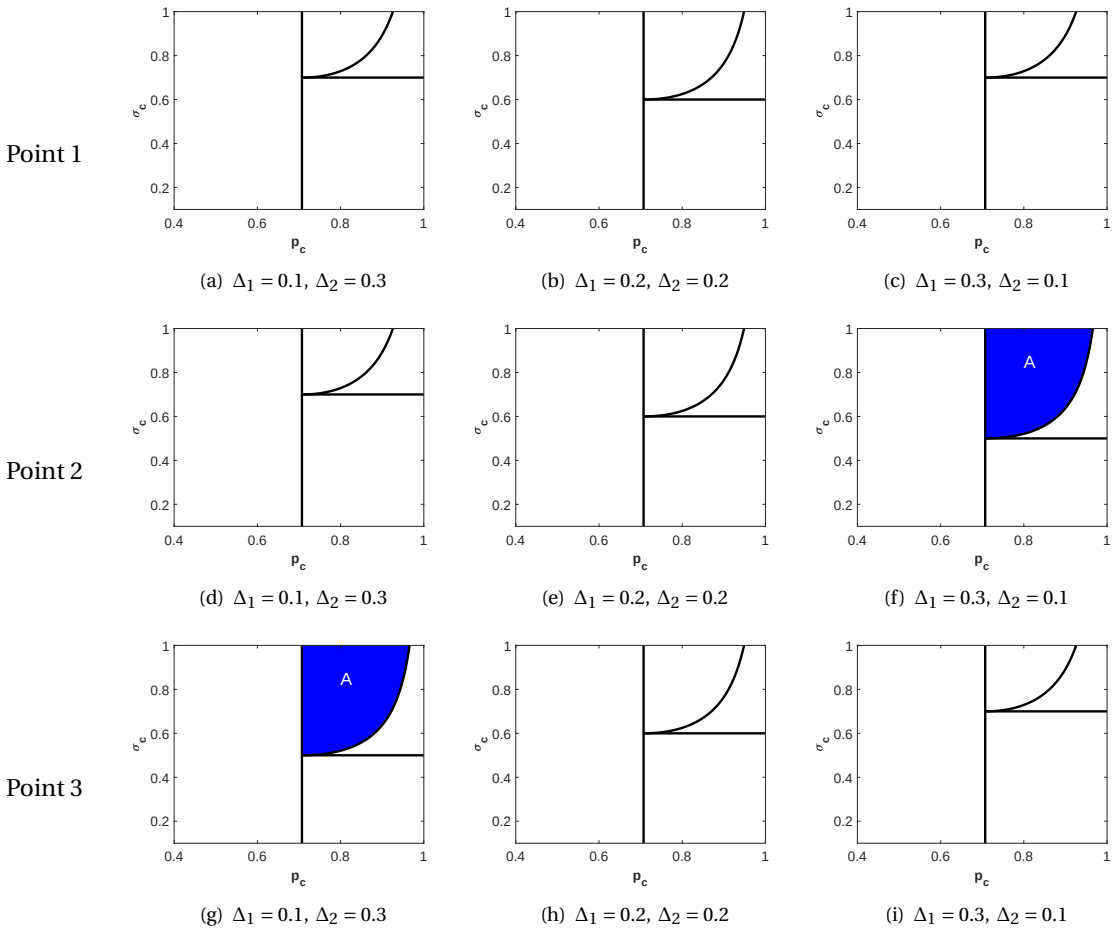


(a) $\Delta_1 = 0.1,\ \Delta_2 = 0.3$ (b) $\Delta_1 = 0.2,\ \Delta_2 = 0.2$ (c) $\Delta_1 = 0.3,\ \Delta_2 = 0.1$

(d) $\Delta_1 = 0.1,\ \Delta_2 = 0.3$ (e) $\Delta_1 = 0.2,\ \Delta_2 = 0.2$ (f) $\Delta_1 = 0.3,\ \Delta_2 = 0.1$

(g) $\Delta_1 = 0.1,\ \Delta_2 = 0.3$ (h) $\Delta_1 = 0.2,\ \Delta_2 = 0.2$ (i) $\Delta_1 = 0.3,\ \Delta_2 = 0.1$

**Figure 5.6.** The parameter range of stability (blue) of the 3 equilibrium points of set 4 for different values of $\Delta_1, \Delta_2$ (of an ordered network). The lines $p_c = \frac{1}{\sqrt{2}}, \sigma_c = \Delta_{max}$ and the curve $\sigma_c = \Sigma_{max}$ are also plotted in each figure.
The upper row shows the first equilibrium point, that is not stable for any value of $\Delta_1, \Delta_2, \sigma_c, p_c$. The middle row shows the second equilibrium point, that has a stable region $A$ if $\Delta_1 > \Delta_2$. The bottom row shows the third equilibrium point, that has a stable region $A$ if $\Delta_2 > \Delta_1$.

Figure 5.6 shows the region of stability for the different equilibrium points of an ordered network ($\omega_1 < \omega_2 < \omega_3$). The stability of each network and equilibrium point is numerically determined by computing the eigenvalues of the corresponding Jacobian. A stable region is indicated with blue. In addition, the lines $p_c = \frac{1}{\sqrt{2}}, \sigma_c = \Delta_{max}$ and the curve $\sigma_c = \Sigma_{max}$ are plotted in each figure.
The figure confirms that the first equilibrium point (upper row panel) is unstable for all values of $\Delta_1, \Delta_2, \sigma_c, p_c$. It shows that the second point (middle row panel) only has a stable region if $\Delta_1 > \Delta_2$. This region ($A$) is indeed enclosed by $p_c > \frac{1}{\sqrt{2}}$ and $\sigma_c > \Sigma_{max}$, as was reasoned above. Finally, it shows that equilibrium point 3 (bottom row pannel) has a stable region if $\Delta_2 > \Delta_1$. This region ($A$) is indeed enclosed by $p_c > \frac{1}{\sqrt{2}}$ and $\sigma_c > \Sigma_{max}$, as was reasoned above.

Finally, is is considered why the first equilibrium point is unstable. Using the same argument as before, it could be assumed that this point could also possibly be stable for $\sigma_c > \Sigma_{max} = \frac{max\{\Delta_1+2\Delta_2, \Delta_2+2\Delta_1\}}{2\sigma_c p_c \sqrt{1-p_c^2}}$. However, Figure 5.6 shows that this argument does not hold for the first equilibrium point. This is explained by using the same phenomenon observed before: frequency dissasortativity (see subsections (5.6.1.1), (5.6.1.2)). In other words, if $|\Delta_i| = |\omega_j - \omega_i|$ is smaller than $|\Delta_j|, |\Delta_k|$, then there is no link between oscillator $i$ and $j$. Seen the nature of the anti-Hebbian coupling and the observations seen in set 1 and 2 (and in the complex adaptive network), this assumption seems reasonable. The following proofs that under this assumption, the first equilibrium point is not well defined for any values of $\Delta_1, \Delta_2$.

*Proof.* Consider the first equilibrium point of the fourth set of an anti-Hebbian network of 3 oscillators, and assume frequency dissasortativity. The oscillators have frequencies *a,b, c* in the given interval of natural frequencies: $a,b,c \in [\omega_{min};\omega_{max}]$, with $a \leq b \leq c$ and $\omega_{min} \neq \omega_{max}$. There are 3 cases we need to consider: $b < \frac{a+c}{2} \quad \vee \quad b = \frac{a+c}{2} \quad \vee \quad b > \frac{a+c}{2}$.

First, we consider $b < \frac{a+c}{2}$. We then have $|a-b| < |b-c| < |c-a|$, thus the nonzero links will occur between $(b,c)$ and $(c,a)$. Thus, in order to have $\alpha_{12}, \alpha_{23} > 0$, we must have $\omega_2 = c$. We can have $\omega_1 = a$ and $\omega_3 = b$ or vice-versa.
Assume $\omega_1 = a$, $\omega_3 = b$. But then we have $\Delta_1 + 2\Delta_2 = (c-a) + 2(b-c) = 2b - (a+c)$ We have $b < \frac{a+c}{2}$, and thus $\Delta_1 + 2\Delta_2 < 0$. But then $\alpha_{23} < 0$ and this is a contradiction. Similarly, assume $\omega_1 = b$, $\omega_3 = a$. We then have $\Delta_1 + 2\Delta_2 = (c-b) + 2(a-c) = 2a - b - c < 0$ (as $a \leq b \leq c$), and thus $\alpha_{12} < 0$. This is again a contradiction.

Secondly, we consider $b = \frac{a+c}{2}$. We then have $|a-b| = |b-c| < |c-a|$, thus the nonzero links will occur between $(c,a)$ and either $(a,b)$ or $(b,c)$.
Assume the links will occur between $(c,a)$ and $(a,b)$. Due to frequency dissasortativity we then must have $\omega_2 = a$ to have $\alpha_{12}, \alpha_{23} > 0$. Independent of the choice of $\omega_1$ and $\omega_2$, we will find that either $\Delta_1 + 2\Delta_2 = 0$ or $\Delta_2 + 2\Delta_1 = 0$, and we again have a contradiction.

Finally, we consider $b > \frac{a+c}{2}$. We then have $|b-c| < |a-b| < |c-a|$, thus the nonzero links will occur between $(b,a)$ and $(c,a)$. Thus, in order to have $\alpha_{12}, \alpha_{23} > 0$, we must have $\omega_2 = a$. We can have $\omega_1 = c$ and $\omega_3 = b$ or vice-versa.
Assume $\omega_1 = c$, $\omega_3 = b$. But then we have $\Delta_2 + 2\Delta_1 = (b-a) + 2(a-c) = a + b - 2c$. We have $a \leq b \leq c$, and thus $\Delta_2 + 2\Delta_1 \leq$. But then $\alpha_{12} \leq 0$ and this is a contradiction. Similarly, assume $\omega_1 = b$, $\omega_3 = c$. We then have $\Delta_2 + 2\Delta_1 = (c-a) + 2(a-b) = c + a - 2b < 0$ (as $b > \frac{a+c}{2}$), and thus $\alpha_{12} < 0$ and this is a contradiction.

We thus conclude that we can not have a combination of oscillators such that this equilibrium point is stable. □

Note that this proof only works for the first equilibrium point, and not for the second and third equilibrium point of the set. However, a similar argument proves that for these two points it must hold that $\Delta_{1,2} > 0$ for the points to be well defined (given frequency dissasortativity).
In addition, it must be noted that the link between the pair of oscillators whose frequencies are most distant, has the largest value in both point 2 and 3. This is again explained by frequency dissasortativity: the preference for distant frequencies.

### Set 5

**Stability conditions**
The third and fourth point of the set have a stable region. A given network can be ordered (such that $\omega_1 < \omega_2 < \omega_3$), and the points are then stable if:

1. $\Delta_1 \neq \Delta_2$, and $\Delta_{1,2} > 0$
2. $p_c > \frac{1}{\sqrt{2}}$
3. $p_c < p_{ki}$, with $k,i$ chosen such that $\alpha_{ki}$ is the vanished link.
4. $\Sigma_{5,2,j} < \sigma_c < \Sigma_{5,1,i}$ ((5.60), (5.61))
5. $\sigma_c > f(\Delta_{i,j,k})$, with $f(\Delta_{i,j,k})$ the numerator of $\Sigma_{5,1,i}$.
6. Equilibrium point 3: $\Delta_1 > \Delta_2$, and for equilibrium point 4: $\Delta_2 > \Delta_1$

**Derivation**
The next set of equilibrium points are given by (5.25)-(5.34). For the sake of completeness first point of this group is also stated below:

$$\phi_1^* = \arccos\left(2p_c^2 - 1\right) \qquad \phi_2^* = \arcsin\left(\frac{\Delta_1 + 2\Delta_2}{\sigma_c}\right), \qquad \alpha_{12}^* = \frac{\Delta_2 + 2\Delta_1}{2\sigma_c p_c \sqrt{1-p_c^2}} \qquad \alpha_{23}^* = 1 \qquad \alpha_{13}^* = 0$$

As with the previous set of equilibrium points, the spectrum of the Jacobian at this equilibrium point is not easily found. Therefore, a similar approach as before will be taken. First, the conditions for stability will be

determined. Then it will be reasoned which equilibrium points may have a stable region, and which points are always unstable, by comparing the point to those analysed before.

In the previous set, it was found that the stability of the points (with two nonzero links), can be determined by considering each link apart, and take the appropriate conditions of the first two sets, as if the other links are zero. These conditions combined, gave the desired conditions for the equilibrium point as a whole. The same approach will be used here. It must be noted that all points in this set have $\alpha_{ij} = 1,\ 0 < \alpha_{jk} < 1$ and $\alpha_{ki} = 0$, with $i, j, k \in \{1,2,3\},\ i \neq j \neq k$.
First, the conditions of $\alpha_{ij} = 1$ are considered. In set 1, it was found that the restricting conditions then originate from $p_c < p_{jk},\ p_{ki}$ and $p_{ij} < p_c$. The first two conditions imply $\alpha_{jk}, \alpha_{ki} = 0$, and the latter implies $\alpha_{ij} = 1$. Thus, $p_{ij} < p_c$ is selected as a stability condition for the equilibrium points in set 5. This implies a critical coupling strength, given by

$$\Sigma_{5,1,i} := \frac{\sigma_c \sin(\phi_i^*)}{2p_c\sqrt{1-p_c^2}} \tag{5.60}$$

with $\phi_i^*$ the phase difference appearing in the formula of $p_{ij}$. For stability, it must hold that $\sigma_c < \Sigma_{5,1,i}$. Moreover, $\phi_i^*$ (and thus the point) is well defined, if $\sigma_c > f(\Delta_{i,j,k})$, with $f(\Delta_{i,j,k})$ the numerator of the argument of $\phi_i^* = \arcsin\left(\frac{f(\Delta_{i,j,k})}{\sigma_c}\right)$. It must be noted that $f(\Delta_{i,j,k})$ is also the numerator of $\Sigma_{5,1,i}$.

Next, the conditions due to the link obeying $0 < \alpha_{jk} < 1$ are considered. In the previous set for such links it is required that $\sigma_c > \Sigma_{5,2,j}$, with $\Sigma_{5,2,j}$ given by

$$\Sigma_{5,2,j} := \sigma_c \alpha_{jk}^* \tag{5.61}$$

Moreover, the link is well defined if $\sigma_c > g(\Delta_{i,j,k})$, where $g(\Delta_{i,j,k})$ is the numerator of the expression of $\alpha_{jk}^*$. It must be noted that $g(\Delta_{i,j,k})$ is also the numerator of $\Sigma_{5,2,j}$.

Thus, the point is well-defined, if $\sigma_c > g(\Delta_{i,j,k})$ and $\sigma_c > f(\Delta_{i,j,k})$. As $\Sigma_{5,2,j} < \sigma_c < \Sigma_{5,1,i}$, it must hold that $g(\Delta_{i,j,k}) < f(\Delta_{i,j,k})$ (as the critical strengths have the same denominator). Thus, the conditions equilibrium point is well defined if just $\sigma_c > f(\Delta_{i,j,k})$.

Now, the vanished link $\alpha_{ki}^*$ is studied. As was already mentioned in set 1, 2 and 3, a vanished link $\alpha_{ki}^*$ comes with an eigenvalue $\lambda = p_c - p_{ki}$. In other words, it must hold that:

$$2p_c^2 - 1 < \cos(\phi_k^*) \tag{5.62}$$

where $\phi_k$ is again the phase difference appearing in the formula of $p_{ki}$. As the other phase differences $\phi_{i,j}$ are already given, $\phi_k$ can be expressed in $\sigma_c$ and $p_c$. Therefore, this inequality can easily be solved numerically. As in set 2, this will imply a lower bound on $\sigma_c$ : $\sigma_c > h(p_c)$.

Using these observations, it can be deduced which points are never stable and which points may have a stable region. These deductions will be discussed briefly, as they are very similar to the conclusions of the previous set of equilibrium points.
The first and second equilibrium points ((5.25), (5.26)) of this set will never be stable. Assuming frequency dissasortativity, either $f(\Delta_{i,j,k})$ or $g(\Delta_{i,j,k})$ is negative. This would either imply $\sigma_c < \Sigma_{5,1,i} < 0$, or $\alpha_{jk} < 0$, which is not allowed.
However, the third and fourth point ((5.27), (5.28)) have a stable region if $\Delta_1 > \Delta_2 > 0$ or $\Delta_2 > \Delta_1 > 0$, respectively. Without loss of generality, a given system can be ordered, such that $\Delta_{1,2} > 0$, as described before.
It can be shown that the last two points of the set ((5.29), (5.34)), are never stable. The corresponding proof shows that either $f(\Delta_{i,j,k}) < g(\Delta_{i,j,k})$, or that $g(\Delta_{i,j,k}) < 0$. The first result implies that it is not possible to have $\Sigma_{5,2,j} < \sigma_c < \Sigma_{5,1,i}$. To obtain the latter result, frequency dissasortativity is again assumed, and it implies that $\alpha_{jk} \leq 0$.

### 5.6.3. Three links

#### Set 6

**Stability conditions**
The point is stable if

1. Equation (5.32) has a solution, i.e. $\phi_1$ is defined
2. $p_{12}, p_{23}, p_{13} < p_c$ (or: $\sigma_c < \Sigma_{6,1}, \Sigma_{6,2}, \Sigma_{6,3}$)

Moreover, a necessary bound is found: $\sigma_c > \frac{\max\{\Delta_1+2\Delta_2\ ;\ 2\Delta_1+\Delta_2\}}{2}$. This bound is also satisfied by all previous sets.

**Derivation**
This set contains one equilibrium point, given by (5.31) and below

$$\phi_2^* = \arcsin\left(\sin(\phi_1) + \frac{\Delta_2-\Delta_1}{\sigma_c}\right) \qquad \phi_1^* + \phi_2^* = \arcsin\left(\frac{2\Delta_1+\Delta_2}{\sigma_c} - \sin(\phi_1)\right) \qquad \alpha_{12}^* = \alpha_{23}^* = \alpha_{13}^* = 1$$

and where $\phi_1^*$ is found by

$$\frac{2\Delta_1+\Delta_2}{\sigma_c} = \sin(\phi_1)\left(1+\sqrt{1-\left(\frac{\Delta_2-\Delta_1}{\sigma_c}+\sin(\phi_1)\right)^2}+\sqrt{1-\sin^2(\phi_1)}\right)+\frac{\Delta_2-\Delta_1}{\sigma_c}\sqrt{1-\sin^2(\phi_1)}$$

By using the same approach as in the previous sets, it is expected that this equilibrium point is stable if $p_{12}, p_{23}, p_{13} < p_c$. Recall that this is the condition for a single link to be equal to 1.

However, the spectrum of the Jacobian matrix of this equilibrium point could also be determined analytically. The following eigenvalues are found:

$$\begin{aligned}
\lambda_1 &= -\sqrt{a^2-ab-ac+b^2-bc+c^2}-a-b-c \\
\lambda_2 &= \sqrt{a^2-ab-ac+b^2-bc+c^2}-a-b-c \\
\lambda_3 &= \sqrt{\frac{1+\cos(\phi_1^*)}{2}}-p_c \\
\lambda_4 &= \sqrt{\frac{1+\cos(\phi_2^*)}{2}}-p_c \\
\lambda_5 &= \sqrt{\frac{1+\cos(\phi_1^*+\phi_2^*)}{2}}-p_c
\end{aligned} \tag{5.63}$$

where $a = \frac{\sigma_c\cos(\phi_1^*)}{3}$, $b = \frac{\sigma_c\cos(\phi_2^*)}{3}$, $c = \frac{\sigma_c\cos(\phi_1^*+\phi_2^*)}{3}$. It can be shown that $a, b, c \geq 0$, and thus obviously $\lambda_1 < 0$, and $\lambda_2 = \sqrt{a^2-ab-ac+b^2-bc+c^2}-(a+b+c) = \sqrt{a^2-ab-ac+b^2-bc+c^2}-\sqrt{a^2+2ab+2ac+b^2+2bc+c^2} < 0$. Thus, $\lambda_1, \lambda_2 < 0$ do not provide any restrictions. The conditions for stability are given by $p_{12}, p_{23}, p_{13} < p_c$, and this corresponds to those predicted. The following critical coupling strengths are found (similar to (5.60)):

$$\Sigma_{6,1} := \frac{\sigma_c\sin(\phi_1^*)}{2p_c\sqrt{1-p_c^2}} \tag{5.64}$$

$$\Sigma_{6,2} := \frac{\sigma_c\sin(\phi_2^*)}{2p_c\sqrt{1-p_c^2}} \tag{5.65}$$

$$\Sigma_{6,3} := \frac{\sigma_c\sin(\phi_1^*+\phi_2^*)}{2p_c\sqrt{1-p_c^2}} \tag{5.66}$$

These curves can be found numerically, and the point is stable if $\sigma_c < \Sigma_{6,1-3}$. Moreover, the point must be well defined. To that extend, it is obliged $\left|\sin(\phi_1^*)+\frac{\Delta_2-\Delta_1}{\sigma_c}\right| \leq 1$ and $\left|\frac{2\Delta_1+\Delta_2}{\sigma_c}-\sin(\phi_1^*)\right| \leq 1$. This will give a

necessary condition for $\sigma_c$, in the following way:

Without loss of generality, the system can be ordered ($\Delta_1, \Delta_2 > 0$). Then, $\frac{2\Delta_1+\Delta_2}{\sigma_c} > 0$. Therefore, $-1 \leq \frac{2\Delta_1+\Delta_2}{\sigma_c} - \sin(\phi_1^*) \leq 1$ can be reduced to: $\frac{2\Delta_1+\Delta_2}{\sigma_c} - \sin(\phi_1^*) \leq 1$, or: $\frac{2\Delta_1+\Delta_2}{\sigma_c} \leq 1 + \sin(\phi_1^*) \leq 2$. Thus the first lower bound is given by $\sigma_c > \frac{2\Delta_1+\Delta_2}{2}$.
Moreover, by adding the inequalities: $-1 \leq \frac{2\Delta_1+\Delta_2}{\sigma_c} - \sin(\phi_1^*) \leq 1$ and $-1 \leq \sin(\phi_1^*) + \frac{\Delta_2-\Delta_1}{\sigma_c} \leq 1$, it is obtained: $-2 \leq \frac{2\Delta_1+\Delta_2+\Delta_2-\Delta_1}{\sigma_c} = \frac{\Delta_1+2\Delta_2}{\sigma_c} \leq 2$. Thus, the second lower bound yields: $\frac{\Delta_1+2\Delta_2}{2} \leq \sigma_c$. It can be concluded, that a necessary condition that must be satisfied is given by

$$\sigma_c > \frac{\max\{\Delta_1 + 2\Delta_2 \; ; \; 2\Delta_1 + \Delta_2\}}{2} \tag{5.67}$$

It must be noted that this condition is also satisfied by all previous points!

### Set 7

**Stability conditions**
It is found that this point is always unstable.

**Derivation**
The next equilibrium point is given by (5.33), or by:

$$\phi_1^* = \phi_2^* = \tfrac{2}{3}\pi, \quad \phi_1^* + \phi_2^* = \tfrac{4}{3}\pi \qquad \alpha_{23}^* = \frac{2(\Delta_2 - \Delta_1)}{\sigma_c\sqrt{3}} + \alpha_{12} \qquad \alpha_{13}^* = \alpha_{12} - \frac{2(2\Delta_1 + \Delta_2)}{\sigma_c\sqrt{3}}$$

with $p_c = \frac{1}{2}$.

Again, the spectrum of the (simplified) Jacobian matrix is not so straightforward. However it is noted that this equilibrium point is only well defined for a specific value of $p_c$, such that it is not possible to obtain a region of stability as before, but only an interval of values of $\sigma_c$ such that this point is stable. Moreover, it is noted that $p_c < \frac{1}{\sqrt{2}}$, and therefore it is expected that this point will not be stable. Indeed, for various values of $\Delta_{1,2}$, there are no values of $\sigma_c$ found such that this point is stable.

## Set 8

**Stability conditions**
The first equilibrium point (with additional term $-2(2p_c^2-1)$ for the link) has a stable region. If a given system is ordered ($\Delta_1, \Delta_2 \geq 0$), this region is given by:

1. $\max\{\Sigma_{8,1,i}, \Sigma_{8,2,j}\} < \sigma_c < \min\{\Sigma_{8,3,i}, \Sigma_{8,4,j}\}$ ((5.68),(5.69),(5.70),(5.71))
2. $\sqrt{a^2-ab-ac+b^2-bc+c^2}-a-b-c<0$, with $a=\frac{\sigma_c\alpha_{12}\cos(\phi_1^*)}{3}$, $b=\frac{\sigma_c\alpha_{23}\cos(\phi_2^*)}{3}$, $c=\frac{\sigma_c\cos\alpha_{13}(\phi_1^*+\phi_2^*)}{3}$. This is an approximated boundary.

Moreover, $\max\{\Sigma_{8,1,i}, \Sigma_{8,2,j}\} < \sigma_c$ again implies $\sigma_c > \frac{\max\{\Delta_1+2\Delta_2\ ;\ 2\Delta_1+\Delta_2\}}{2}$.

**Derivation**
The set of equilibrium point is given by (5.35)-(5.37). The first equilibrium point is given by

$$\phi_1^* = \phi_2^* = \arccos\left(2p_c^2-1\right), \quad \alpha_{12}^* = \frac{2\Delta_1+\Delta_2}{2\sigma_c p_c\sqrt{1-p_c^2}} \pm 2(2p_c^2-1) \quad \alpha_{23}^* = \frac{2\Delta_2+\Delta_1}{2\sigma_c p_c\sqrt{1-p_c^2}} \pm 2(2p_c^2-1) \quad \alpha_{13}^* = 1$$

All points in this set have two links $0<\alpha_{ij},\alpha_{jk}<1$ and one link $\alpha_{ki}=1$. Again, the spectrum of the Jacobian matrix is hard to analyse, so a different approach is desired. However, it must be noted, that the structure of these links is different from those in set 1 and 2, and not all conditions can be copied from the these sets.

First it is stated, that only the equilibrium points with the additional terms $\pm 2(2p_c^2-1)$ may have a stable region. It can be assumed that in order to have $\alpha_{ki}=1$, it is obliged to have $p_{ki}<p_c$. The points without the additional terms, have for the phase difference $\phi_k^*$ appearing in $p_{ki}$, that $\phi_k^*=0$. This implies $1<p_c$, but $p_c$ is restricted to the unit interval. Only the points with additional terms are thus considered.

First, the links $0<\alpha_{ij},\alpha_{jk}<1$ are studied. Still, the lower bounds $\sigma_c>\sigma_c\alpha_{ij}$ and $\sigma_c>\sigma_c\alpha_{jk}$ seem to be reasonable, as these imply $\alpha_{ij},\alpha_{jk}<1$. For the first equilibrium point (with $-2(2p_c^2-1)$), and for $p_c>\frac{1}{2}$, these bounds can be rewritten to the critical coupling strengths

$$\Sigma_{8,1,i} := \frac{2\Delta_1+\Delta_2}{2(1+2(2p_c^2-1))p_c\sqrt{1-p_c^2}} \tag{5.68}$$

$$\Sigma_{8,2,j} := \frac{\Delta_1+2\Delta_2}{2(1+2(2p_c^2-1))p_c\sqrt{1-p_c^2}} \tag{5.69}$$

where $\alpha_{ij,jk}<1$, if $\sigma_c>\Sigma_{8,1,i},\Sigma_{8,2,j}$, or $\sigma_c>\max\{\Sigma_{8,1,i},\Sigma_{8,2,j}\}$. Note that for $p_c<\frac{1}{2}$, the term $2(1+2(2p_c^2-1)$ becomes negative, and therefore the inequality sign flips (as solving for $\sigma_c$ implies dividing by this term), implying that $\sigma_c$ is negative. Therefore, $p_c>\frac{1}{2}$. Moreover, it easily shown that this boundary again implies $\sigma_c>\frac{\max\{\Delta_1+2\Delta_2\ ;\ 2\Delta_1+\Delta_2\}}{2}$. This is the lower bound for $\sigma_c$ found in the previous point.

However, these critical coupling strengths will not be sufficient. It must be noticed that due to the additional term, $\alpha_{ij,jk}$ may become smaller than 0. Therefore, critical coupling strengths must be introduced, such that $\alpha_{ij,jk}>0$. Solving this inequality yields the following critical coupling strengths:

$$\Sigma_{8,3,i} := \frac{2\Delta_1+\Delta_2}{4(2p_c^2-1)p_c\sqrt{1-p_c^2}} \tag{5.70}$$

$$\Sigma_{8,4,j} := \frac{\Delta_1+2\Delta_2}{4(2p_c^2-1)p_c\sqrt{1-p_c^2}} \tag{5.71}$$

where the link is well defined if $\sigma_c<\Sigma_{8,3,i},\Sigma_{8,4,j}$, or just $\sigma_c<\min\{\Sigma_{8,3,i},\Sigma_{8,4,j}\}$. Obviously, these critical coupling strengths must be positive. Note that for $p_c<\frac{1}{\sqrt{2}}$, the inequality sign would flip. However, seen all previous sets of equilibrium point, it is a save guess to assume $p_c>\frac{1}{\sqrt{2}}$.
As $\alpha_{13}$ is the strongest link, it is expected that the frequencies of the corresponding oscillators are most distant. Thus, a given system must be order from lowest to largest frequency to have positive critical coupling

strength.

Now the link $\alpha_{ki} = 1$ is considered. In the sets before, this implied a critical coupling strength: $\sigma_c < \frac{\sigma_c \sin(\phi_1^*)}{2p_c\sqrt{1-p_c^2}}$. Note that this was the result of $p_{ki} < p_c$, where the phase difference appearing in $p_{ki}$ is given by $\phi_i^* = \arcsin(\frac{f(\Delta_1,\Delta_2(,p_c))}{\sigma_c})$. However, for this point $\phi_1^*$ is not in this form, so this critical coupling strength can not be used. For point 1, $\phi_1^* + \phi_2^* = 2\arccos(2p_c^2 - 1)$. Solving $p_{ki} < p_c$, then yields (for $p_c > \frac{1}{\sqrt{2}}$): $2p_c^2 - 1 < p_c$, and this is alwasy true in the given interval.

As in the previous set, the stability can also be determined by evaluating the eigenvalues of the Jacobian matrix of the equilibrium point at each $(p_c, \sigma_c)$. The region where all eigenvalues have real nonpositive part, is shown in the right panel of 5.7. The lower curve is given by $\max\{\Sigma_{8,1,i}, \Sigma_{8,2,j}\}$, the upper curve is given by $\min\{\Sigma_{8,3,i}, \Sigma_{8,4,j}\}$, and the vertical line is given by $p_c = \frac{1}{\sqrt{2}}$. The left panel shows what is expected from the reasoning above.

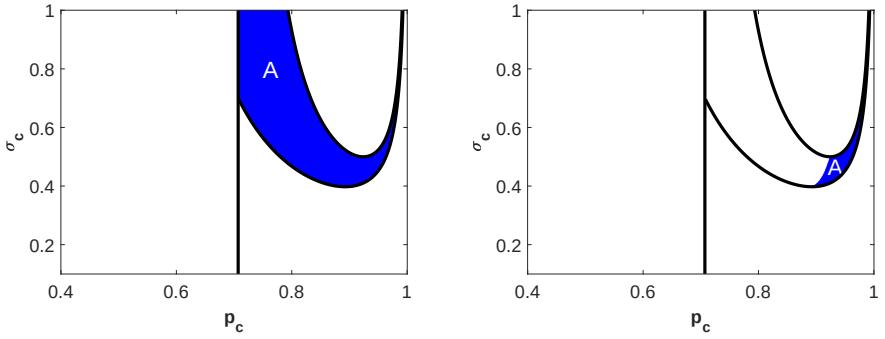


(a) (b)

**Figure 5.7.** Stable region of the first equilibrium point of set 8 for $\Delta_1 = 0.1$ and $\Delta_2 = 0.3$. In a) the stable region bounded by reasoned conditions, and in b) the numerical determined stable region. It is clear that one condition is still missing

It is shown that the two curves are indeed very accurate. However, it is clear that one condition is missing, resulting in a largely overestimation of the region of stability. This last condition can not be found analytically, but it is possible to make an estimate, by observing the previous eigenvalues:
First, define $a = \frac{\sigma_c \alpha_{12}\cos(\phi_1^*)}{3}$, $b = \frac{\sigma_c \alpha_{23}\cos(\phi_2^*)}{3}$, $c = \frac{\sigma_c \cos\alpha_{13}(\phi_1^*+\phi_2^*)}{3}$. In the case that there are three links equal to 1, it was found $\lambda = \sqrt{a^2 - ab - ac + b^2 - bc + c^2} - a - b - c$. By taking a look at the Jacobian, this is explained by noting that the terms $\frac{\alpha_{ij}(1-\alpha_{ij})\sin(\phi_i)}{2\sqrt{2+2\cos(\phi_i)}}$ vanish. Now it is noted that the term corresponding to $\alpha_{13}$ also vanishes, and that the terms corresponding to $\alpha_{23}, \alpha_{13}$ are relatively small in the overestimated region $A$ of figure 5.7. For $\Delta_1 = 0.1, \Delta_2 = 0.3$, these terms have values of $\pm 0.01$, while for example the term $(p_c - p_{13})(1 - 2\alpha_{13}$ is more than 10 times as big. Therefore, the terms are approximated by 0, resulting in the eigenvalue $\lambda = \sqrt{a^2 - ab - ac + b^2 - bc + c^2} - a - b - c$.

In Figure 5.8, the stable region of the first equilibrium point is shown for different values of $\Delta_1$ and $\Delta_2$ (upper row panels: $\Delta_1 = 0.1, \Delta_2 = 0.3$, middle row panels $\Delta_1 = 0.15, \Delta_2 = 0.25$, bottom row panels $\Delta_1 = \Delta_2 = 0.2$). The left panels are the stable regions found by implementing this extra condition $\lambda < 0$. The right panels show again the regions where all eigenvalues of the Jacobian matrix at the first equilibrium point are nonpositive. It is clear that the condition $\lambda < 0$ is not the exact condition, and slightly underestimates the stable region. However, it can be said that it is a good approximation.

$\Delta_1 = 0.10$,
$\Delta_2 = 0.30$

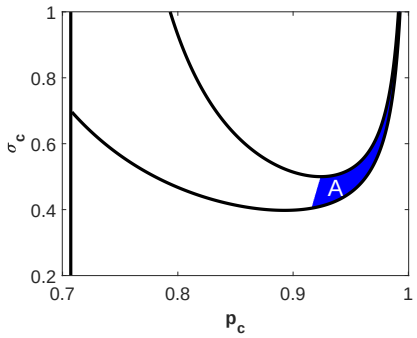


(a)

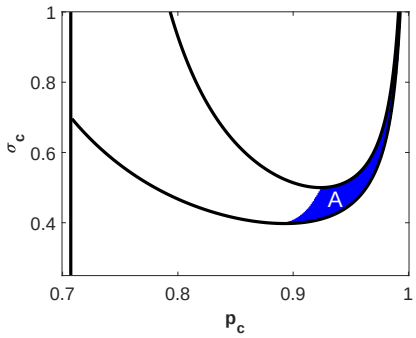


(b)

$\Delta_1 = 0.15$,
$\Delta_2 = 0.25$

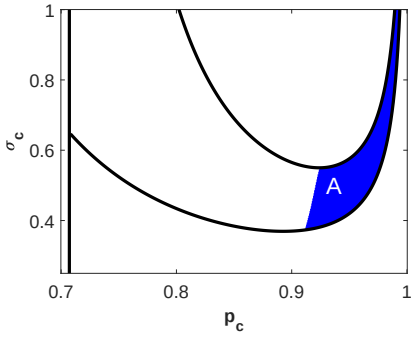


(c)

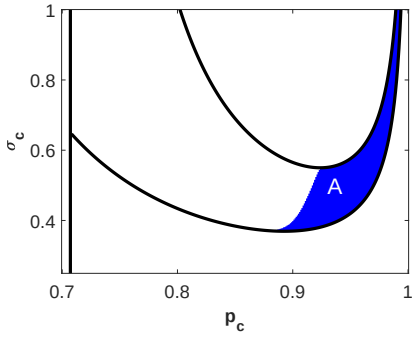


(d)

$\Delta_1 = 0.20$,
$\Delta_2 = 0.20$

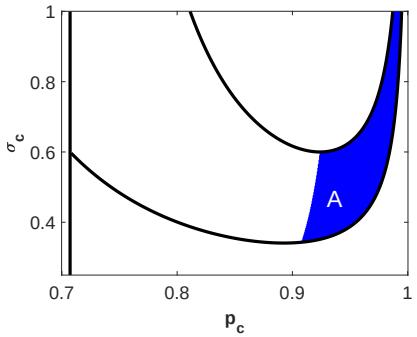


(e)

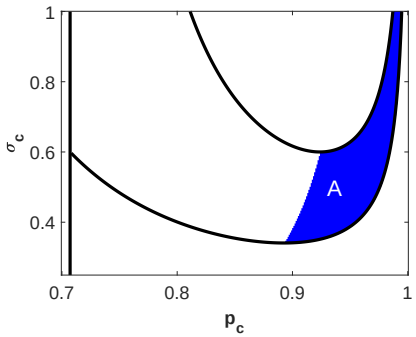


(f)

**Figure 5.8.** Stable region of the first equilibrium point of set 8 for $\Delta_1 = 0.1$ and $\Delta_2 = 0.3$. In a) the reasoned stable region, and in b) the numerical determined stable region.

Finally, it is noted that the first equilibrium point with: $+2(2p_c^2 - 1)$ as additional term is always unstable. The same holds for (all variants of) the second and third equilibrium point. The term $+2(2p_c^2 - 1)$ pushes the weight of the link out of the unit interval.

### Set 9

**Stability conditions**
The first and second equilibrium point may have a stable region. If a given system is ordered ($\Delta_1, \Delta_2 \geq 0$), then the points are stable if:

1. $\Sigma_{9,3,k} < \sigma_c < \Sigma_{9,2,i}, \Sigma_{9,2,j}$ ((5.72),(5.73),(5.74))
2. $\sqrt{a^2 - ab - ac + b^2 - bc + c^2} - a - b - c < 0$, with $a = \frac{\sigma_c \alpha_{12} \cos(\phi_1^*)}{3}$, $b = \frac{\sigma_c \alpha_{23} \cos(\phi_2^*)}{3}$, $c = \frac{\sigma_c \cos\alpha_{13}(\phi_1^* + \phi_2^*)}{3}$. This is an approximated boundary.
3. For the first point, $\Delta_2 > \Delta_1$ and equation (5.39) is satisfied ($\phi_2^*$ is defined)
4. For the second point, $\Delta_1 > \Delta_2$ and equation (5.41) is satisfied ($\phi_1^*$ is defined)

Moreover, it is numerically found that again $\sigma_c > \frac{\max\{\Delta_1 + 2\Delta_2\ ;\ 2\Delta_1 + \Delta_2\}}{2}$.

**Derivation**
The set of equilibrium points is given by (5.38)-(5.42). The first point is given by

$$\phi_1^* = \arccos(2p_c^2 - 1) \qquad \alpha_{12}^* = \frac{\Delta_1 - \Delta_2 + \sigma_c \sin(\phi_2^*)}{2\sigma_c p_c \sqrt{1 - p_c^2}} \qquad \alpha_{23}^* = \alpha_{13}^* = 1$$

where $\phi_2^*$ can be found by solving

$$\frac{2\Delta_2 + \Delta_1}{\sigma_c} = 2p_c^2 \sin(\phi_2^*) + 2p_c \sqrt{1 - p_c^2} \cos(\phi_2^*)$$

All points in this set thus have two links $\alpha_{ij}, \alpha_{jk} = 1$ and one link $0 < \alpha_{ki} < 1$. Again, each link is treated apart, as if it is the only nonzero link. Thus, the critical coupling strengths are given by

$$\Sigma_{9,1,i} := \frac{\sigma_c \sin(\phi_i^*)}{2p_c \sqrt{1 - p_c^2}} \tag{5.72}$$

$$\Sigma_{9,2,j} := \frac{\sigma_c \sin(\phi_j^*)}{2p_c \sqrt{1 - p_c^2}} \tag{5.73}$$

$$\Sigma_{9,3,k} := \sigma_c \alpha_{ki} \tag{5.74}$$

and for stability, it must hold that $\Sigma_{9,3,k} < \sigma_c < \Sigma_{9,1-2,i-j}$. These conditions originate from the requirements $p_{ij}, p_{jk} < p_c$ and $\alpha_{ki} \leq 1$. These boundaries can only be solved numerically. As in the previous set of equilibrium points, it is found that these conditions only are not enough: the region of stability is then somewhat overestimated. Again, define $a = \frac{\sigma_c \alpha_{12} \cos(\phi_1^*)}{3}$, $b = \frac{\sigma_c \alpha_{23} \cos(\phi_2^*)}{3}$, $c = \frac{\sigma_c \cos\alpha_{13}(\phi_1^* + \phi_2^*)}{3}$. Then the last condition is approximated by $\sqrt{a^2 - ab - ac + b^2 - bc + c^2} - a - b - c < 0$. This again results in a slightly underestimated region of stability, similar to the previous set.
It is found that the first equilibrium point is stable, if $\Delta_2 > \Delta_1$, whereas the second point is stable, if $\Delta_1 > \Delta_2$. Note that this also implies that the weakest link occurs between the two oscillator whose frequencies are the closest. The third point of the set is never stable.

Moreover, it is numerically found that again $\sigma_c > \frac{\max\{\Delta_1 + 2\Delta_2\ ;\ 2\Delta_1 + \Delta_2\}}{2}$.

## 5.7. Bifurcation Diagram

In this section, the bifurcation diagram shown in Figure 5.1 is reconsidered, and studied more extensively. The bifurcation diagram is shown in Figure 5.9. In the left panel, the stable regions are determined by computing the eigenvalues of the Jacobian at each equilibrium point and at each $(p_c, \sigma_c)$. The right panel shows the regions of stability using the conditions that were found for each point in the previous section. Again, the different colors represent different (stable) equilibrium points. In the following, all equilibrium points and their region of stability will be discussed.

As $\Delta_1 \neq \Delta_2$, it immediately follows that points of the first two sets are always unstable. It was already shown that set 3 is always unstable. However the fourth set has a stable point. As $\Delta_2 > \Delta_1$, this the third point of this set ((5.24), $\alpha_{12} = 0, 0 < \alpha_{23,13} < 1$). This point is stable in region $A$, that is given by $\sigma_c > \frac{0.5}{2p_c\sqrt{1-p_c^2}}$ and $p_c > \frac{1}{\sqrt{2}}$. The left panel confirms these boundaries (as was also shown in the previous section).
Moreover, it is expected that the fourth point of set 5 ((5.28), $\alpha_{12} = 0, 0 < \alpha_{23} < 1, \alpha_{13} = 1$) is stable in region $B$, given by $0.5 < \sigma_c < \frac{0.5}{2p_c\sqrt{1-p_c^2}}$, $p_c > \frac{1}{\sqrt{2}}$ and $p_c < p_{12}$. The left panel again confirms these boundaries.
The point where all links have maximal value (set 6, (5.31)), $\alpha_{12} = \alpha_{23} = \alpha_{13} = 1$) is stable if $p_{12}, p_{23}, p_{13} < p_c$. This region is given by $E$, and again this region is the same for the left and right panel.
Obviously, set 7 is always unstable and is therefore not considered.
In region $C$ the first point of set 8 is stable ((5.35), ). This region is enclosed by $\frac{0.7}{2(1+2(2p_c^2-1))p_c\sqrt{1-p_c^2}} < \sigma_c < \frac{0.5}{4(2p_c^2-1)p_c\sqrt{1-p_c^2}}$, and estimated boundary $\sqrt{a^2-ab-ac+b^2-bc+c^2}-a-b-c<0$, with $a = \frac{\sigma_c\alpha_{12}\cos(\phi_1^*)}{3}$, $b = \frac{\sigma_c\alpha_{23}\cos(\phi_2^*)}{3}$, $c = \frac{\sigma_c\cos\alpha_{13}(\phi_1^*+\phi_2^*)}{3}$. Comparing the left and right panel shows that this boundary results in a less curved (left) boundary of $C$, as was already highlighted in the previous section.
The first point of set 9 ((5.38), $0 < \alpha_{12} < 1, \alpha_{23} = \alpha_{13} = 1$) has a stable region. This is region $D$, and it is given by $\sigma_c\alpha_{12} < \sigma_c < \frac{\sigma_c\min\{\sin(\phi_1);\sin(\phi_1+\phi_2)\}}{2p_c\sqrt{1-p_c^2}}$ and the same estimated boundary $\sqrt{a^2-ab-ac+b^2-bc+c^2}-a-b-c<0$ as for set 8. Again, it is shown that region $D$ is slightly underestimated by this boundary. Finally, in the regions $F1, F2$ no equilibrium point is stable. In the region $F2$ (where $p_c > \frac{1}{\sqrt{2}}$), it is expected that the weight of the links will tend the maximum value 1, which is not enough for synchronizing the oscillators (just as with 2 oscillators). In region $F1$, the weight of the links will tend to 0, resulting in 3 disconnected oscillators.

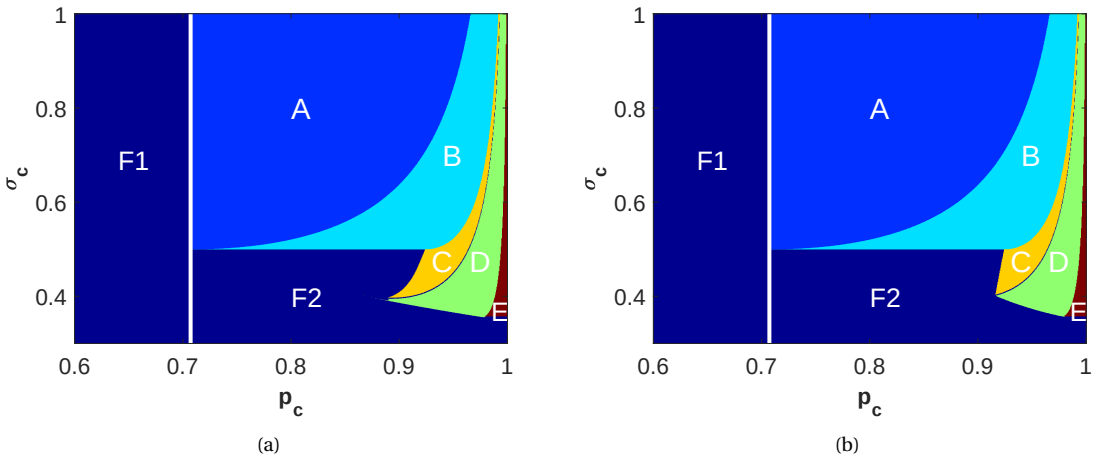


**Figure 5.9.** Stability diagram of all the equilibrium points of the network (with $\Delta_1 = 0.1, \Delta_2 = 0.3$. In a) these regions are determined by computing the eigenvalues of the Jacobian at each equilibrium point and at each $(p_c, \sigma_c)$), whereas in b) the (estimated) conditions for stability are used.

Thus, although regions $C$ and $D$ are slightly underestimated, the right panel is in general a very accurate representation of the stability of the points. Obviously, analyzing networks using such stability conditions is much more efficient than computing the spectrum of the Jacobian for each equilibrium point and each combination of parameters. Therefore, the results of the stability conditions were used in the comparison with the simulated network. The asymptotic values of the characteristics of the network at $(p_c, \sigma_c)$ are obviously the asymptotic values of the equilibrium point that is stable at $(p_c, \sigma_c)$.

## 5.8. Conclusion

To conclude, the analysis of the network of three oscillators revealed that for oscillators $i$ and $j$, the value of the link connecting these oscillators does not only depend on the properties of these two oscillators only, but on all $\Delta_i$ of the network. The most important and interesting rules that were found are

1. $p_{ij} < p_c$, then $\alpha_{ij} = 0$ and this occurs for $\sigma_c > f(p_c, \Delta_1, \Delta_2)$.
2. $p_{ij} = p_c$, then $\alpha_{ij} = g_1(p_c, \sigma_c, \Delta_1, \Delta_2)$ and this occurs for $g_2(p_c, \Delta_1, \Delta_2) < \sigma_c < g_3(p_c, \Delta_1, \Delta_2)$.
3. $p_{ij} > p_c$ then $\alpha_{ij} = 1$ and this occurs for $\sigma_c < h(p_c, \Delta_1, \Delta_2)$.
4. If $|\omega_i - \omega_j| > |\omega_j - \omega_k|$, then $\alpha_{ij} \geq \alpha_{jk}$ for all synchronous states.

It was found that the dynamics of this network in general has the same structure in parameter space as the complex network ($N = 300$). Therefore it may be suggested that these rules also capture the dynamics of a network of $N$ oscillators. The dependence on $(\Delta_1, \Delta_2)$ in the functions is then expanded by dependence on $(\Delta_1, \Delta_2, \ldots, \Delta_{N-1})$. More details on these functions ($f, g_1, g_2, g_3$ and $h$) can be found in the stability analysis.

Moreover, a lower bound on $\sigma_c$ ((5.67)) for the existence of possible synchronized solutions is found. Comparing this to the known lower bound for finite networks (2.9) reveals that these lower bounds are equal if $\Delta_1 = \Delta_2$. However, if $\Delta_1 \neq \Delta_2$, it can be shown that the lower bound found in this study is larger then the known lower bound. In other words, in that case, the found lower bound is more accurate for a network of 3 oscillators.

Finally, the above analysis clearly reveals that even in the synchronous network ($R \approx 1$) links are pruned. Only where set 6 is stable, all links are equal to 1. In the regions $A, B, C$ and $D$ the network also synchronizes, but here links are weakened or vanish completely.

# 6

# Synchronization of chemical oscillators

## 6.1. Introduction

As was mentioned in the introduction of this thesis, the study of collective synchronization is of multidisciplinary importance in science. In this chapter, one of the many applications will be encountered: the synchronization of a population of chemical oscillators. This is based on the paper *Emerging Coherence in a Population of Chemical Oscillators* [38]. In this paper experiments are reported that experimental verify the Kuramoto model for such a population. That is, whether a phase transition occurs due to the global coupling in the population of chemical oscillators. It must be noted that this experiment is not repeated, although some of the figures are reproduced using the available data.

## 6.2. Experimental set-up

A schematic of the experimental set-up used in this paper is depicted in Figure 6.1. The system consists of an array of 64 nickel electrodes in sulfuric acid. The electrodes are connected to the potentiostat through random parallel resistors with mean resistance $R_p$ and a standard deviation of 21 Ω and a series resistor with resistance $R_s$.

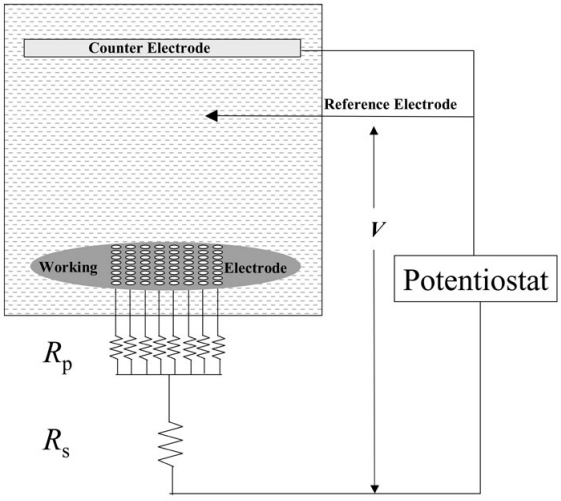


**Figure 6.1.** Schematic of experimental set-up. Reprinted from *Emerging Coherence in a Population of Chemical Oscillators*[38]

.

The contact of nickel and sulfuric acid initiates the anodic reaction of nickel, which is an electrochemical reaction and in general written as [39].

$$Ni \longrightarrow Ni^{2+} + 2e \tag{6.1}$$

The rate of the reaction, and thus of the nickel dissolution, depends on the applied potential at each electrode and is proportional to the current measured (on each electrode). In this experiment, the current is measured at a constant applied potential. It is known that this results in chaotic or periodic oscillations, depending on, for example, the concentration of the acid ([40]), or the applied potential [41]. As the surfaces of the nickel electrodes are obviously not all identical, the frequencies of the oscillators are distributed. During the experiment, the overall coupling strength $\sigma_c$ is varied. The value of $\sigma_c$ is controlled by varying $R_s, R_p$, while the total resistance $R_{tot} = R_s + \frac{R_p}{64}$ is kept constant. To be more specific, $\sigma_c$ is given by

$$\sigma_c := \frac{R_s}{R_{tot} - R_s} \tag{6.2}$$

In must be noted that this is not an adaptive network, thus the strength of the coupling is equal for all oscillators (=$\sigma_c$ ).

In order to determine the global synchronization $R(t)$ of the system, the individual phases of the oscillators must be known. A widely used method in signal processing to define the phase of a signal is based on the Hilbert Transform (HT) [42, 43]. In this approach, the analytic signal $\psi(t)$ is determined. This is a unique complex time function associated to a signal $s(t)$, defined by [44]

$$\psi(t) = s(t) + i\bar{s}(t) = A(t)e^{i\phi(t)} \tag{6.3}$$

where $\bar{s}(t)$ is given by the Hilbert Transform of $s(t)$

$$\bar{s}(t) = H(s(t)) := \frac{1}{\pi}\int_{-\infty}^{\infty} \frac{s(\tau)}{\tau - t} d\tau \tag{6.4}$$

The argument $\phi(t)$ of the complex time function $\psi(t)$ is the phase of the signal.

The signal of the chemical oscillators is given by

$$s(t) = I(t) - \langle I \rangle \tag{6.5}$$

where $I(t)$ the measured current at time $t$ and $\langle I \rangle$ the temporal mean of $I$, such that the signal is symmetric around $s = 0$. The complex time function is thus given by $\psi(t) = (I(t) - \langle I \rangle) + i\,H(I(t) - \langle I \rangle)$.

The global synchronization $R(t)$ is now defined by [38]

$$R(t) := \frac{|\sum_{k=1}^{64} \psi_k(t)|}{\sum_{k=1}^{64} |\psi_k(t)|} \tag{6.6}$$

where $\psi_k(t)$ is the complex time function of oscillator $k$. This definition is quite similar to the order parameter introduced by Kuramoto, in equation (2.5). In the study it is experimentally verified that this specific definition of $\phi(t)$ and $R(t)$ do not affect the results [38].

## 6.3. Results

First, the dynamics are shown of uncoupled periodic oscillators, i.e. $\sigma_c = 0$. In the experiment, it was found that the natural frequency distribution is unimodal with mean $f = 0.4526$ Hz and a standard deviation of $\sigma = 6.54$ mHz. A similar set of frequencies is reproduced. In Figure 6.2 a histogram of the natural (angular) frequencies is shown of this set, where $\omega = 2\pi f$.

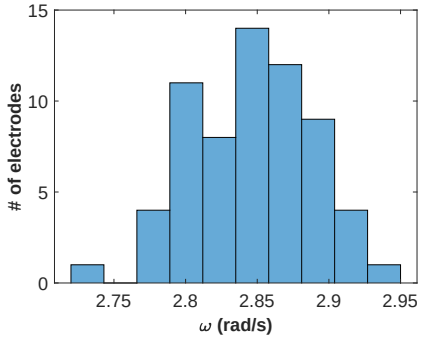


**Figure 6.2.** A histogram of the set of natural (angular) frequencies of the 64 electrodes, that are unimodal distributed with mean $f = 0.4526$ Hz and a standard deviation of $\sigma = 6.54$ mHz.

The time series of $I(t)$ of the second and third electrodes are given in the paper. This data is extracted from the plot to estimate the phase shift $\phi_I$ between the current of two electrodes, the amplitude $A$ and temporal mean $\langle I \rangle$ of the signal, such that $I(t)$ can be modelled as $I(t) = \langle I \rangle + A\sin(\omega t + \phi_I)$. It must be noted that $\phi_I$ is not the phase of the signal, as defined in (6.3). It is estimated that $A \approx \frac{1}{12.5}$ mA, $\langle I \rangle = 0.165$ mA and $\phi_I \approx 3$ rad. In Figure 6.3(a) and 6.3(b) the extracted data versus the modelled (with estimated $A, \langle I \rangle, \phi_I$) is plotted for electrode 2 and 3, respectively. The frequencies are not exactly the same, caused by the separate executed unimodal distributions. In Figure 6.3(c) the modelled signals of the two electrodes are plotted in the same figure.

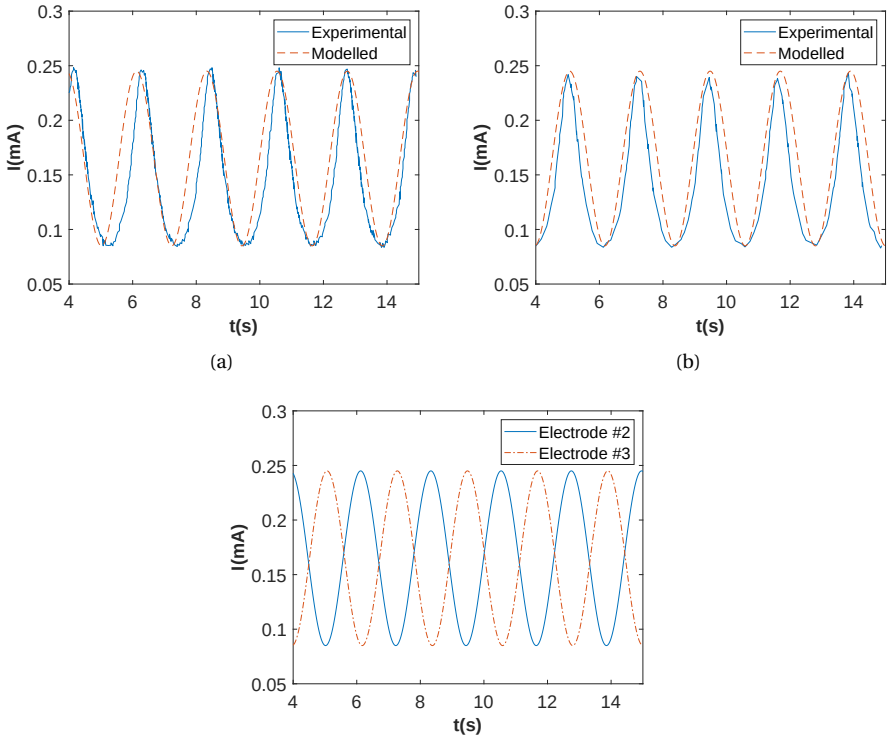


**Figure 6.3.** Times series of two electrodes. In a) and b) the experimental data is plotted vs. the modelled signals (with estimated $A, \langle I \rangle, \phi_I$) per oscillator. In c) the modelled signals of the two electrodes are plotted.

It now is assumed that all electrodes have the same $\phi_I (\approx 3$ rad) relative to the previous electrode, and that all electrodes have the same $A$ and $\langle I \rangle$, such that signals are constructed for all electrodes.

Figure 6.4 depicts a phase portrait snapshot of the 64 oscillators, i.e. the imaginary part $\bar{s}(t)$ is plotted against the real part $s(t)$ of the complex time function $\psi(t)$. The left panel shows the phase portrait of the modelled signal, and the right panels shows the phase portrait that is given in the paper (the data is directly extracted). The modelled data do not form a clear limit cycle, whereas the experimental data does.

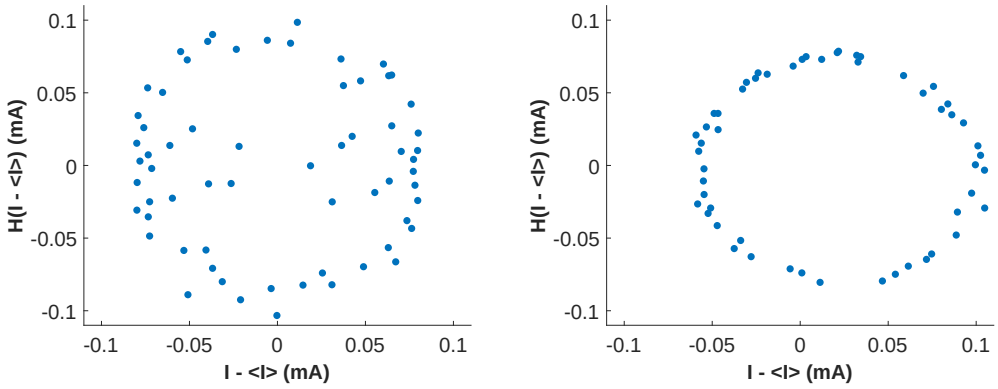


(a) (b)

**Figure 6.4.** Phase portrait snapshot of the 64 oscillators of a) the modelled signal and b) the experimental data

The global synchronization can be found as function of $t$ from these phase portraits, see equation (6.6). In Figure 6.5 $R(t)$ based on the modelled data (left panel) and based on the experimental data (right panel) is plotted. The data of the right panel is directly extracted from Figure 1C of the paper. Both figures reveal a similar trend, but the global synchronization is consistently underestimated for the modelled data.

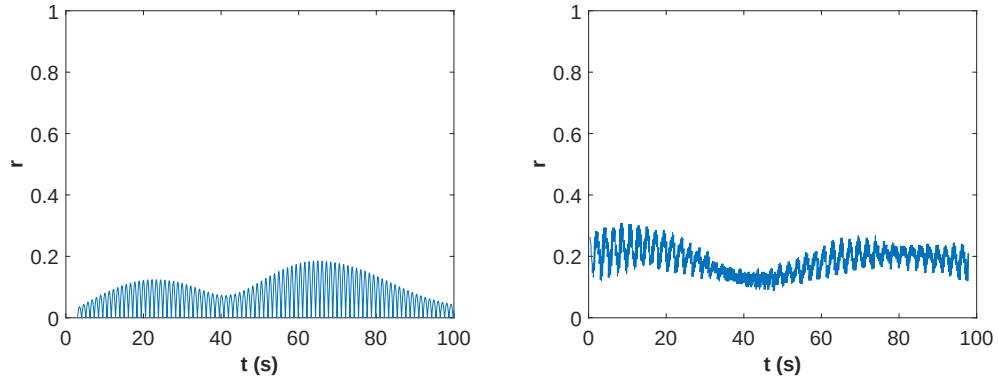


(a) (b)

**Figure 6.5.** Time series of the global synchronization $R$ for a) the modelled signal and b) the experimental data

From Figure 6.3 it can be concluded that the signals can indeed be modelled as sines with a nonzero amplitude, phase difference and temporal mean. However, from Figures 6.4 and 6.5 it can be concluded that the assumption that all electrodes have the same phase difference and temporal mean is incorrect. It would be more plausible to suggest that these parameters are also distributed. It is expected that this is also caused by heterogeneity's of the electrode surface, and therefore the distribution will be related to the distribution of the natural frequencies. It is clear that this relation is not known, and that the data of all electrodes is required rather than the time series of only two electrodes.

In particular, if the data is known of all electrodes and for different values of $\sigma_c$, then $R$ can be plotted as function of $\sigma_c$. Unfortunately, it was not possible to get in touch with the authors of the paper, to receive this data. As the paper originates from 2002, it is likely that the contact details are now outdated.

However, in the paper a characteristic similar to Figure 2.3 was found for the periodic (and chaotic) oscillators. Thus, the global coupling of these oscillators indeed causes a phase transition, such that some of the oscillators synchronize. This is exactly what the Kuramoto model predicts.

# 7

# Conclusion and discussion

In conclusion, in this work the Kuramoto model is discussed, and extended to an adaptive network by introducing adaptation rules, such that the strength of coupling can differ per pair of oscillators. The adaptation rules considered are the anti-Hebbian and Hebbian adaptation rules. The anti-Hebbian adaptation rule promotes(/weakens) links between oscillators that are in anti-phase(/in phase), while the Hebbian adaptation rule promotes(/weakens) links between oscillators that are in phase(/in anti-phase). The dynamics of large ($N = 300$) networks are studied for both rules. For both networks explosive synchronization (ES) is revealed. This phenomenon receives currently many attention in, among others, neuroscience. In particular, it is recently linked to seizures and anesthetic-induced unconsciousness [23, 24, 21].

In the **anti-Hebbian** network, link pruning occurs in the synchronous network, thereby preventing the existence of redundant links. It is found that the network organizes itself in such way, that *frequency dissasortativity* is observed, i.e. links occur between oscillators whose frequencies are most distant. Both the weakening or completely pruning of the links and the frequency dissasortativity are confirmed in a stability analysis of a simple network of 2 and 3 oscillators. The pruning of nodes is an important feature of an anti-Hebbian network. In the Introduction, it was mentioned that synchronization plays an important role in the brain [4], but that excessive synchronization may lead to epilepsy [5, 6, 21]. In previous studies it is shown that anti-Hebbian rules are important for the control of oversynchronization in the brain [45, 46]. This study may help understanding the dynamics and principles of link pruning.
In the stability analysis of 3 oscillators, some additional 'linking' rules were found, that determine the value of the weight of the link. It may be suggested that these nontrivial rules also capture the dynamics of the large network. Most importantly, the weight of the link between two oscillators and its stability depends not only on the properties of these two oscillators only, but on the properties of all the oscillators in the network.

In the **Hebbian** network link pruning only occurs only in the transition from the synchronous to the incoherent network. The opposite phenomenon of frequency dissasortativity is observed for the Hebbian network, although its presence is less significant. In the stability analysis of a simple Hebbian network with 2 oscillators, it was found that the weight of a link will always evolve to one of the extreme values, i.e. $\alpha = 1$ or $\alpha = 0$. It may be expected that in a network of 3 (or $N$) oscillators, only the equilibrium point with all $\alpha_{ij} = 1$ is stable.

Finally, a simple application of the Kuramoto oscillators was considered: the global coupling of chemical oscillators. Although the results of a previously preformed experiment could not be reproduced, as not all data was available, a real application of the model is shown. Indeed, in the experiment described, it was found that global coupling of chemical oscillators causes a phase transition, such that the oscillators synchronize.

The reliability of the results is impacted by the numerical method used to solve the differential equations (Modified Euler). In Chapter 3 an adaptive complex network with an anti-Hebbian and an Hebbian rule is studied. The network with an anti-Hebbian network is an reproduction of the study preformed in [21]. The obtained results confirm the results of this paper. However the dynamics of the largest component (Figure 3.3(a)) are slightly different, although it reveals the same trend as in the paper. It is assumed that this is caused by errors due to the Modified Euler method. In Chapters 4 and 5 similar problems arose in the comparison of

a simulated network with the asymptotic values. In the paper, RK4 is used to simulate the network. However, the implementation of RK4 caused a significant delay in computation time (even though a larger time step may be used), while in general, the method of Modified Euler gave almost exactly the same results. Therefore, Modified Euler is used in this study. Still, it would be plausible that a numerical method with a lower order error will result in more accurate results.

In further research, the dynamics of a network where a fraction of the oscillators have a Hebbian adaptation rule, and a fraction have an anti-Hebbian adaptation rule may be studied. It would also be interesting to extend the stability analysis to a network of $N$ Kuramoto oscillators, and verify whether the linking rules found in this study would still hold. In addtion, a stability analysis of a Hebbian network with 3 (or $N$) oscillators could be preformed, to test whether the equilibrium point with all links equal to 1 is indeed the only stable point. Finally, it would be interesting to investigate other applications of the adaptive network. This could be in the field of social networks. In this field it is known that some people are way more connected than others [47], it may be suggested that this can be modelled using frequency dissartotativity. Other examples may be found in economic flows, or ecological evolution, where synchronization is already observed [34].

# A

# Appendix

## A.1. MATLAB Codes

The computations in this study are executed in MATLAB on a High Performance Computing Cluster (HPC). In this section, the most essential MATLAB codes are be presented. Sometimes codes are used for multiple purposes, by making a few adjustments. These adjustments are indicated per code. It must be noted that codes of simple or less relevant calculations, codes that helped understanding the network (i.e. the computations are not included in this report), codes that sent assignments to the cluster or codes that construct figures are left out. If desired, all codes can be delivered.

### A.1.1. Simulation of the network, Macroscopic characteristics

The code below simulates a network of $N$ oscillators, and computes the global synchronization $R$, total strength $S$, the largest component and the average degree $\langle k \rangle$. The method of Modified Euler is used to solve the differential equations. The function RK4 couldn't be implemented in this code. However, a similar code is written to solve the differential equations using RK4 (manually). With a small adjustment, the code can also be used for the Hebbian network. The code can also be used for a small network (2 or 3 oscillators). However, in this case, the characteristics in time (and their derivatives) are also saved (each 500 time steps), such that evolution in time can be considered.

```
%Input
N =300;                                     % number of coupled oscillators
omin=0.8;                                   % minimum value natural frequency
omax=1.2;                                   % maximum value natural frequency
sigmamin=0.2;                               % minimum value global coupling strength
sigmamax=1;                                 % maximum value global coupling strength
pcmin=0;                                    % minimum value correlation threshold
pcmax=0.4;                                  % maximum value correlation threshold
h=0.01;                                     % timestep
n=1500;                                     % number of timesteps
t=0:h:h*n;                                  % all timesteps
res=100;                                    % resolution of the heatmap (nxn)
tau=0.8;                                    % link threshold
M=4;                                        % number of parallel nodes used hpc

%% Create vectors
sigmac=sigmamin:(sigmamax-sigmamin)/res:sigmamax;    % 1st tuning parameter (coupling
    strength)
pc=pcmin:(pcmax-pcmin)/res:pcmax;                    % 2nd tuning parameter (
    correlation threshold)
length2=numel(sigmac);                               % number of coupling strengths
length1=numel(pc);                                   % number of correlation thresholds
```

```
omega = omin+(omax-omin)*rand(N,1);                    % Natural frequancies of N
    oscillators, uniform distributed in [omin,omax]
theta=2*pi*rand(N,1).*ones(N,length1,length2);         % Initial value of the phase (same
     initial values for all different values of sigma, pc)

a=rand(N);                                             % NxN uniformly distributed values
     in [0,1]
a_lm=abs((a+a')/2-eye(N).*a);                          % Create initial weigthed matrix
    with weighted links (symmetric, hollow, uniformly distributed in [0,1])
a_lm=a_lm.*ones(N,N,length1,length2);                  % Set as initial weigthed matrix
    for all tuning parmaters

%% Time simulation - Modified Euler Method
parfor (k=1:length1,M)                                    % Use M parallel nodes
    for m=1:length2                                       % Time simulation of all values
         of pc, sigma
            for j=1:n
                fntheta=dtheta(omega,sigmac(1,m),N,a_lm(:,:,k,m),theta(:,k,m));
                                                  % f(t_n,w_n), dtheta is D.E. of theta
                fna_lm=da_lm(N,pc(1,k),theta(:,k,m),a_lm(:,:,k,m));
                                                    % f(t_n,w_n), da_lm is D.E.
                    of weight of link
                predtheta=theta(:,k,m)+h*fntheta;
                                                                          % predictor
                     of theta
                preda_lm=a_lm(:,:,k,m)+h*fna_lm;
                                                                           %
                    predictor of weight of link
                a_lm(:,:,k,m)=a_lm(:,:,k,m)+(h/2)*(fna_lm+da_lm(N,pc(1,k),predtheta,
                    preda_lm));           % approximation a_lm  (n+1)
                theta(:,k,m)=theta(:,k,m)+(h/2)*(fntheta+dtheta(omega,sigmac(1,m),N,
                    preda_lm,predtheta)); % approximation theta (n+1)
            end
        R(m,k)=(1/N)*abs(sum(exp(1i*theta(:,k,m))));    % Kuramoto order parameter
        S(m,k)=(sum(sum(a_lm(:,:,k,m))))/(2*N);         % Global Strength
    end
end
%% Construct Adjacency matrix
a_lmround=round(a_lm-(tau-0.5));                       % Constructing adjacency matrix
     (>tau --> 1, otherwise 0)

%% Calculate Largest Component (LC)
Nc=zeros(length2,length1);                             % Create matrix with value of
    Largest Component for (sigma,pc) (LC=300)
LC=zeros(length2,length1);                             % Create matrix with value of
    Largest Component for (sigma,pc) (LC/=300)
n0=zeros(length2,length1);                             % Algebraic multiplicity
    eigenvalue 0 for (sigma,pc)
n1=0;                                                  % number of elements connected
    to first element
conelemi=[1];

for m=1:length2                                                  % Determine LC
    for (sigma, pc)
    for j=1:length1
        di=sum(a_lmround(:,:,j,m),2);                            % Degree of
```

```
            each oscillator
        Delta=diag(di);                                                 % Degree matrix
        Q=Delta-a_lmround(:,:,j,m);                                     % Laplacian
        eigenvalues=round(eig(Q),5);                                    % Compute
            eigenvalues of Laplacian
        n0(m,j)=length(eigenvalues)-length(find(eigenvalues));          % Algebraic
            multiplicity eigenvalue 0
        if n0(m,j) == 1                                                 % 1 connected
            component -> LC=300
            Nc(m,j)=N;
        else
            Nl=zeros(n0(m,j),1);                                        % Create vector
                 with size of connected component 1, 2, ..., n0
            [Nl(1), conelemi]=component(a_lmround(:,:,j,m),1);          % Compute [size
                 of connected component 1, vector of oscillators part of component]
            Compare=2:1:N;                                              % Vector of all
                 oscillators in network (from 2 - N)
            connected=ismember(Compare,conelemi)-1;
            for i=2:n0
                connected=ismember(Compare,conelemi)-1;                 % Create
                    logical matrix - val=-1 if oscillator is not contained in a checked
                     component
                newrow=find(connected)+1;                               % Oscillators
                    that are not part of a checked component
                row=newrow(1);                                          % Select
                    oscillator in unchecked component (+1, as Compare starts from 2)
                [Nl(i),newcolomeni]=component(a_lmround(:,:,j,m),row);  % check new
                    component, [size connected component i, oscillators part of
                    component i]
                conelemi=[conelemi newcolomeni];                        % All
                    oscillators that are part of a checked connected component
            end
            LC(m,j)=max(Nl);                                            % Pick largest
                component
        end
    end
end
Largestcomponent=Nc+LC;                                                 % Largest
    component for all (sigma,pc)
%% Calculate average degree <k>
di=zeros(N,length2,length1);
averagedegree=zeros(length2,length1);
for m=1:length2
    for j=1:length1
        di(:,m,j)=sum(a_lmround(:,:,j,m),2);            % Degree of each oscillator
        averagedegree(m,j)=sum(di(:,m,j),1)/N;          % Average degree
    end
end

%% Output
save('LC_antiheb_n1500.mat','sigmac','pc','Largestcomponent','averagedegree','R','S')
    % Save macroscopic characteristics
save('network_antiheb.mat','a_lm','a_lmround','theta','omega','-v7.3')         % Save
    charateristics network

%% Functions
```

```
% Functions for time evoluation of the phase, weight of the link, and to
% find the size of each component
%% Differential equation for theta
function f=dtheta(omega,sigmac,N,a_lm,theta)                % Differential equation (D.
    E.) for phase theta
som=sum(a_lm.*sin(theta*ones(1,N)-ones(N,1)*theta'))';
f=omega+(sigmac/N)*som;
end
%% Differential equation a_lm
function g=da_lm(N,pc,theta,a_lm)                           %D.E. for weight of link
    a_lm
L=ones(N,1)*theta';                                         %defining matrices for
    theta_l en theta_m
M=theta*ones(1,N);
p_lm=0.5*abs(exp(1i*L)+exp(1i*M));                          %instantaneous phase
    correlation
g=(pc-p_lm).*a_lm.*(1-a_lm);
end
%% Function to find largest component
function [Nc,conelemi]=component(adjacency,row)             % Input (adjacency matrix
    of network, connected component with oscillator 'row' in it
n1=0;                                                       % Output [Size of component
    , oscillators in component]
conelemi=[find(adjacency(row,:))];                          % Vector with all
    oscillators connected to oscillator 'row'. (first design largest component)
    for k = 1:3
        n1=n1+1;
        n2=length(conelemi);                                % All oscillators connected
             to oscillator 'row' are checked for new connected oscillators
        for i=n1:n2
            row=conelemi(i);                                % Check oscillators that
                are connected to element i (element i connected to element 'row')
            conelem=find(adjacency(row,:));                 % Find all connections with
                 components
            if length(conelem)> 0
                conelemi=[conelemi conelem];                % Add connected oscillators
                     to component
                conelemi=unique(conelemi);                  % Delete copies
            end
        end                                                 % Repeat procedure (study
            the connectivity of discovered connected oscillators)
    end
        Nc=length(conelemi);                                % Size of component
end
```

### A.1.2. Microscopic characteristics

The microscopic characteristics of network can be computed easily from the data generated in the previous code. For the Hebbian network, other values of $p_c$ are used.
It is also possible to fix a natural frequency in a network, and compute the microscopic characteristics for this oscillator (after simulating the network), such that the characteristics are computed for all values of $\omega_i$. However, it was chosen to use the data from the previous code, such that the structure of a network is more clear, and to make sure that the circumstances are equal for all different values of $\omega_i$.

```
 clear all
 load('Nodestructure_ah_theta.mat') %See details below
%%
```

```
% Input data is:
% 3 adjacency-matrices for pc=0.61, pc=0.75 and pc=0.95 (and sigma=0.6 for all three)

% 3 vectors with the phases of the oscillators for pc=0.61, pc=0.75
% and pc=0.95 (and sigma=0.6 for all three

% Vector containing all natural frequencies
%% Standard information of network (could also be obtained from input)
omin=0.8;                   % Limits for plots
omax=1.2;

N=300;                      % Number of oscillators
pc=[0.61 0.75 0.95]

plots=length(pc);           % Number of plots

a_lmround(:,:,1)=alm_pc061; %pc = 0.61
a_lmround(:,:,2)=alm_pc075; %pc = 0.75
a_lmround(:,:,3)=alm_pc095; %pc = 0.95

theta(:,1,1)=mod(theta_pc_061_sig_06,2*pi); %pc = 0.61
theta(:,2,1)=mod(theta_pc_075_sig_06,2*pi); %pc = 0.75
theta(:,3,1)=mod(theta_pc_095_sig_06,2*pi); %pc = 0.95

%% Degree node
degreenode=sum(a_lmround,2);
%% Neighborhood detuning
neighborhood=zeros(N,plots);
connectedomega=zeros(N,1);
averageomega=zeros(N,1);
for k=1:plots
connectedomega=a_lmround(:,:,k)*omega;  %Create matrix with the nat. freq. of connected
     oscillators
averageomega=sum(connectedomega,2)./degreenode(:,1,k);  %Compute average nat. freq. <
    omega>
neighborhood(:,k)=omega-averageomega;   %Node neighborhood detuning for all oscillators
end
%% Connectivity of the network
omega_sort=sort(omega);
a_lm2=zeros(N,N,plots);
for h = 1:plots      % This for loop reorders the adjacency matrix, such that
    oscillator 1
    for i = 1:N      % has the lowest nat. freq., and oscillator N the largest nat.
        freq.
        for j = 1:N  % without changing the structure of the network
            result1 = find(omega_sort==omega(i));
            result2 = find(omega_sort==omega(j));
            a_lm2(result1,result2,h)=a_lmround(i,j,h);
        end
    end
end
```

### A.1.3. Stability analysis 3 oscillators

The next code is used to reveal the asymptotic characteristics of the network. The stability of each equilibrium point is given by the stability conditions that were found in chapter 5. For each equilibrium point the

characteristics are found by filling in the asymptotic values of phase difference and weight of the link or by solving analytical expressions for these variables. This code only works for $\Delta_1 < \Delta_2$. Similar codes are written for $\Delta_1 = \Delta_2$ and $\Delta_1 > \Delta_2$. These can also be combined, such that for any input, the output will be asymptotic characteristics of the network. For simplicity and compactness, only one case is given here.

Instead of using the stability conditions, a very similar code is written that computes the eigenvalues of the Jacobian at each equilibrium point (using the (solved) asymptotic values of the phase difference and weight of the link)

```
%% Network of 3 oscillators (AH)
% This code generates the bifurcation matrix, and all
% microscopic/macroscopic characteristics of a network of 3 oscillators,
% with 0<Delta1<Delta2
%%
clear all
%% Frequencies of the network (input)
omega1=0.8;
omega2=0.9;
omega3=1.2;

pcstart=0.4;        %xlimit of figure
sigmastart=0.1;     %ylimit of figure

%% Determine Delta1, Delta2
Delta1=omega2-omega1;
Delta2=omega3-omega2;
clearvars omega1 omega2 omega3 %Not relevant
%% Define variables
sigma=(sigmastart:0.0005:1)';   %all values of sigma
pc=(pcstart:0.0005:1);          %all values of pc

x=length(pc);
y=length(sigma);
z=length(sinphi);

hm=zeros(y,x);                  %Bifurcation matrix

sinphi=(0:0.0005:1)';       `   %possible values of sin(phi_1) (used to solve
    analytical implicit expressions)
sinphi1=zeros(y,1);
sinphi2=zeros(y,x)+10;
%% Set 1 - Only for Delta1=Delta2
%% Set 2 - Only for Delta1=Delta2
%% Set 3 - Not stable for any network
%% Set 4
% Delta1<Delta2
% Properties of the point
phi2=acos(2.*pc.^2-1);
phi12=phi2;
phi1=phi12-phi2;

a12=0;
a23=(Delta2-Delta1)./(2.*sigma*(pc.*sqrt(1-pc.^2))).*ones(y,x);
a13=(Delta2+2*Delta1)./(2.*sigma*(pc.*sqrt(1-pc.^2))).*ones(y,x);

%Stability
% Construct logical array of pc>1/sqrt(2)
```

```
lpc=pc>1/sqrt(2);

% Construct logical matrix of sigma > Maximum Critical Coupling Strength
MaxDelta=max(Delta2-Delta1,Delta2+2*Delta1);
CritSig=MaxDelta./(2.*(pc.*sqrt(1-pc.^2))).*ones(y,x);
lsigma=sigma.*ones(y,x)>CritSig;

% Bifurcation matrix (stable region)
hm4=lsigma.*lpc;
%  Characteristics
S4=hm4.*(a12+a23+a13)./(3-1); %Total Strength
Bif4=hm4.*0.5;                %Different colors for Bifurcation diagram
phi14=hm4.*phi1;              %value of phi1
R4=(1/3)*abs(exp(0)+exp(1i.*phi1)+exp(1i.*phi12)).*hm4; %The phase difference is given.
     Choose theta1=0, then theta2=phi1 and theta3=phi12

%% Set 5
% Delta1<Delta2
% Properties of the point
phi2=acos(2.*pc.^2-1);
phi12=asin((Delta2+2*Delta1)./sigma);
phi1=phi12-phi2;

a12=0;
a23=(Delta2-Delta1)./(2.*sigma*(pc.*sqrt(1-pc.^2))).*ones(y,x);
a13=1;

%Stability
% Construct logical array where p12>pc
p12=sqrt((1+cos(phi1))./2);
lp12=p12>pc;

% Construct logical matrix where sigma < Critical Coupling strength
% The Coupling Strength is the same as of point 4
lsigma=sigma.*ones(y,x)<CritSig;
lsigma2=MaxDelta<sigma;

% Construct logical array where pc>1/sqrt(2)
% This is the same lpc as of point 4

% Bifurcation matrix (stable region)
hm5=lsigma.*lsigma2.*lpc.*lp12;
%  Characteristics
S5=hm5.*(a12+a23+a13)./(3-1); %Total Strength
Bif5=hm5;                     %Different colors for Bifurcation diagram
phi15=hm5.*phi1;              %value of phi1
R5=(1/3)*abs(exp(0)+exp(1i.*phi1)+exp(1i.*phi12)).*hm5; %The phase difference is given.
     Choose theta1=0, then theta2=phi1 and theta3=phi12

%% Set 6
% Find smallest solution of sin(phi1) satisfying condition
for m = 1:y         %sigma
   for k = 1:z      %possible values of sin phi
    A = sinphi(k);
    term= ((Delta2-Delta1)/sigma(m)) + sinphi(k);
    B = sinphi(k)*sqrt(1-term^2);
```

```
    C = term*sqrt(1-sinphi(k)^2);
    D = (2*Delta1+Delta2)/sigma(m);
    condition= A + B + C - D ;              % Condition on phi_1
        if abs(condition)<10^-3             % Accuracy
            sinphi1(m)=sinphi(k);
            break
        end
   end
end
clearvars condition A B C D term

% Properties of the point
phi1=asin(sinphi1);
phi2=asin(sin(phi1)+(Delta2-Delta1)./sigma);
phi12=phi1+phi2;

a12=1;
a23=1;
a13=1;

% Stability
% Construct logical array where p12<pc
p12=sqrt((1+cos(phi1))./2);
lp12=p12.*ones(y,x)<pc.*ones(y,x);
% Construct logical array where p23<pc
p23=sqrt((1+cos(phi2))./2);
lp23=p23<pc.*ones(y,x);
% Construct logical array where p13<pc
p13=sqrt((1+cos(phi12))./2);
lp13=p13<pc.*ones(y,x);

% Bifurcation matrix (stable region)
hm6=lp12.*lp23.*lp13;
%  Characteristics
S6=hm6.*(a12+a23+a13)./(3-1); %Total Strength
Bif6=hm6.*3;                  %Different colors for Bifurcation diagram
phi16=hm6.*phi1;              %value of phi1
R6=(1/3)*abs(exp(0)+exp(1i.*phi1)+exp(1i.*phi12)).*hm6; %Choose theta1=0, then theta2=
    phi1 and theta3=phi12

%% Set 8

% Properties of the point
phi1=acos(2.*pc.^2-1);
phi2=phi1;
phi12=phi1+phi2;

a12=(2*Delta1+Delta2)./(2*sigma*pc.*sqrt(1-pc.^2))-2*(2.*pc.^2-1);
a23=(2*Delta2+Delta1)./(2*sigma*pc.*sqrt(1-pc.^2))-2*(2.*pc.^2-1);
a13=1;

%Stability

% Construct logical matrix where sigma < Critical Coupling strength
MinDelta=min(2*Delta2+Delta1,Delta2+2*Delta1);
CritSigMax=(MinDelta)./(2.*pc.*sqrt(1-pc.^2).*2.*(2.*pc.^2-1));
```

```
157 lsigma1=sigma<CritSigMax;
158
159 % Construct logical matrix where sigma > Critical Coupling strength
160 MaxDelta=max(2*Delta2+Delta1,Delta2+2*Delta1);
161 CritSigMin=(MaxDelta)./(2.*pc.*sqrt(1-pc.^2).*(1+2.*(2.*pc.^2-1)));
162 lsigma2=sigma>CritSigMin;
163
164 % Construct logical matrix where lambda < 0
165 a=(sigma*cos(phi1)).*a12./(3-1); %Matrix multiplications such that matrix has dimension
      y-by-x and element m,n has sigma(m)*cos(k)*a12(m,k)
166 b=(sigma*cos(phi2)).*a23./(3-1);
167 c=2.*(sigma*cos(phi12))./(3-1);
168 lambda=sqrt(a.^2-2*a.*b-2*a.*c+b.^2-2*b.*c+c.^2)-a-b-c;
169 llambda=lambda<0;
170
171 % Bifurcation matrix (stable region)
172 hm8=lsigma1.*lsigma2.*llambda;
173 %  Characteristics
174 S8=hm8.*(a12+a23+a13)./(3-1); %Total Strength
175 Bif8=hm8.*2;                  %Different colors for Bifurcation diagram
176 phi18=hm8.*phi1;              %value of phi1
177 R8=(1/3)*abs(exp(0)+exp(1i.*phi1)+exp(1i.*phi12)).*hm8; %The phase difference is given.
      Choose theta1=0, then theta2=phi1 and theta3=phi12
178 %% Set 9
179
180 % Find smallest solution of sin(phi2)
181 A=sinphi*(2.*pc.^2);                            %dimensions z(=sin)-by-x(=pc)
182 B=(sqrt(1-sinphi.^2))*(2.*pc.*sqrt(1-pc.^2));   %Use sin instead of angle to limit
      domain
183 Right=A+B;
184 Left = (2*Delta2+Delta1)./sigma;
185
186 for k = 1:x %pc
187     for m = 1:y %sigma
188          for n=1:z %sinphi
189             condition= Right(n,k) - Left(m); %Condition on phi1, see set of eq. points
                  7
190          if abs(condition)<10^-2
191             a12=(Delta1-Delta2+sigma(m)*sinphi(n))/(2*sigma(m)*pc(k)*sqrt(1-pc(k)^2));
192             if a12>0 && a12<=1 && sinphi2(m,k)==10 %smallest solution
193                 sinphi2(m,k)=sinphi(n);
194             end
195          end
196     end
197     end
198 end
199
200 % Properties of the point
201 phi1=acos(2.*pc.^2-1);
202 phi2=asin(sinphi2);
203 phi12=phi1+phi2;
204
205 a12=(Delta1-Delta2+sigma.*sin(phi2))./(2*sigma*(pc.*sqrt(1-pc.^2)));
206 a23=1;
207 a13=1;
208
```

```
% Stability

% Construct logical array where sigma>sigma*a12
la12=sigma>sigma.*a12;

% Construct logical matrix where sigma < Critical Coupling strengths
CritSigMax1=sigma.*sin(phi2)./((2.*pc.*sqrt(1-pc.^2)).*ones(y,x));
CritSigMax2=sigma.*sin(phi12)./((2.*pc.*sqrt(1-pc.^2)).*ones(y,x));
CritSig=min(CritSigMax1,CritSigMax2);
lsigma=sigma<CritSig;

% Construct logical matrix where lambda < 0
a=(sigma*cos(phi1)).*a12./(3-1); %Matrix multiplications such that matrix has dimension y-by-x and element m,n has sigma(m)*cos(k)*a12(m,k)
b=(sigma.*cos(phi2))./(3-1);
c=2.*(sigma.*cos(phi12))./(3-1);
lambda=sqrt(a.^2-2*a.*b-2*a.*c+b.^2-2*b.*c+c.^2)-a-b-c;
llambda=lambda<0;

% Bifurcation matrix (stable region)
hm9=la12.*lsigma.*llambda;
% Characteristics
S9=hm9.*(a12+a23+a13)./(3-1); %Total Strength
Bif9=hm9.*1.5;
phi19=hm9.*phi1;              %value of phi1
R9=(1/3)*abs(exp(0)+exp(1i.*phi1)+exp(1i.*phi12)).*hm9; %The phase difference is given. Choose theta1=0, then theta2=phi1 and theta3=phi12
%%  Characteristics of all points
% Bifurcation diagram
Bif=Bif4+Bif5+Bif6+Bif8+Bif9;     %Bifurcation diagram (different colors)

% Total strength
S=S4+S5+S6+S8+S9;                   %Total Strength of stable points
LS= S==0;
LS=LS.*lpc.*1.5;                    %Region F2 has maximum strength
S=S+LS;                             %S for all (sigma,pc)

% Phi1
Phi1=phi14+phi15+phi16+phi18+phi19;                 %value of phi in stable region

Lphi1= Phi1==0;                                     %Construct oscillating phase difference in region F2
lsigma=sigma<MinDelta;
Lphi1=Lphi1.*lpc.*lsigma.*2.*pi.*sin(sigma.*300.*pi);

Lphi2= Phi1==0;
lpc2=pc<1/sqrt(2);                                  %Define phi1 = pi/3 (random) in region F1
Lphi2= Lphi2.*lpc2;

Phi1=Phi1+Lphi1+Lphi2;                              %Phi for all (sigma,pc)

% Global Synchronization
RF1=(1/3)*abs(exp(0)+exp(1i.*Lphi1)+exp(1i.*2.*Lphi1)).*lpc.*lsigma.*Lphi1; %R in unstable region F1
RF2=(1/3)*abs(exp(0)+exp(1i*2/3*pi)+exp(1i*4/3*pi)).*lpc2;                  %R in
```

```
    unstable region F2
R=R4+R5+R6+R8+R9+RF1+RF2;                              %R for all (sigma,pc)
```

### A.1.4. Chemical oscillators

The code below is used to generate the data required for the figures in Chapter 6.

```
%% Distribution of the frequencies
mu=0.4526;                                  % Mean of distribution (frequencies)
StanDev=6.54*10^-3;                         % Standard Deviation of distribution
omega=normrnd(mu,StanDev,[64 , 1])*2*pi;    % Omega=2*pi*f

%% Construct I(t) for 64 oscillators
t=3:0.005:160;
phasedif=(0:63)';
I_average=0.165;
A=1/12.5;
I=I_average+A*sin(omega.*t+phasedif*3);

%% Data phase portrait
j=50;                                   % Timestamp snapshot (arbitrary)
s=I(:,j)-I_average;                     % Signal s(t)
psi=hilbert(s);                         % Complex time function

%% Order parameter
s=I-0.165; %note: x2=t
sbar=imag(hilbert(s));
r=zeros(1,length(t));
for k=1:length(t)
    r(1,k)=abs(sum(s(:,k)+sbar(:,k)))/sum(sqrt(s(:,k).^2+sbar(:,k).^2));
end
```

# Bibliography


[1] S.H. Strogatz. *Sync: How Order Emerges From Chaos In the Universe, Nature, and Daily Life*. Hyperion, 2012. ISBN: 9781401304461.

[2] Z. Néda et al. "Physics of the rhythmic applause". In: *Physical Review E* 61 (June 2000).

[3] D.C. Michaels, E.P. Matyas, and J. Jalife. "Mechanism of Sinoatrial Pacemaker Synchronization: A New Hypothesis". In: *Circulation Research* 61 (1987), pp. 704–714.

[4] M.V.L Bennett and R.S. Zukin. "Electrical Coupling and Neuronal Synchronization in the Mammalian Brain". In: *Neuron* 41.4 (2004), pp. 495–511.

[5] R.D. Traub and R.K. Wong. "Cellular mechanism of neuronal synchronization in epilepsy". In: *Science* 216.4547 (1982), pp. 745–747.

[6] M. Chavez et al. "Functional Modularity of Background Activities in Normal and Epileptic Brain Networks". In: *Phys. Rev. Lett.* 104 (11 Mar. 2010).

[7] K. Wiesenfeld, P. Colet, and S.H. Strogatz. "Synchronization Transitions in a Disordered Josephson Series Array". In: *Physical Review Letters* 76.3 (1996), pp. 404–407.

[8] K. Wiesenfeld, P. Colet, and S.H. Strogatz. "Frequency locking in Josephson arrays: Connection with the Kuramoto model". In: *Physical Review E - Statistical Physics, Plasmas, Fluids, and Related Interdisciplinary Topics* 57.2 (1998), pp. 1563–1569.

[9] Z. Jiang and M. Mc Call. "Numerical simulation of a large number of coupled lasers". In: *Journal of the Optical Society of America B: Optical Physics* 10.1 (1993), pp. 155–163.

[10] S.Yu. Kourtchatov et al. "Theory of phase locking of globally coupled laser arrays". In: *Physical Review A* 52.5 (1995), pp. 4089–4094.

[11] G. Filatrella, A. H. Nielsen, and N. F. Pedersen. "Analysis of a power grid using a Kuramoto-like model". In: *The European Physical Journal B* 61.4 (Feb. 2008), pp. 485–491.

[12] K. Xi, J. L. A. Dubbeldam, and H.X. Lin. "Synchronization of cyclic power grids: Equilibria and stability of the synchronous state". In: *Chaos: An Interdisciplinary Journal of Nonlinear Science* 27.1 (2017), p. 013109.

[13] R.A. York and R.C. Compton. "Quasi-Optical Power Combining Using Mutually Synchronized Oscillator Arrays". In: *IEEE Transactions on Microwave Theory and Techniques* 39.6 (1991), pp. 1000–1009.

[14] A. Pikovsky, M. G. Rosenblum, and J. Kurths. *Synchronization, A Universal Concept in Nonlinear Sciences*. Cambridge University Press, 2001.

[15] N. Wiener. *Nonlinear Problems in Random Theory*. The Massachusetts Institute of Technology, 1958.

[16] S. H. Strogatz. "From Kuramoto to Crawford: exploring the onset of synchronization in populations of coupled oscillators". In: *Physica D: Nonlinear Phenomena* 143.1 (2000).

[17] F.A. Rodrigues et al. "The Kuramoto model in complex networks". In: *Physics Reports* 610 (2016), pp. 1–98.

[18] A. T. Winfree. "Biological rhythms and the behavior of populations of coupled oscillators". In: *Journal of Theoretical Biology* 16.1 (1967), pp. 15–42.

[19] Y. Kuramoto. *Chemical Oscillations, Waves and Turbulence*. Berlin: Springer, 1984.

[20] Y. Kuramoto. "Self-entrainment of a population of coupled non-linear oscillators". In: *International Symposium on Mathematical Problems in Theoretical Physics*. Ed. by Huzihiro Araki. 1975, pp. 420–422.

[21] V. Avalos-Gaytán et al. "Emergent explosive synchronization in adaptive complex networks". In: *Phys. Rev. E* 97 (4 2018).

[22] I. Leyva et al. "Explosive transitions to synchronization in networks of phase oscillators". In: *Scientific reports* 3 (2013), p. 1281.

[23] R.B. Yaffe et al. “Physiology of functional and effective networks in epilepsy”. In: *Clinical Neurophysiology* 126.2 (2015), pp. 227–236.

[24] M. Kim et al. “Functional and Topological Conditions for Explosive Synchronization Develop in Human Brain Networks with the Onset of Anesthetic-Induced Unconsciousness”. In: *Frontiers in Computational Neuroscience* 10 (2016), p. 1.

[25] V. Latora, V. Nicosia, and G. Russo. *Complex networks: Principles, Methods and Applications*. Cambridge University Press, 2017.

[26] V. Chapela, R. Criado, and M. Romance S. Moral. *Intentional Risk Management through Complex Networks Analysis*. Springer International Publishing, 2015.

[27] T. C. Silva and L. Zhao. *Machine Learning in Complex Networks*. Springer International Publishing, 2016.

[28] K. Aardal, L. van Iersel, and R. Janssen. *Lecture Notes TW2020 Optimization*. Delft University of Technology, 2018.

[29] P. van Mieghem. *Graph Spectra for Complex Networks*. Cambridge University Press, 2010.

[30] U. von Luxburg. *A Tutorial on Spectral Clustering*. Tech. rep. Max Planck Institute for Biological Cybernetics, 2006.

[31] Y. Kuramoto. “Cooperative Dynamics of Oscillator Community: A Study Based on Lattice of Rings”. In: *Progress of Theoretical Physics Supplement* 79 (1984), pp. 223–240.

[32] N. Chopra and M.W. Spong. “On Exponential Synchronization of Kuramoto Oscillators”. In: *IEEE Transactions on Automatic Control* (2009).

[33] F. Dörfler and F. Bullo. “On the critical coupling for Kuramoto Oscillators”. In: *SIAM Journal on Applied Dynamical Systems* (2011).

[34] A. Arenas et al. “Synchronization in complex networks”. In: *Physics Reports* 469.3 (2008).

[35] P. Grassberger et al. “Explosive Percolation is Continuous, but with Unusual Finite Size Behavior”. In: *Phys. Rev. Lett.* 106 (22 May 2011), p. 225701.

[36] Arrowsmith D.K. and Place C.M. *Dynamical Systems: Differential equations, maps and chaotic behaviour*. Chapmann & Hall, 1992.

[37] J.K. Hale and H. Kocak. *Dynamics and Bifurcations*. Springer, 1991.

[38] I. Z. Kiss, Y. Zhai, and J. L. Hudson. “Emerging Coherence in a Population of Chemical Oscillators”. In: *Science* 296.5573 (2002), pp. 1676–1678.

[39] N. Sato and G. Okamoto. “Kinetics of the Anodic Dissolution of Nickel in Sulfuric Acid Solutions”. In: *Journal of the Electrochemical Society* 111.8 (1964), pp. 897–903.

[40] O. Lev et al. “Bifurcations to periodic and chaotic motions in anodic nickel dissolution”. In: *Chemical Engineering Science* 43.6 (1988), pp. 1339–1353.

[41] W. Wang, I.Z. Kiss, and J.L. Hudson. “Clustering of Arrays of Chaotic Chemical Oscillators by Feedback and Forcing”. In: *Phys. Rev. Lett.* 86 (21 May 2001), pp. 4954–4957.

[42] A. S. Pikovsky et al. “Phase synchronization of chaotic oscillators by external driving”. In: *Physica D: Nonlinear Phenomena* 104.3 (1997), pp. 219–238.

[43] Michael Rosenblum and Jürgen Kurths. “Analysing synchronization phenomena from bivariate data by means of the Hilbert transform”. In: *Nonlinear analysis of physiological data*. Springer, 1998, pp. 91–99.

[44] D. Gabor. *Theory of communication*. Institution of Electrical Engineering, 1946.

[45] E. Harvey-Girard, J. Lewis, and L. Maler. “Burst-Induced Anti-Hebbian Depression Acts through Short-Term Synaptic Dynamics to Cancel Redundant Sensory Signals”. In: *Journal of Neuroscience* 30.17 (2010), pp. 6152–6169.

[46] K. Bol et al. “Frequency-Tuned Cerebellar Channels and Burst-Induced LTD Lead to the Cancellation of Redundant Sensory Inputs”. In: *Journal of Neuroscience* 31.30 (2011), pp. 11028–11038.

[47] J. Scott. *Social Network Analysis: A Handbook*. Sage Publications, 2000.